SLAC-PUB-2946
June 1982
(A)

COHERENT INSTABILITIES OF A RELATIVISTIC BUNCHED BEAM*

Alexander W. Chao

Stanford Linear Accelerator Center

Stanford University, Stanford, California 94305

Lectures Presented at the Second Summer School

on High Energy Particle Accelerators

Stanford Linear Accelerator Center

Stanford, California

August 2-13, 1982

---

*Work supported by the Department of Energy, contract DE-AC03-76SF00515.

ABSTRACT

A charged particle beam contained in an accelerator vacuum chamber interacts electromagnetically with its environment to create a wake field. This field then acts back on the beam, perturbing the particle motion. If the beam intensity is high enough, this beam-environment interaction may lead to an instability and to subsequent beam loss. The beam and its environment form a dynamical system, and it is this system that will be studied.

In Section I, the Maxwell equations are solved to obtain the wake field of a beam with a rigid particle distribution, i.e., the action of the wake field on the particle distribution is neglected. The concepts of wake function and impedance will be introduced and their properties discussed. As an illustration, the special case of a pure resistive wall will be presented explicitly.

In Section II, the influence of wake fields on the beam will be studied, but with a simplified model for the beam distribution. In fact, the beam will be represented as a point charge without any internal structure. The beam-environment system is solved self-consistently with the restriction that the beam is allowed to have only center-of-mass motion. This simplified view allows a few of the instability mechanisms to be studied. These one-particle models are sufficiently successful that the treatment is extended to include a few two-particle models, in which the beam is represented as two point macroparticles interacting with each other through the wake forces. This picture gives an insight into the internal motions within the beam. Seven of these one- and two-

particle models will be treated. The equation used in this Section II is basically F = ma.

A self-consistent treatment of the beam-environment system that permits a full evaluation of the internal beam motions will be included in Section III. Here the equation of motion -- the Vlasov equation -- is established to describe the system. The formalism that allows this equation to be solved will then be presented. Results obtained in Section II, as well as some additional results on coherent effects, will be derived in this section. For pedagogical purposes, the material is treated using simplified models as illustrations.

TABLE OF CONTENTS

I. RESPONSE OF ENVIRONMENT TO BEAM

A charged particle beam interacts with its vacuum chamber environment in an accelerator. As a first step in our treatment of the beam-environment system, we will study the properties of the wake electromagnetic fields generated by the beam in the environment. For this purpose, the beam is considered to be rigid and unaffected by the wake field it generates (and therefore no instabilities). The beam is assumed to move with the speed of light. The wake field that we are most interested in is that seen by a test charge that follows the beam at a fixed distance.

We will first work out the wake field in some detail for the case in which the environment is that of a smooth cylindrical pipe with resistive wall surface. In the process we will point out the general features of all wake fields.

It is inevitable that the concept of impedance also be introduced. The impedance is essentially the Fourier transform of the wake field and we will discuss its properties as well. Finally we will include in this section a discussion of the parasitic energy loss of the beam in the environment.

1.1. Free Space and Perfectly Conducting Pipe

The electromagnetic field carried by a relativistic point charge q in free space is a familiar subject treated in text books.[1,2] The field distribution is sketched in Fig. 1(a). The EM field distribution is Lorentz contracted into a thin disk perpendicular to the particle's

direction of motion with angular spread of the order of $1/\gamma$. In the ultrarelativistic limit of $v = c$, the disk actually shinks into a δ-function thickness, as shown in Fig. 1(b). The electric field $\vec{E}$ points strictly radially outward from the point charge. The magnitude of E is most easily obtained by drawing a pill box with radius r and infinitesimal height around the charge q, as sketched in Fig. 1(b), and apply the Gauss law. The result is*

$$E_r = \frac{2q}{r}\,\delta(z-ct) \tag{1.1}$$

where we have adopted a cylindrical coordinate system with z pointing in the direction of motion of q. Similarly, an application of Ampere's law gives

$$B_\theta = \frac{2q}{r}\,\delta(z-ct) \tag{1.2}$$

which is equal to E_r.

We now consider the case in which the point charge moves along the axis of a cylindrically symmetric vacuum chamber pipe that is perfectly conducting, as shown in Fig. 1(c). The same application of the Gauss and Ampere laws again gives results (1.1) and (1.2). The sole function of the pipe wall is to truncate the field lines by terminating them onto the image charges on the wall.

---

* We use cgs units.

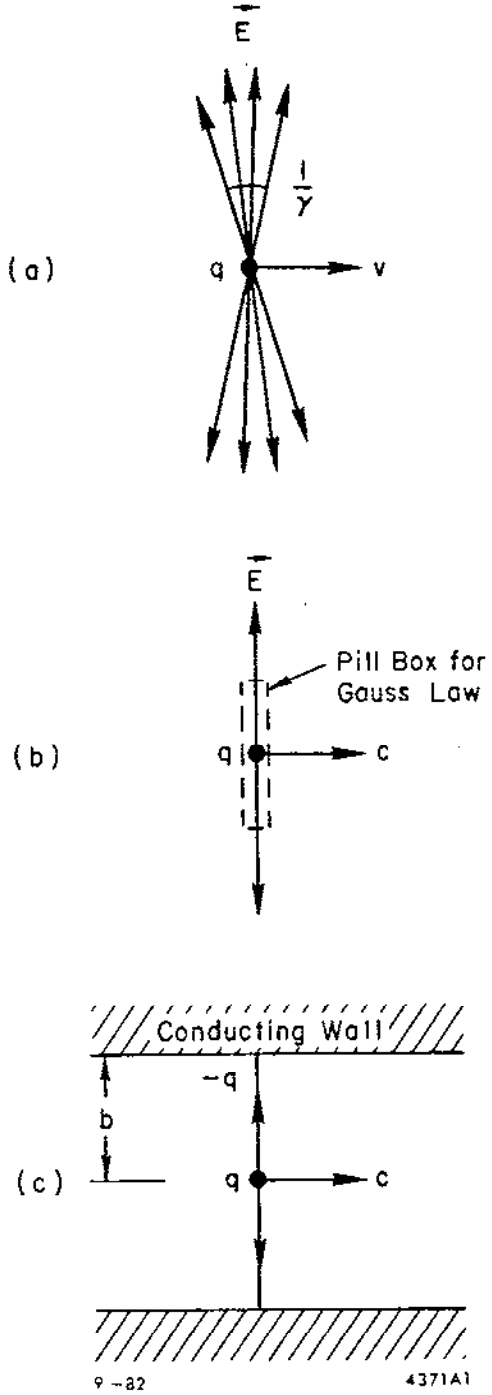

Fig. 1. Electromagnetic field carried by an ultrarelativistic point charge in free space and in a perfectly conducting smooth pipe.

The above result with the pipe simply truncating the field lines without deformation works only if the charge moves along the pipe axis. It is no longer correct for a point charge moving off-axis, in which case the beam will be represented as a superposition of multipole moments. One can consider for instance a distribution with a pure m-th moment:

$$\rho = \frac{I_m}{\pi a^{m+1}} \delta(z-ct)\, \delta(r-a) \cos m\theta$$

$$\vec{j} = c\, \rho\, \hat{z} \qquad (1.3)$$

i.e., the charge is distributed as an infinitesimally thin ring with radius a and with a cos $m\theta$ angular dependence. The quantity I_m is the m-th moment of the beam charge distribution.

The reason that the pipe no longer simply truncates the free space field lines in this case is that now the electric field is no longer perpendicular, and the magnetic field is no longer parallel, to the pipe wall. Indeed, the electromagnetic field carried by the source (1.3) is obtained by solving the Maxwell equations together with proper boundary conditions. The result is

$$E_r = \begin{cases} 2I_m \left(\dfrac{1}{b^{2m}} - \dfrac{1}{a^{2m}} \right) r^{m-1} \cos m\theta \; \delta(z-ct) & r < a \\ 2I_m \left(\dfrac{1}{r^{m+1}} + \dfrac{r^{m-1}}{b^{2m}} \right) \cos m\theta \; \delta(z-ct) & a < r < b \end{cases}$$

$$E_\theta = \begin{cases} -2I_m \left(\dfrac{1}{b^{2m}} - \dfrac{1}{a^{2m}} \right) r^{m-1} \sin m\theta \; \delta(z-ct) & r < a \\ 2I_m \left(\dfrac{1}{r^{m+1}} - \dfrac{r^{m-1}}{b^{2m}} \right) \sin m\theta \; \delta(z-ct) & a < r < b \end{cases}$$

$$B_r = - E_\theta$$

$$B_\theta = E_r \quad . \tag{1.4}$$

The derivation of Eqs. (1.4) is omitted here. It can be reproduced as a special case of what we will discuss in Section 1.3. The important facts here are that the particle has generated a field that has angular dependence of sin mθ and cos mθ and that the field is Lorentz contracted into a δ-function in its longitudinal distribution. No wake field is left behind the particle as a result of this particle-environment interaction.

In free space or in a perfectly conducting pipe, therefore, a particle does not see the fields carried by other particles in the beam. (Unless the two particles move side by side with exactly the same longitudinal position, in which case they see each other's fields but do not experience any Lorentz force because the electric force and the

magnetic force cancel exactly in the limit $\vec{v} = c\hat{z}$.)* Consequently, there can be no coherent instability.

1.2. Resistive Wall Wake, $m \neq 0$

In case the vacuum chamber is not a smooth pipe or if it is smooth but not perfectly conducting, a beam will generate behind it an electromagnetic wake. See Fig. 2. In this and the next sections, the case of a resistive pipe wall [Fig. 2(b)] will be worked out in detail. For simplicity, we assume that the beam moves with the speed of light and that the pipe wall has infinite thickness. The more general considerations are treated in Refs. 3, 4 and 5. We also assume the beam has a distribution given by (1.3).

Let us first explicitly write down the Maxwell equations, component by component in cylindrical coordinates:

$$\frac{1}{r}\frac{\partial(rE_r)}{\partial r} + \frac{1}{r}\frac{\partial E_\theta}{\partial \theta} + \frac{\partial E_z}{\partial z} = 4\pi\rho$$

$$\frac{1}{r}\frac{\partial B_z}{\partial \theta} - \frac{\partial B_\theta}{\partial z} = \frac{4\pi}{c} j_r + \frac{1}{c}\frac{\partial E_r}{\partial t}$$

$$\frac{\partial B_r}{\partial z} - \frac{\partial B_z}{\partial r} = \frac{4\pi}{c} j_\theta + \frac{1}{c}\frac{\partial E_\theta}{\partial t}$$

---

* It is true that there is an electrostatic force in the rest frame of the beam, but when observed in the laboratory frame, motions are infinitely time dilated.

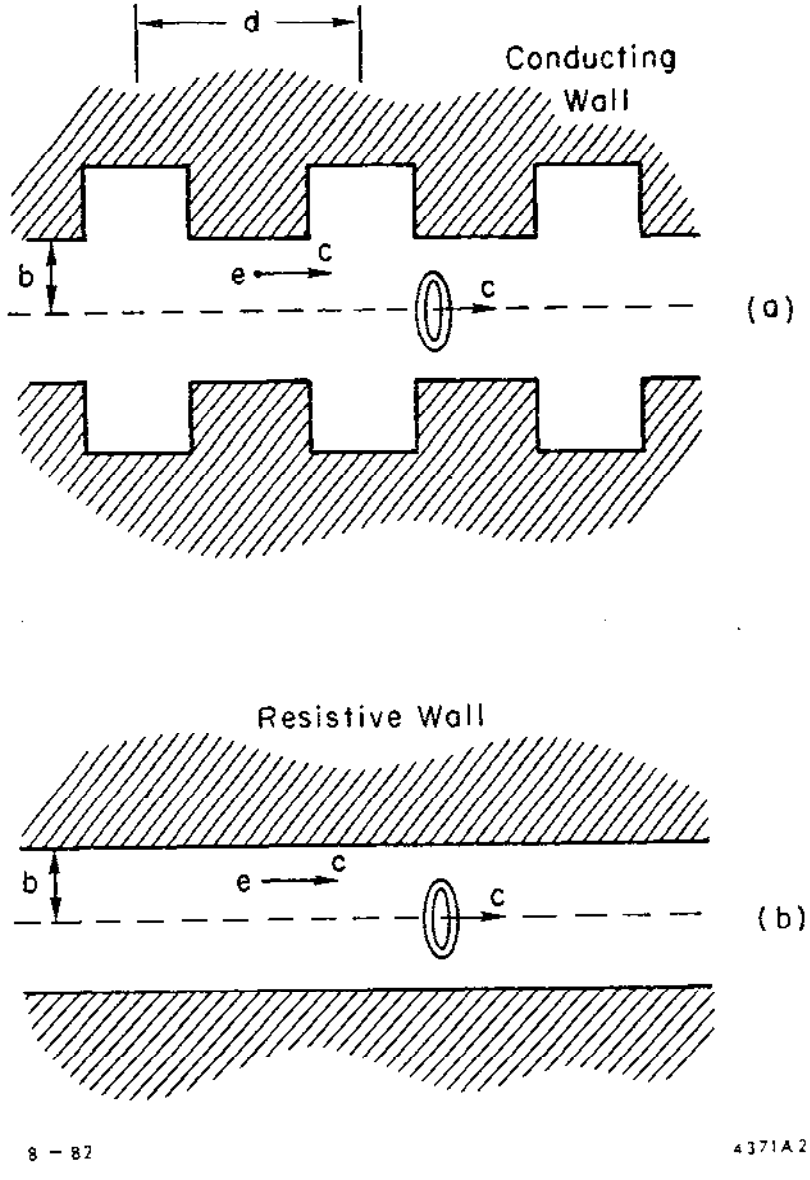

Fig. 2. Examples of vacuum chamber pipe that generates wake fields. The beam is represented here as a ring possessing a multipole moment with cos mθ distribution.

$$\frac{1}{r}\frac{\partial(rB_\theta)}{\partial r} - \frac{1}{r}\frac{\partial B_r}{\partial \theta} = \frac{4\pi}{c} j_z + \frac{1}{c}\frac{\partial E_z}{\partial t}$$

$$\frac{1}{r}\frac{\partial(rB_r)}{\partial r} + \frac{1}{r}\frac{\partial B_\theta}{\partial \theta} + \frac{\partial B_z}{\partial z} = 0$$

$$\frac{1}{r}\frac{\partial E_z}{\partial \theta} - \frac{\partial E_\theta}{\partial z} = -\frac{1}{c}\frac{\partial B_r}{\partial t}$$

$$\frac{\partial E_r}{\partial z} - \frac{\partial E_z}{\partial r} = -\frac{1}{c}\frac{\partial B_\theta}{\partial t}$$

$$\frac{1}{r}\frac{\partial(rE_\theta)}{\partial r} - \frac{1}{r}\frac{\partial E_r}{\partial \theta} = -\frac{1}{c}\frac{\partial B_z}{\partial t} \quad . \tag{1.5}$$

Given that ρ and j_z are proportional to cos $m\theta$, the angular θ dependence of the field components can be obtained by inspection: E_r, E_z and B_θ are proportional to cos $m\theta$, while E_θ, B_z and B_r are proportional to sin $m\theta$. One also expects that the dependence on z and t are such that all quantities depend on the the combined variable z-ct. We then write the field components in terms of Fourier transformations*

$$\begin{aligned}(E_r, E_z, B_\theta) &= \cos m\theta \int_{-\infty}^{\infty} dk\, e^{ik(z-ct)}\, (\tilde{E}_r, \tilde{E}_z, \tilde{B}_\theta) \\ (E_\theta, B_z, B_r) &= \sin m\theta \int_{-\infty}^{\infty} dk\, e^{ik(z-ct)}\, (\tilde{E}_\theta, \tilde{B}_z, \tilde{B}_r)\end{aligned} \tag{1.6}$$

---

* There is a theorem saying that when you have only partial knowledge of the solution to a differential equation and do not know what to do next, the thing to do is to make a Fourier transform.

where $\tilde{E}_r$, etc. are functions of k and r. Due to causality, our solution must satisfy the condition that no wake field will be produced ahead of the beam, i.e., in the region $z-ct > 0$.

In the rest of this section, we will work out the case $m = 0$. The $m \geq 1$ cases are discussed in Section 1.3. The beam is thus represented as a thin ring with total charge q. The field components E_θ, B_z and B_r vanish.

Setting $m = 0$ in (1.6) and substituting the result into (1.5), we obtain three equations. [There are eight equations in (1.5), but five of them are redundant.] They are rather easy to solve, yielding

$$\tilde{E}_z = A \qquad r < b$$

$$\tilde{E}_r = \tilde{B}_\theta = \begin{cases} -ikA\dfrac{r}{2} & r < a \\ -ikA\left(\dfrac{r}{2} + \dfrac{q}{\pi r}\right) & a < r < b \end{cases} \tag{1.7}$$

where A is a constant that depends only on k and is yet to be determined. Note that there is no discontinuity of $\tilde{E}_z$ at $r = a$. The quantity A is closely related to something called the impedance to be discussed in Section 1.5.

For a perfectly conducting wall, $\tilde{E}_z$ vanishes at $r = b$; this means $A = 0$, and an inverse Fourier transform of (1.7) gives (1.1) and (1.2). In case the wall is resistive, one needs to obtain A from the boundary conditions at $r = b$, and to do that, the fields inside the wall, $r > b$, need to be found.

Substituting (1.6) into the Maxwell Eq. (1.5) and setting $\rho = 0$ and $\vec{j} = \sigma\vec{E}$ in the metal wall, where σ is the conductivity, we again obtain three non-redundant equations:

$$\frac{1}{r}\frac{\partial}{\partial r}\left(r \frac{\partial \tilde{E}_z}{\partial r} \right) + \lambda^2 \tilde{E}_z = 0$$

$$\tilde{E}_r = \frac{ik}{\lambda^2}\frac{\partial \tilde{E}_z}{\partial r} \tag{1.8}$$

$$\tilde{B}_\theta = \left(1 + \frac{\lambda^2}{k^2} \right) \tilde{E}_r$$

where we have defined, following Refs. 3 and 4, a parameter

$$\lambda = \sqrt{\frac{2\pi\sigma|k|}{c}}\,[i + \mathrm{sgn}(k)] \tag{1.9}$$

with

$$\lambda^2 = \frac{4\pi\sigma i k}{c} \quad .$$

The parameter λ^{-1} has dimensionality of length; it defines the skin depth as a function of frequency $\omega = kc$ inside the metal wall.

In what follows, we will assume $|\lambda|$ is much larger than b^{-1}, i.e., the skin depth is much shorter than the pipe radius b. This assumption is good if the wave number $|k|$ is much greater than $c/4\pi\sigma b^2$, or equivalently if we are interested in the region

$$|\, z-ct \,| \ll b/\chi \tag{1.10}$$

where χ is a small dimensionless parameter defined by

$$\chi \equiv c/4\pi\sigma b \quad . \tag{1.11}$$

For example, if $b = 5$ cm and the wall is made of aluminum with $\sigma = 3 \times 10^{17}$ sec^{-1}, we have $\chi = 1.6 \times 10^{-9}$ and our approximation breaks down at a distance $\gtrsim 3 \times 10^{7}$ m behind the beam. (In case the vacuum chamber wall has a finite thickness Δ, our approximation also requires $|\lambda| \gg \Delta^{-1}$.) Under this approximation, the equation for $\tilde{E}_z$ in (1.8) becomes $\partial^2\tilde{E}_z/\partial r^2 + \lambda^2\tilde{E}_z = 0$, which has the solution*

$$\tilde{E}_z = A\, e^{i\lambda(r-b)} \tag{1.12}$$

where the coefficient A is the same as that appeared in Eq. (1.7) to assure continuity of $\tilde{E}_z$. From Eq. (1.8), we then have

$$\begin{aligned} \tilde{E}_r &= -\frac{k}{\lambda} A\, e^{i\lambda(r-b)} \\ \tilde{B}_\theta &= -\frac{k}{\lambda}\left(1 + \frac{\lambda^2}{k^2}\right) A\, e^{i\lambda(r-b)} \quad . \end{aligned} \tag{1.13}$$

The coefficient A is determined by the continuity of $\tilde{B}_\theta$ at $r = b$, yielding the result

$$A = \frac{q}{\pi b\left(\frac{ikb}{2} - \frac{\lambda}{k}\right)} \quad . \tag{1.14}$$

---

* If we do not make the assumption $|\lambda| \gg b^{-1}$, $\tilde{E}_z$ will be written in terms of Bessel functions. This complication is not needed for our purposes.

Note that it would be incorrect to demand a continuity on $\tilde{E}_r$ at $r = b$, because there is a surface charge on the wall pipe.

What we will have to do next is to make inverse Fourier transforms on $\tilde{E}_r$, $\tilde{E}_z$ and $\tilde{B}_\theta$ to obtain the fields. To simplify the mathematics, we will make the approximation that $|\lambda/k| \gg |kb|$. This condition on k in frequency space is equivalent to requiring in physical space the condition

$$| z-ct | \gg \chi^{1/3} b \quad . \tag{1.15}$$

Again taking $\sigma = 3 \times 10^{17}$ sec^{-1} and $b = 5$ cm, this condition excludes from study the wake fields within a distance ~0.06 mm behind the beam.

Under the assumptions (1.10) and (1.15), the parameter A becomes

$$A \approx -\frac{qk}{\pi b \lambda} \quad . \tag{1.16}$$

The inverse Fourier transform can then be readily performed for the region $r < b$. The results for $z-ct < 0$, i.e., behind the charge, are

$$E_z = \frac{q}{2\pi b}\sqrt{\frac{c}{\sigma}}\,\frac{1}{|z-ct|^{3/2}}$$

$$B_\theta = E_r = -\frac{3}{4}\frac{q}{2\pi b}\sqrt{\frac{c}{\sigma}}\,\frac{r}{|z-ct|^{5/2}} \quad . \tag{1.17}$$

The fields vanish for $z-ct > 0$ due to causality. In deriving (1.17), we have used the formulas given in Table I.[3,6]

TABLE I

Fourier transform pairs $F(z) = \int_{-\infty}^{\infty} dk\, e^{ikz}\, \tilde{F}(k)$. The quantity λ is given by Eq. (1.9). The function $F(z)$ vanishes for $z > 0$.

$\tilde{F}(k)$	$F(z)$ $(z < 0)$
$1/k$	$2\pi i$
$1/k^2$	$-2\pi z$
$1/k^3$	$-\pi i z^2$
λ/k^2	$-8\pi i \sqrt{\frac{\sigma}{c}}\, \lvert z\rvert^{1/2}$
λ/k^3	$-\frac{16\pi}{3} \sqrt{\frac{\sigma}{c}}\, \lvert z\rvert^{3/2}$
$1/\lambda$	$-i \sqrt{\frac{c}{\sigma}}\, \lvert z\rvert^{-1/2}$
k/λ	$-\frac{1}{2} \sqrt{\frac{c}{\sigma}}\, \lvert z\rvert^{-3/2}$
k^2/λ	$\frac{3}{4} i \sqrt{\frac{c}{\sigma}}\, \lvert z\rvert^{-5/2}$

Equation (1.17) shows that E_z decreases algebraically with $|z-ct|^{-3/2}$ and is uniform in the transverse dimension (independent of r and θ), while the transverse field components decrease faster with $|z-ct|^{-5/2}$ and is proportional to r. The field components in the metal wall are more difficult to find and in any case are not useful later, so they are omitted from Eq. (1.17).

Note that in the region of interest the field components are continuous across r = a and in fact are even independent of a. By taking the limit $a \to 0$, we see that the results are also applicable to the case when the beam is represented as a point charge.

There is something disturbing about Eq. (1.17). Consider a test charge trailing the beam at a certain distance z. The sign of the longitudinal electric field E_z is such that the test charge gets accelerated if its charge has the same sign as q. If this were true for $z \to 0$, one would expect that the point charge q will <u>gain</u> energy as it travels down the resistive pipe. To make sure this unphysical phenomenon does not happen, we have to compute the field at very short distances behind the beam, which so far has been excluded by the condition (1.15). For this purpose, we take now the opposite limit to (1.15), i.e. we take $|\lambda/k| \ll |kb|$, or equivalently $|z-ct| \ll \chi^{1/3} b$. The parameter A then is approximately given by*

---

* The short range behavior of the wake field depends on the assumption that the beam moves with the speed of light. The upper range of k in reality has a cutoff around γ/b. This introduces the condition that in order for Eq. (1.19) to be valid, the beam energy must be high enough so that $\gamma \gg \chi^{-1/3}$. Another cutoff in k occurs if the beam has a finite length σ_z; then k is restricted to the region $k \lesssim \sigma_z^{-1}$.

$$A \approx \frac{2q}{i\pi k b^2} \quad . \tag{1.18}$$

Using Table I, we perform inverse Fourier transforms to obtain

$$\begin{aligned} E_z &\approx -\frac{4q}{b^2} && r < b \\ B_\theta &= E_r \approx \frac{16q}{b^2}\sqrt{\frac{\sigma}{c}}\,|z-ct|^{1/2} && r = b \quad . \end{aligned} \tag{1.19}$$

Again these expressions are valid for $z-ct < 0$; the fields vanish for $z-ct > 0$. One finds that E_z immediately behind the charge q is indeed decelerating. Note that although E_z is independent of the wall conductivity σ in Eq. (1.19), the range of validity of Eq. (1.19) does depend on σ. In the limit $\sigma \to \infty$, a beam with finite length or a point charge with $v < c$, of course, does not lose energy to the vacuum chamber.

One can obtain the rate of energy loss of the charge q by equating it to the heat generated in the resistive wall. This gives

$$\begin{aligned} \frac{d\mathcal{E}}{dz} &= -\frac{1}{c}\int_{\text{wall}} dV\ \vec{j}\cdot\vec{E} \\ &= -\frac{1}{c}\int_{\text{wall}} dV\ \sigma\vec{E}^2 \\ &= -\frac{2\pi\sigma}{c}\int_b^\infty 2\pi b\ dr \int_{-\infty}^{\infty} dk\ [|\tilde{E}_z|^2 + |\tilde{E}_r|^2] \quad . \end{aligned} \tag{1.20}$$

Using expressions (1.12) and (1.13) for $\tilde{E}_z$ and $\tilde{E}_r$ and (1.14) for A in the metal wall and making the approximation that $\chi = c/4\pi\sigma b \ll 1$, we find

$$\frac{d\epsilon}{dz} = -\frac{2q^2}{b^2} \quad . \tag{1.21}$$

If we then associate this energy loss to an equivalent electric field as seen by the charge q, we find that it is exactly equal to half of the value of $E_z(z-ct)$ in the limit $|z-ct| \to 0$, given by Eq. (1.19). That is

$$E_z\Big|_{\text{seen by } q} = \frac{1}{2} E_z\Big|_{(z-ct) \to 0^-} \quad . \tag{1.22}$$

The expression (1.22) actually is a general result, sometimes referred to as the "fundamental theorem of beam loading."[7] The factor 1/2 comes from the fact that charges in a beam see the wake produced only by those charges in front of it and as a result see on the average only 1/2 of the total beam charge.

To prove (1.22) in general, consider a beam with short but finite length that has an otherwise arbitrary longitudinal density $\rho(z)$. The beam loses energy at a rate

$$\frac{d\epsilon}{dt} = -\int_{-\infty}^{\infty} dz' \, \rho(z') \int_{z'}^{\infty} dz \, \rho(z) \, E_z(z-z') \tag{1.23}$$

where $E_z(z-z')$ is the wake produced by a unit point charge and seen by another point charge a distance $z-z'$ behind in an arbitrary vacuum chamber environment. If the bunch length is short enough that E_z behaves like a step function within the bunch distribution, Eq. (1.23) becomes

$$\frac{d\epsilon}{dt} \approx - E_z(0^+) \int_{-\infty}^{\infty} dz' \, \rho(z') \int_{z'}^{\infty} dz \, \rho(z) \quad .$$

An integration by parts then gives

$$\frac{d\epsilon}{dt} \approx - \frac{q^2}{2} E_z(0^+) \quad ,$$

which proves (1.22). The derivation assumed nothing but causality.

Figures 3(a) and 3(b) show the qualitative behavior of E_z and E_r at the wall surface as functions of z-ct based on the results (1.17) and (1.19). In Fig. 3(c) we constructed qualitatively the pattern of electric field in the pipe region.

Problem 1. Assuming $|\lambda/k| \ll |kb|$, derive Eq. (1.19) from Eq. (1.18). Then try to find the next order term by keeping the next order term in A, i.e., use

$$A \approx \frac{2q}{i\pi kb^2} \left(1 + \frac{2\lambda}{ik^2 b} \right) \quad .$$

Compare the results with Figs. 3(a) and 3(b).

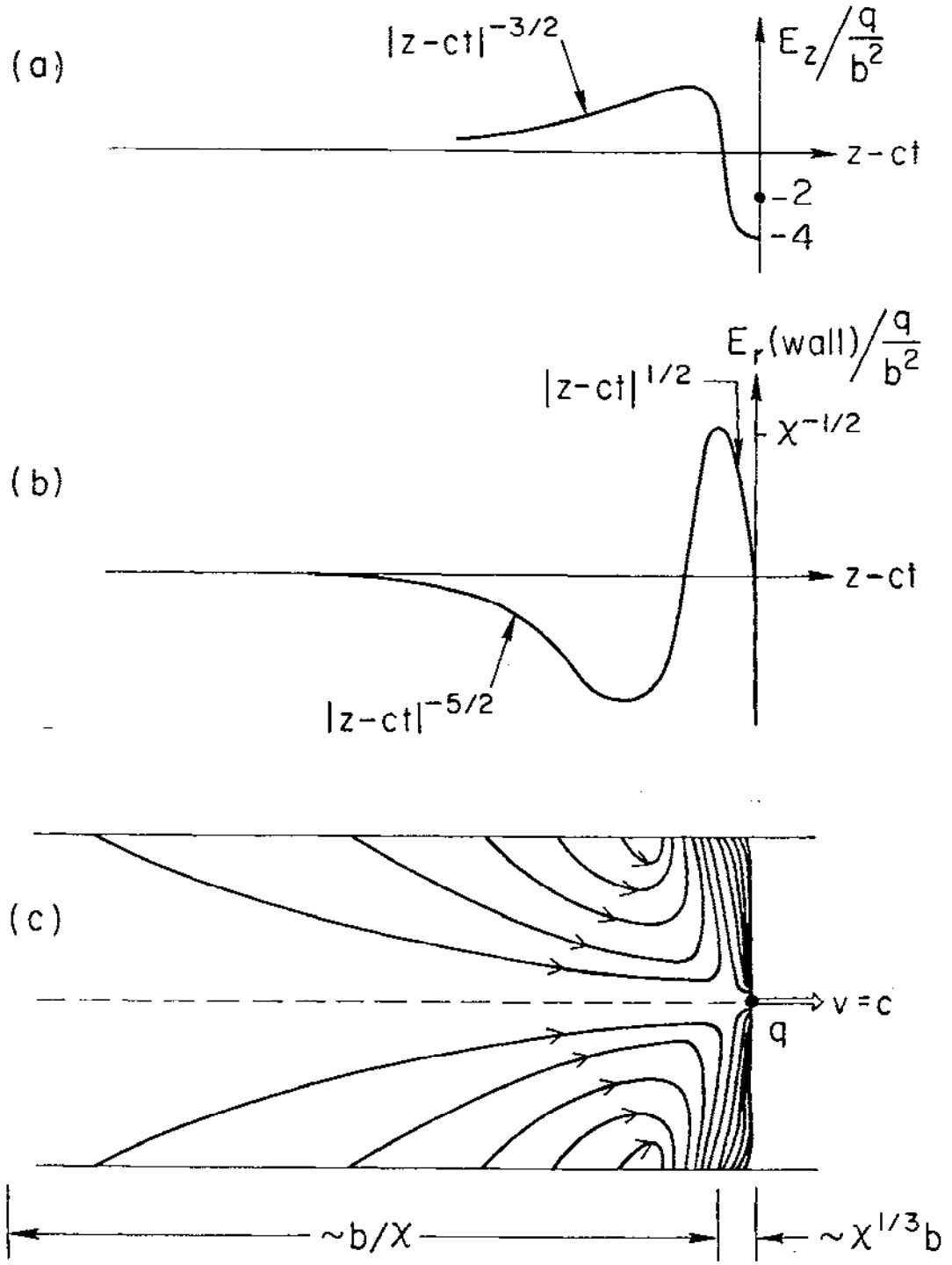

Fig. 3. (a) and (b). The electric field components E_z and E_r at the wall surface as functions of distance behind the charge q. The fields are normalized by q/b^2. The radial field component is typically much larger than the longitudinal component by a factor $\sim\chi^{-1/3}$, but decays behind the charge much faster. Both field components switch sign at a distance of the order of $\chi^{1/3}b$. (c) A schematic drawing of the wake field lines in the pipe. The value of χ in these drawings has been exaggerated by a factor of $\sim 10^8$.

1.3. Resistive Wall Wake, m ≥ 1

In the previous section, electromagnetic wake fields are obtained for the case m = 0. The fields are excited as the charge (i.e., the "monopole moment") of the beam interacts with the resistive wall surroundings. If the beam possesses higher moments (m = 1 for dipole, m = 2 for quadrupole, etc.) in its transverse distribution, it will interact differently and generate different wake field patterns. In this section, we will work out the wake fields for cases m ≥ 1.

Substituting Eq. (1.6) into the Maxwell Eq. (1.5), we obtain the following results in the region r < b

$$\frac{\partial \tilde{E}_z}{\partial r} = -\frac{m}{r}\tilde{B}_z$$

$$\frac{\partial \tilde{B}_z}{\partial r} = -\frac{m}{r}\tilde{E}_z$$

$$\frac{1}{r}\frac{\partial}{\partial r}(r\tilde{E}_r) - \frac{m}{r}\tilde{B}_r = \frac{2I_m}{\pi a^{m+1}}\delta(r-a) - i\left(k + \frac{m^2}{kr^2}\right)\tilde{E}_z$$

$$\frac{1}{r}\frac{\partial}{\partial r}(r\tilde{B}_r) - \frac{m}{r}\tilde{E}_r = -i\left(k + \frac{m^2}{kr^2}\right)\tilde{B}_z$$

$$\tilde{B}_\theta = \tilde{E}_r + \frac{m}{ikr}\tilde{B}_z$$

$$\tilde{E}_\theta = -\tilde{B}_r - \frac{m}{ikr}\tilde{E}_z \quad . \tag{1.24}$$

The first two of these equations are used to obtain $\tilde{E}_z$ and $\tilde{B}_z$; the second two equations can then be solved for $\tilde{E}_r$ and $\tilde{B}_r$; then $\tilde{B}_\theta$ and $\tilde{E}_\theta$ are found from the last two expressions. The solutions for the longitudinal components are easy to find:

$$\begin{aligned} \tilde{E}_z &= A\, r^m \qquad r < b \\ \tilde{B}_z &= -A\, r^m \qquad r < b \end{aligned} \tag{1.25}$$

where A is some coefficient that depends on k. Note that $\tilde{E}_z$ and $\tilde{B}_z$ are continuous across r = a.

The solution for the other field components is not difficult to obtain. One needs only to observe that they generally can be written as polynomials in r, each containing three terms proportional to r^{m-1}, r^{m+1} and r^{-m-1} respectively. By properly choosing the coefficients for each of the terms for the two regions r < a and a < r < b, the solution is found to be

$$\tilde{E}_r = \begin{cases} -\dfrac{ikA}{2(m+1)}\, r^{m+1} + \dfrac{1}{2}\left(-\dfrac{imA}{k} + B - \dfrac{2I_m}{\pi a^{2m}} \right) r^{m-1} & r < a \\ \dfrac{I_m}{\pi r^{m+1}} - \dfrac{ikA}{2(m+1)}\, r^{m+1} + \dfrac{1}{2}\left(-\dfrac{imA}{k} + B \right) r^{m-1} & a < r < b \end{cases}$$

$$\tilde{E}_\theta = \begin{cases} -\dfrac{ikA}{2(m+1)}\, r^{m+1} + \dfrac{1}{2}\left(\dfrac{imA}{k} - B + \dfrac{2I_m}{\pi a^{2m}} \right) r^{m-1} & r < a \\ \dfrac{I_m}{\pi r^{m+1}} - \dfrac{ikA}{2(m+1)}\, r^{m+1} + \dfrac{1}{2}\left(\dfrac{imA}{k} - B \right) r^{m-1} & a < r < b \end{cases}$$

$$\tilde{B}_r = \begin{cases} \dfrac{ikA}{2(m+1)} r^{m+1} + \dfrac{1}{2}\left[\dfrac{imA}{k} + B - \dfrac{2I_m}{\pi a^{2m}}\right] r^{m-1} & r < a \\ -\dfrac{I_m}{\pi r^{m+1}} + \dfrac{ikA}{2(m+1)} r^{m+1} + \dfrac{1}{2}\left[\dfrac{imA}{k} + B\right] r^{m-1} & a < r < b \end{cases}$$

$$\tilde{B}_\theta = \begin{cases} -\dfrac{ikA}{2(m+1)} r^{m+1} + \dfrac{1}{2}\left[\dfrac{imA}{k} + B - \dfrac{2I_m}{\pi a^{2m}}\right] r^{m-1} & r < a \\ \dfrac{I_m}{\pi r^{m+1}} - \dfrac{ikA}{2(m+1)} r^{m+1} + \dfrac{1}{2}\left[\dfrac{imA}{k} + B\right] r^{m-1} & a < r < b \end{cases}$$

(1.26)

The field components in region $r < a$ do not contain r^{-m-1} terms since they are unphysical at $r = 0$. The parameter A appeared in (1.25) while B is an additional coefficient. Both A and B are yet to be determined.

In the case of a perfectly conducting wall, $A = 0$ because E_z must vanish at $r = b$. The condition that $\tilde{E}_\theta = 0$ at $r = b$ then gives $B = 2I_m/\pi b^{2m}$. The reader should be able to make an inverse Fourier transform to obtain Eq. (1.4).

To find A and B for the resistive wall case, we need to solve for the fields in the metal wall. Inserting again (1.6) into the Maxwell equations and setting $\vec{j} = \sigma\vec{E}$ and $\rho = 0$, we obtain these results:

$$\frac{1}{r}\frac{\partial}{\partial r}\left[r\frac{\partial \tilde{E}_z}{\partial r}\right] + \left[\lambda^2 - \frac{m^2}{r^2}\right]\tilde{E}_z = 0$$

$$\frac{1}{r}\frac{\partial}{\partial r}\left[r\frac{\partial \tilde{B}_z}{\partial r}\right] + \left[\lambda^2 - \frac{m^2}{r^2}\right]\tilde{B}_z = 0$$

$$\tilde{E}_r = \frac{c}{4\pi\sigma}\left(\frac{m}{r}\tilde{B}_z + \frac{\partial\tilde{E}_z}{\partial r}\right)$$

$$\tilde{E}_\theta = -\frac{c}{4\pi\sigma}\left(\frac{m}{r}\tilde{E}_z + \frac{\partial\tilde{B}_z}{\partial r}\right)$$

$$\tilde{B}_r = \frac{c}{4\pi\sigma}\frac{\partial\tilde{B}_z}{\partial r} + \left(\frac{c}{4\pi\sigma} - \frac{1}{ik}\right)\frac{m}{r}\tilde{E}_z$$

$$\tilde{B}_\theta = \frac{c}{4\pi\sigma}\frac{m}{r}\tilde{B}_z + \left(\frac{c}{4\pi\sigma} - \frac{1}{ik}\right)\frac{\partial\tilde{E}_z}{\partial r} \quad . \qquad (1.27)$$

After the first pair of equations are solved for $\tilde{E}_z$ and $\tilde{B}_z$, the other field components are obtained from the remaining four equations. The parameter λ is given by Eq. (1.9).

Following what we did for the m = 0 case, we assume again that the skin depth is much shorter than b, i.e., we are interested in the region specified by Eq. (1.10). The first two equations in (1.27) then have the solution

$$\tilde{E}_z = -\tilde{B}_z = A\, b^m\, e^{i\lambda(r-b)} \qquad r > b \quad . \qquad (1.28)$$

Knowing $\tilde{E}_z$ and $\tilde{B}_z$, the rest of the field components are found to be

$$\tilde{E}_r = \tilde{E}_\theta = -\frac{k}{\lambda} A\, b^m\, e^{i\lambda(r-b)}$$

$$\tilde{B}_\theta = -\left(\frac{k}{\lambda} + \frac{\lambda}{k}\right) A\, b^m\, e^{i\lambda(r-b)} \qquad (1.29)$$

$$\tilde{B}_r = \left(\frac{k}{\lambda} + \frac{im}{kb}\right) A\, b^m\, e^{i\lambda(r-b)} \quad .$$

The requirement that $\tilde{E}_\theta$, $\tilde{B}_r$ and $\tilde{B}_\theta$ be continuous at $r = b$ (the component $\tilde{E}_r$ is not continuous across $r = b$ due to a surface charge on the wall) gives

$$A = \frac{2I_m k}{\pi b^{2m+1}\left(\frac{ik^2 b}{m+1} - \lambda\right)}$$

$$B = \frac{2I_m}{\pi b^{2m}\left(\frac{ik^2 b}{m+1} - \lambda\right)}\left(\frac{im}{b} - \lambda\right) \quad . \qquad (1.30)$$

If we further restrict our interest to the region specified by Eq. (1.15), the coefficients A and B become

$$A \approx -\frac{2I_m k}{\pi b^{2m+1}\lambda}$$

$$B \approx \frac{2I_m}{\pi b^{2m}}\left(1 + i\frac{k^2 b}{(m+1)\lambda} - \frac{im}{b\lambda}\right) \quad . \qquad (1.31)$$

Table I' can then be used to find the field components, yielding

$$E_z = \frac{I_m}{\pi b^{2m+1}} \sqrt{\frac{c}{\sigma}}\, r^m \cos m\theta \, \frac{1}{|z-ct|^{3/2}}$$

$$E_r = -\frac{3I_m}{4\pi b^{2m+1}} \sqrt{\frac{c}{\sigma}}\, \frac{1}{(m+1)}\, r^{m-1} \cos m\theta \, (r^2+b^2) \, \frac{1}{|z-ct|^{5/2}}$$

$$E_\theta = -\frac{3I_m}{4\pi b^{2m+1}} \sqrt{\frac{c}{\sigma}}\, \frac{1}{(m+1)}\, r^{m-1} \sin m\theta \, (r^2-b^2) \, \frac{1}{|z-ct|^{5/2}}$$

$$B_z = -\frac{I_m}{\pi b^{2m+1}} \sqrt{\frac{c}{\sigma}}\, r^m \sin m\theta \, \frac{1}{|z-ct|^{3/2}}$$

$$B_r = -E_\theta - \frac{2I_m}{\pi b^{2m+1}} \sqrt{\frac{c}{\sigma}}\, m r^{m-1} \sin m\theta \, \frac{1}{|z-ct|^{1/2}}$$

$$B_\theta = E_r - \frac{2I_m}{\pi b^{2m+1}} \sqrt{\frac{c}{\sigma}}\, m r^{m-1} \cos m\theta \, \frac{1}{|z-ct|^{1/2}} \quad . \qquad (1.32)$$

These expressions are valid for regions behind the beam and inside the pipe. Again, the field vanishes in front of the beam. Note that the beam dimension a does not appear explicitly in the fields, indicating that for a given m-th moment of the beam the wake field is independent of the detailed shape of the beam distribution. See Fig. 4.

According to (1.32), the longitudinal field components E_z and B_z behaves like $|z-ct|^{-3/2}$, just like the m = 0 case as described by

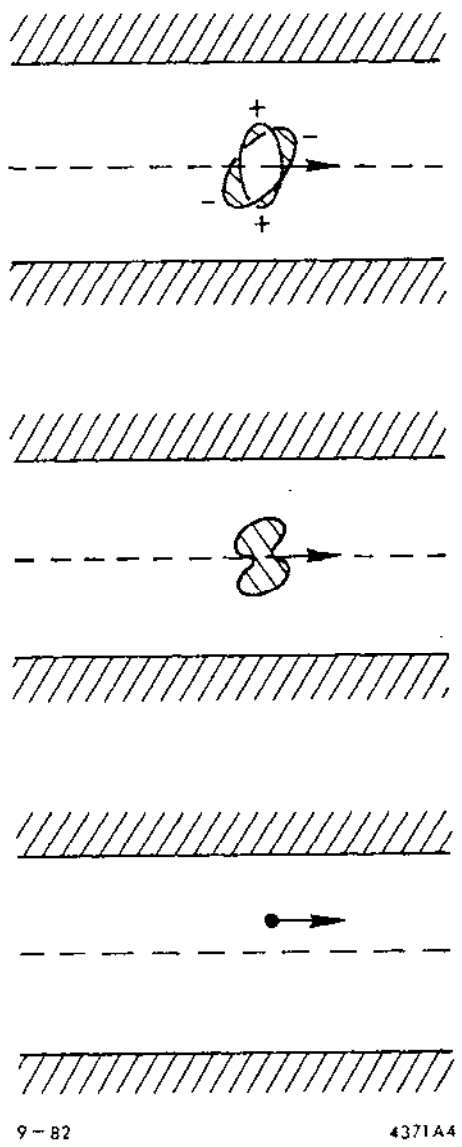

Fig. 4. The wake field is independent of the detailed beam distribution. The same wake field is generated as long as the beam has the same m-th moment. Cases shown are for m = 2.

Eq. (1.17). On the other hand, the transverse field components behave very differently from the m = 0 case. For example, the transverse electric field and magnetic field are comparable at distances $|z-ct| \lesssim b$ behind the beam, but the magnetic field, having a long $|z-ct|^{-1/2}$ tail, dominates at distances $|z-ct| \gtrsim b$. An alternative derivation of some of these results can be found in Ref. 8.

Problem 2. Follow procedure similar to that in Section 1.2 to compute the electromagnetic field components in the short range $z \ll \chi^{1/3}b$ for the case $m \geq 1$. This result will supplement the expressions (1.32). Show that the longitudinal electric field E_z switches sign in the region $0 < z \lesssim \chi^{1/3}b$.

1.4. Wake Functions

In Fig. 2, we showed cases for which a beam with multipole moment can excite a pattern of an electromagnetic wake field that, in general, contains both longitudinal and transverse components. Consider now a test charge e trailing behind the cos mθ-ring-beam in an environment shown in Fig. 2(a) or 2(b). The test charge experiences an electromagnetic wake force. The vacuum chamber pipe is considered to be cylindrically symmetric.

We assume that both the beam and the trailing test charge move with the speed of light c. The wake force pattern generated by the beam then also moves with a phase velocity equal to c.

We will average the wake force over the wall periods [e.g., over the separation d in Fig. 2(a)] so that the fast varying part of the wake force associated with the pipe structure periods is smoothed out. The wake force experienced by the test charge then depends only on r, θ and Z, where we use the upper case Z to designate the longitudinal separation between the test charge and the beam, i.e., $Z = -(z-ct)$. The assumption that the wake force has the translational symmetry (i.e., depends only on Z and not on t and z separately) presupposes that the vacuum chamber pipe has open ends and that the beam has been in the pipe since $t = -\infty$.

The Lorentz force $\vec{F} = e(\vec{E} + \hat{z} \times \vec{B})$ has the longitudinal component $F_\parallel = F_z = eE_z$ and the transverse component $\vec{F}_\perp = F_\theta\hat{\theta} + F_r\hat{r}$, where

$$\begin{aligned} F_\theta &= e(E_\theta + B_r) \\ F_r &= e(E_r - B_\theta) \end{aligned} \tag{1.33}$$

The wake force seen by the test charge e for the resistive wall case is given by, using Eq. (1.32)

$$\begin{aligned} F_\parallel &= \frac{eI_m}{\pi b^{2m+1} p_m} \sqrt{\frac{c}{\sigma}}\, r^m \cos m\theta\, Z^{-3/2} \\ \vec{F}_\perp &= \frac{2e\, I_m}{\pi b^{2m+1} p_m} \sqrt{\frac{c}{\sigma}}\, m r^{m-1} Z^{-1/2} (\hat{r} \cos m\theta - \hat{\theta} \sin m\theta) \end{aligned} \tag{1.34}$$

where

$$p_m = \begin{cases} 2 & \text{if} \quad m = 0 \\ 1 & \text{if} \quad m \geq 1 \end{cases}$$

This expression also gives the correct answer for $m = 0$ if we set $I_0 = q$ [see Eq. (1.17)].

It is interesting to observe that the transverse force comes solely from the $Z^{-1/2}$ term of the magnetic field. What happens is that the image current penetrates into the metal wall and, as it slowly resurfaces, drives the $Z^{-1/2}$ tail of the magnetic field. The same thing does not occur to the electric field because the image charges stay on the wall surface without penetration into the metal.

There actually exists a general form of the wake force once it is averaged over the structure period; Eq. (1.34) is only a special case of it for a resistive wall boundary. To obtain the general form, the Maxwell equations (1.5) are linearly combined into four equations for the quantities F_z, F_r, F_θ and eB_z. The result is, surprisingly, rather simple:

$$\begin{aligned} -\frac{e}{r}\frac{\partial}{\partial\theta}B_z &= \frac{\partial}{\partial z}F_r = \frac{\partial}{\partial r}F_z \\ e\frac{\partial}{\partial r}B_z &= \frac{\partial}{\partial z}F_\theta = \frac{1}{r}\frac{\partial}{\partial\theta}F_z \end{aligned} \tag{1.35}$$

In deriving (1.35), we have used the fact that, in the region $r < b$, the source terms satisfy $j_z = j_\theta = 0$ and $j_z = c\rho$, and that all quantities depend on z and t only as functions of $Z \equiv ct - z$. Equation (1.35) is especially interesting since it does not contain source terms explicitly, neither does it depend on the boundary conditions.

Recalling that F_z and F_r are proportional to cos $m\theta$ while B_z and F_θ are proportional to sin $m\theta$, Eq. (1.35) can easily be solved. We find as a result

$$\begin{aligned} \vec{F}_\perp &= eI_m W_m(Z)\, mr^{m-1} (\hat{r} \cos m\theta - \hat{\theta} \sin m\theta) \\ F_z &= - eI_m W'_m(Z)\, r^m \cos m\theta \\ eB_z &= eI_m W'_m(Z)\, r^m \sin m\theta \end{aligned} \qquad (1.36)$$

where W_m is a function of Z satisfying causality, W'_m is the derivative of W_m. The $m = 0$ case is included provided we set $I_0 = q$.

The explicit form of W_m, of course, can only be determined after imposing the boundary conditions as was done for the resistive wall. It is interesting, however, to note that all the explicit r, θ and Z dependencies in (1.36) are derived without referring to the boundary conditions at all, except that the boundary is infinitely periodic and has cylindrical symmetry. The property (1.36) applies to the force components and not necessarily to the EM field components.

The result (1.36) can be combined to say that, with z-ct dependencies, the transverse gradient of the longitudinal force is equal to the longitudinal gradient of the transverse force, i.e.,

$$\nabla_\perp F_z = \frac{\partial}{\partial Z} \vec{F}_\perp \quad . \qquad (1.37)$$

This expression is sometimes referred to as the Panofsky-Wenzel theorem,[7,9] although the original form of the theorem looks rather different.

The function $W_m(Z)$ in Eq. (1.36) is called the wake function; it describes the shock response of the vacuum chamber environment to a δ-function beam. Mathematically W_m is equivalent to a Green's function. Sometimes it may be more convenient to call $W_m(Z)$ the transverse wake function and $W'_m(Z)$ the longitudinal wake function for reasons that should be obvious from Eq. (1.36). The dimensionality of W_m is L^{-2m-1} in the cgs units.

For the special case of a resistive wall, the wake function is

$$W_m(Z) = \frac{2}{\pi b^{2m+1} p_m} \sqrt{\frac{c}{\sigma}}\, Z^{-1/2} \quad . \tag{1.38}$$

The range of validity of (1.38) is $b/\chi \gg Z \gg \chi^{1/3} b$, where χ is the small parameter defined in (1.11).

Immediately following the beam, we expect to see a longitudinal electric field that retards the beam regardless of vacuum chamber properties. This means the quantity $j_z F_z$ must be negative definite, which implies

$$W'_m(Z) > 0 \quad \text{for} \quad Z \to 0^+ \quad . \tag{1.39}$$

It follows that the longitudinal wake $W'_m(Z)$ of a resistive wall must switch sign in the range between $Z = 0$ and $Z \approx \chi^{1/3} b$ since W'_m obtained from (1.38) is negative. This result was considered in Problem 2.

Another consequence of (1.39) is that the transverse wake function W_m rises monotonically with Z, starting from $W_m = 0$ at $Z = 0^-$, after the

point charge beam. If W'_m does not diverge at Z = 0 faster than 1/Z, then $W_m(0) = 0$. It follows that a particle does not experience a deflection due to its own transverse wake. This is in contrast to the longitudinal dimension in which a particle does see its own retarding wake field. In other words, the longitudinal wake is cosine-like and the transverse wake is sine-like. See Fig. 5.

We now define a Cartesian coordinate system with $x = r \cos\theta$ and $y = r \sin\theta$, and orient the charge density in the x-y system with an angle θ_0 [i.e., in the expression (1.3) for ρ, $\cos m\theta$ is replaced by $\cos m(\theta-\theta_0)$]. In this Cartesian system, the beam now has two components of m-th moments -- one normal and another skewed. Table II lists the two moments (first the normal moment and then the skewed moment) and the associated wake forces. A bracket $\langle\ \rangle$ means averaging over the transverse distribution of the beam; $\hat{x}$ and $\hat{y}$ are the unit vectors in the x and y directions. The wake forces are those seen by a test charge e with transverse coordinates x, y and follows the beam at a distance Z behind.

The transverse wake force for m = 1 listed in Table II behaves like the bending force seen in a horizontal or vertical dipole magnet. Similarly, the wakes act like quadrupole and skew quadrupole magnets for m = 2, sextupole and skew sextupole magnets for m = 3, etc. The m = 0 case does not have a transverse wake force because the longitudinal wake does not have a transverse gradient.

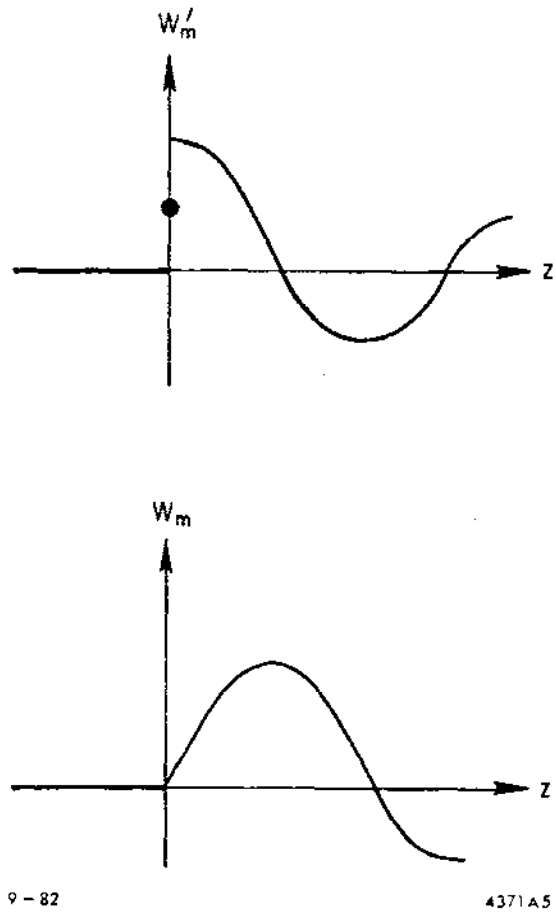

Fig. 5. Sketches of the longitudinal wake function $W'_m(z)$ and the transverse wake function $W_m(z)$.

TABLE II

m	Distribution Moments of Beam	Longitudinal Wake Force	Transverse Wake Force
0	q	$-eq\, W'_0(Z)$	0
1	$q\langle x\rangle$	$-eq\langle x\rangle\, x\, W'_1(Z)$	$eq\langle x\rangle\, W_1(Z)\, \hat{x}$
	$q\langle y\rangle$	$-eq\langle y\rangle\, y\, W'_1(Z)$	$eq\langle y\rangle\, W_1(Z)\, \hat{y}$
2	$q\langle x^2-y^2\rangle$	$-eq\langle x^2-y^2\rangle\, (x^2-y^2)\, W'_2(Z)$	$2eq\langle x^2-y^2\rangle\, W_2(Z)\, (x\hat{x}-y\hat{y})$
	$q\langle 2xy\rangle$	$-eq\langle 2xy\rangle\, 2xy\, W'_2(Z)$	$2eq\langle 2xy\rangle\, W_2(Z)\, (y\hat{x}+x\hat{y})$
3	$q\langle x^3-3xy^2\rangle$	$-eq\langle x^3-3xy^2\rangle(x^3-3xy^2)W'_3(Z)$	$3eq\langle x^3-3xy^2\rangle\, W_3(Z)\cdot[(x^2-y^2)\hat{x}-2xy\hat{y}]$
	$q\langle 3x^2y-y^3\rangle$	$-eq\langle 3x^2y-y^3\rangle(3x^2y-y^3)W'_3(Z)$	$3eq\langle 3x^2y-y^3\rangle\, W_3(Z)\cdot[2xy\hat{x}+(x^2-y^2)\hat{y}]$

One can also say something about the polarity of these transverse wake forces using Table II. To do that, imagine a short beam travelling down the accelerator with a displacement in x. The head of the beam bunch will generate a wake force that kicks the particles in the tail further away from the accelerator axis since $W_1(Z) > 0$ if Z is short enough. Similarly, if the beam has an elliptical shape in its transverse distribution and thus possesses a quadrupole moment, the transverse wake force is such that it tends to elongate the ellipse further in the bunch tail. In general, one finds that the polarity of the transverse wake forces is such that it always hurts a short beam. See Fig. 6.

As Z increases, W'_m and W_m may change signs and the wake forces become beneficial. In particular, W'_0 may become negative at some finite distance behind the head of the beam. Therefore, if one injects two beam bunches into the accelerator and if the separation of the two bunches are chosen strategically, the trailing bunch will be <u>accelerated</u> by the wake field of the leading bunch. This mechanism is an important means of accelerating particles.[10-12] (In some sense, one special case of wake field accelerators is the klystrons, which have already been widely used to accelerate particles. The difference is that, for klystrons, the wake fields are generated in a special-purpose vacuum chamber, optimized by various means and then sent by waveguides to accelerate the trailing beam. The new generation of wake field accelerators and the klystrons of course have different regions of applicability.)

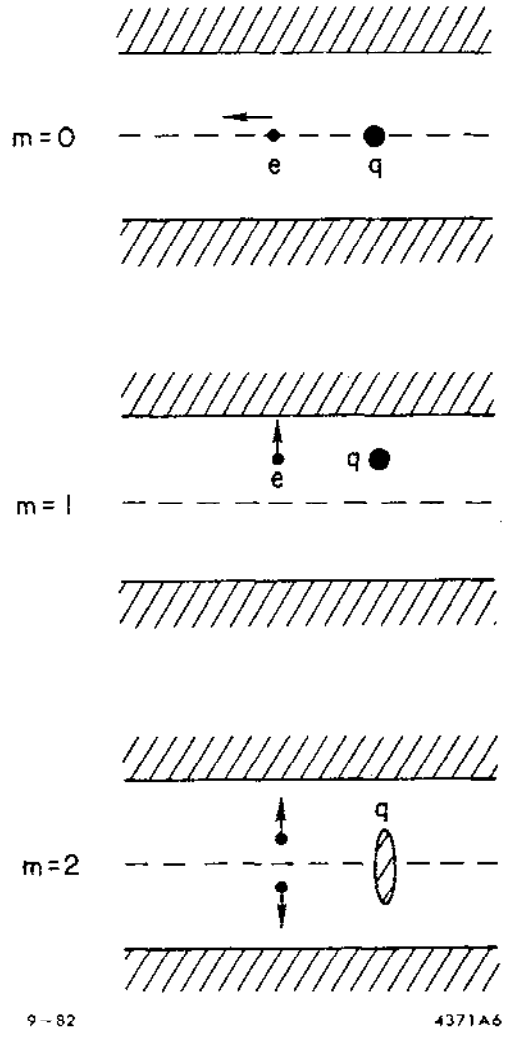

Fig. 6. The polarity of the wake field always hurts a short beam. For m = 0, the longitudinal wake force is retarding. For m = 1, the transverse wake force further deflects the test charge e. For m = 2 the tail portion of an elliptical beam becomes further elongated. Arrows represent the wake force.

There are several interesting properties of the wake functions. One has been listed in Eq. (1.39). Some of these properties for the longitudinal wake function $W'_m(Z)$ are given in Problem 3 below. Here let us show how property (c) can be reached; other properties can be shown similarly. Consider a point charge q followed by another point charge q at a distance Z behind. The first q loses energy at a rate $(q^2/2)W'_0(0)$ due to the wake generated by itself [see Eq. (1.22)]. The trailing q loses energy at a rate $(q^2/2)W'_0(0) + q^2W'_0(Z)$, where the second term is due to the wake left by the leading charge. Physically, the two-charge system can never gain energy; this means $W'_0(Z) \geq -W'_0(0)$ for any Z. Similarly, if the second charge is -q rather than q, one proves $W'_0(Z) \leq W'_0(0)$. Property (c) of Problem 3 is thus proved for m = 0.

Problem 3. Show that the longitudinal wake function $W'_m(Z)$ is unphysical unless the following properties are satisfied:

(a) $W'_m(Z) = 0$ if $Z < 0$.

(b) $W'_m(0) \geq 0$.

(c) $W'_m(0) \geq |W'_m(Z)|$ for all Z.

(d) If $W'_m(\alpha) = W'_m(0)$ for some α, then $W'_m(Z)$ is periodic with period α, i.e., $W'_m(Z+\alpha) = W'_m(Z)$ for $Z \geq 0$.

(e) If $W'_m(\alpha) = - W'_m(0)$ for some α, then $W'_m(Z+\alpha) = - W'_m(Z)$.

(f) $\int_0^\infty W'_m(Z)\, dZ \geq 0$.

(g) $1 \geq [W'_m(Z_1)\, W'_m(Z_2)\, W'_m(Z_1+Z_2)]/[W'_m(0)]^3 \geq -1/8$

for any Z_1, Z_2.

Use these results to show that the wake functions sketched in Fig. 7 are unphysical.

In the previous two sections, we worked out in some detail the case of a resistive wall. The reason for using the resistive wall as an example is that it can be handled with relative ease and yet it does contain most of the important features of a general wake. In reality, the resistive wall wake contributes very little to the wake fields found in an accelerator. Most of the wake field comes from effects associated with discontinuities in the vacuum chamber pipe [see Fig. 2(a)].

The computation of wake functions analytically for a non-smooth pipe is rather involved. Here we are forced to make drastic approximations. For example, one may represent the pipe structure by a series of closed pill-boxes,[13-15] or to take a perturbative approach which is valid when the pipe wall is only slightly varied from that of a smooth pipe.[16-18] Indeed, the most realistic approach, it seems, is to seek the help of the almighty computer.[19-24]

In Fig. 8 we show the results obtained by Bane, Wilson and Zotter[7,22] for the SLAC linac. Their wake functions W'_0, W_1 and W_2 are plotted using our language and units. For comparison, we also show the resistive wall wakes in Fig. 9 assuming an aluminum pipe. The wakes in Fig. 8 oscillate as functions of z, indicating the electromagnetic wake field "rings" after being excited. The ringing wave length is comparable to the cavity structure dimensions.

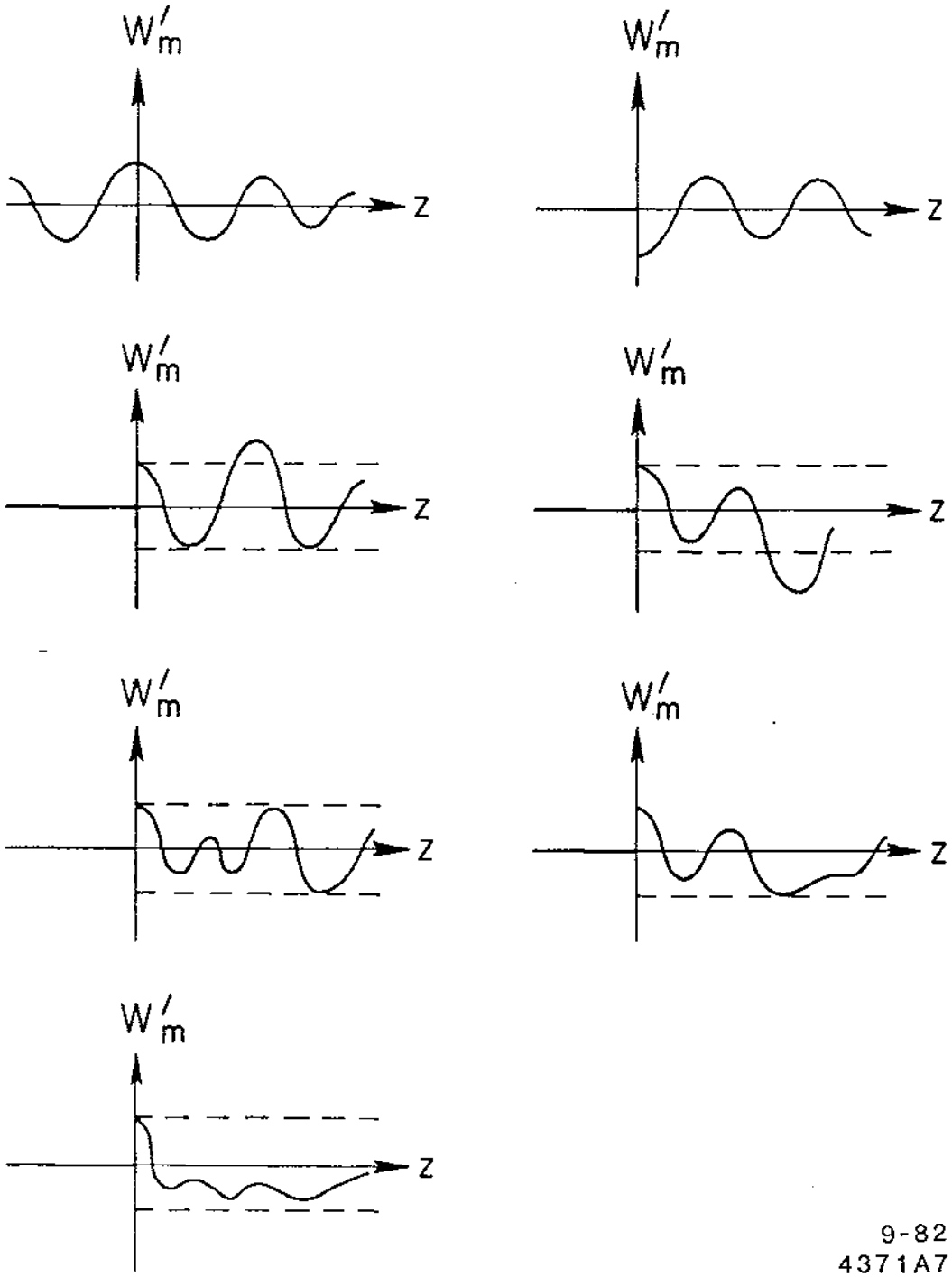

Fig. 7. Sketches of some unphysical wake functions $W'_m(Z)$.

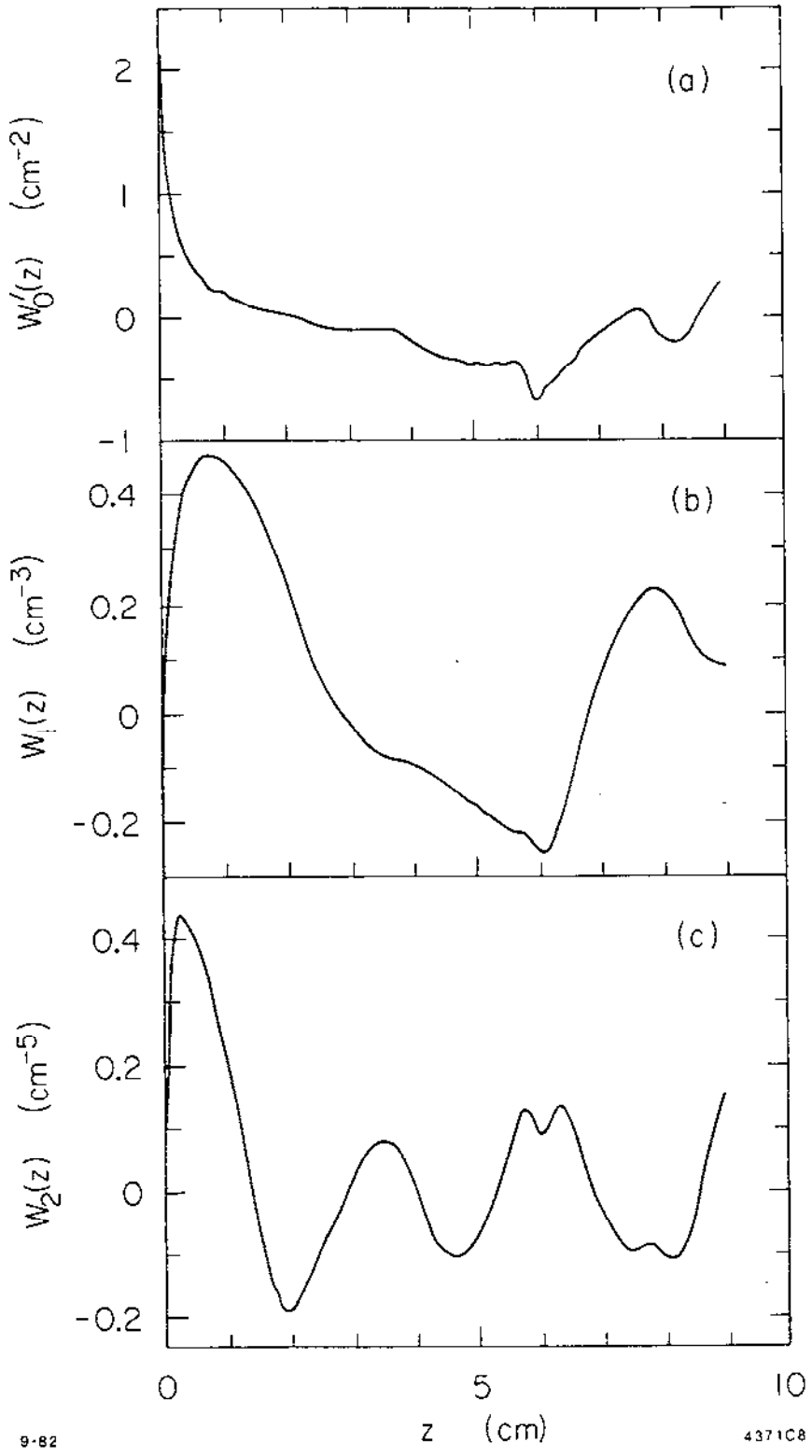

Fig. 8. Wake functions W'_0, W_1 and W_2 for the SLAC linac.

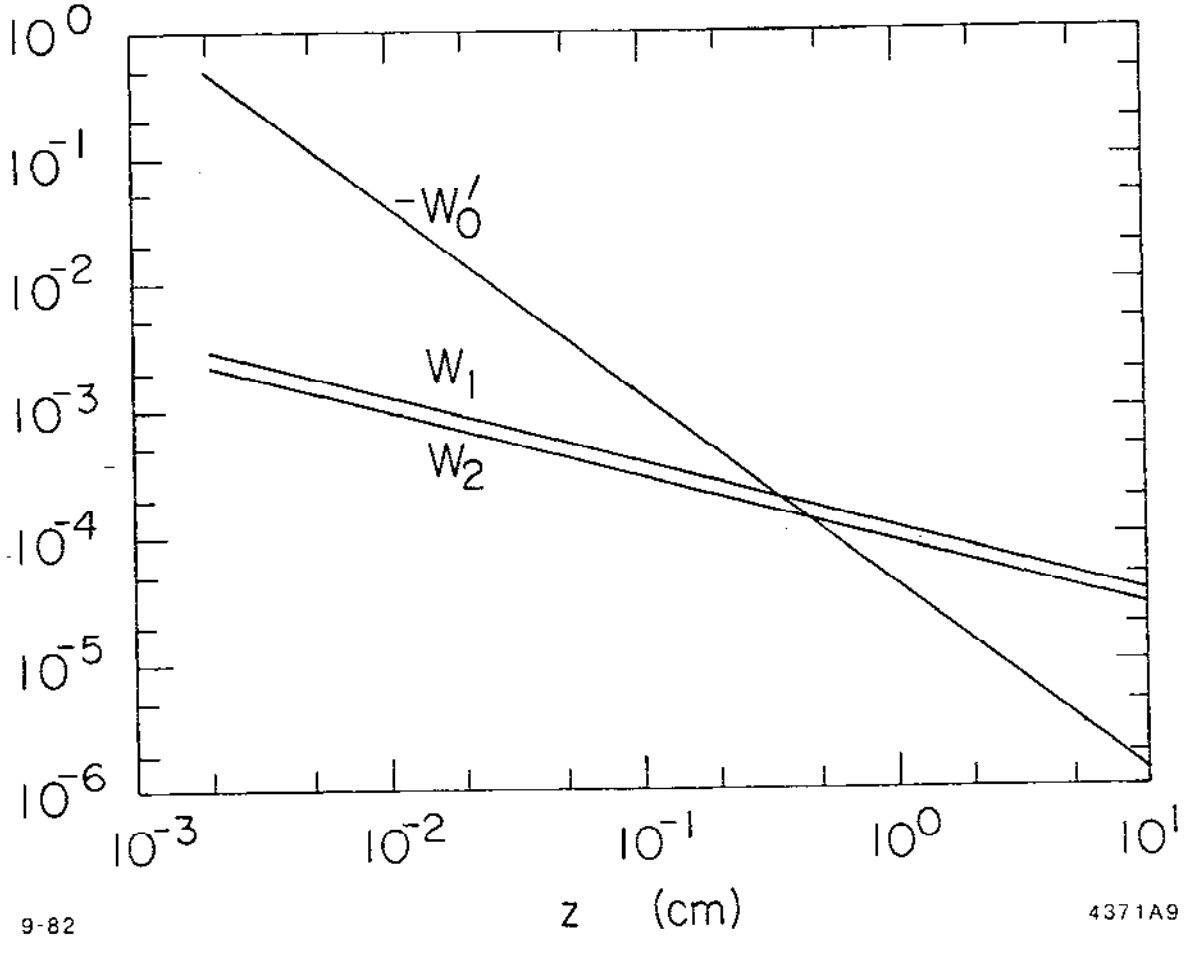

Fig. 9. The resistive wall wakes W'_0, W_1 and W_2. These curves are not to be extrapolated into the region $Z \leq 0.002$ cm. The pipe radius b is chosen to be 1.163 cm in order to compare with Fig. 8. The units for W'_0, W_1 and W_2 are cm^{-2}, cm^{-3} and cm^{-5}, respectively.

1.5. Impedance

So far the wake fields have been introduced as a function of time after the δ-function beam has passed by. It is often useful to examine the frequency content of the wake field by making a Fourier transform on it. One indication of the usefulness of this procedure is the fact that we introduced the Fourier transformed quantities $\tilde{E}$ and $\tilde{B}$ when we worked out the resistive wall. Another perhaps more important reason for its usefulness is that the wake response often contains a number (say, 20) of sharply defined frequencies. Such a situation does not occur for a resistive wall wake but does occur if the wake is generated by a cavity pipe structure. The Fourier transform of the wake function is called the impedance.

Needless to say, the descriptions of the wake force in terms of wake functions in the time domain and in terms of impedances in the frequency domain are exactly identical. It is only a matter of taste as to which view to take. For many later developments, we find it convenient to use the time domain description to set up the equations of motion ($F = ma$) and then use the Fourier transform techniques to solve those equations once they are written down.

So far we have considered δ-function beams. Wakes produced by other beam distributions can be constructed using the δ-function result. For example, consider a beam that has a current

$$I_0(z,t) = \hat{I}_0 \, e^{ikz - i\omega t} \quad . \tag{1.40}$$

Only the real part of (1.40) is meaningful. The m = 0 wake at position z is a superposition of the wakes produced by all charges in the beam that passed by position z at previous times, i.e.,

$$E_z(z,t) = -\frac{1}{c}\int_0^{\infty} dz'\, I_0[z,t-(z'/c)]\, W'_0(z') \qquad (1.41)$$

which is equal to

$$-\frac{1}{c} I_0(z,t) \int_{-\infty}^{\infty} dz'\, e^{i\omega z'/c}\, W'_0(z') \quad .$$

The lower limit of integration has been replaced by $-\infty$ since $W'_0 = 0$ for $z' < 0$. We have used the fact that the wake field is insensitive to the cross sectional area of the beam so we can integrate J_z over the cross section to obtain I_0.

Let the accelerator section that contains the wake field be of length L. One can define a retarding voltage across the section due to the wake field by $V(z,t) = -E_z(z,t)L$, we then have the expression

$$V(z,t) = -I_0(z,t)\cdot Z_0''(\omega) \qquad (1.42)$$

where the quantity $Z_0''(\omega)$ is called the longitudinal impedance for the m = 0 mode at frequency ω; it is related to the wake function through a Fourier transformation:

$$Z_0''(\omega)/L = \int_{-\infty}^{\infty} \frac{dz'}{c}\, e^{i\omega z'/c}\, W'_0(z') \qquad (1.43)$$

and it describes the frequency content of the longitudinal wake W'_0. Instead of Eqs. (1.40) to (1.42), an alternative view is to simply take Eq. (1.43) as the definition of the impedance.

Similarly, if the beam current possesses a multipole moment

$$I_m(z,t) = \hat{I}_m e^{ikz-i\omega t} \quad , \tag{1.44}$$

one can define the relationship $V = -E_z L = -I_m Z_m'' r^m \cos m\theta$ through a longitudinal impedance per unit length

$$Z_m''(\omega)/L = \int_{-\infty}^{\infty} \frac{dz'}{c} e^{i\omega z'/c} W'_m(z') \quad . \tag{1.45}$$

For the beam (1.44), one can further write the transverse force according to

$$\vec{F}_\perp(z,r,\theta,t) = ie\, I_m(z,t)\, m r^{m-1} (\hat{r}\cos m\theta - \hat{\theta}\sin m\theta)\, Z_m^\perp(\omega) \tag{1.46}$$

where $Z_m^\perp(\omega)$ is the transverse impedance given by

$$Z_m^\perp(\omega)/L = \frac{1}{i} \int_{-\infty}^{\infty} \frac{dz'}{c} e^{i\omega z'/c} W_m(z') \quad . \tag{1.47}$$

In the cgs system, the dimensionality is TL^{-2m-1} for the longitudinal impedance Z_m'' and TL^{-2m} for the transverse impedance $Z_m^\perp$. Sometimes it is more convenient to express the impedances using ohm as unit; for that one can use the conversion factor that 1 ohm = 1.11×10^{-12} sec/cm.

Note that a minus sign is included in Eq. (1.42) for the reason that the voltage tends to be retarding, i.e., 180^0 out of phase with the beam current. Similarly, we have included a factor i in Eqs. (1.46) and (1.47) since the transverse force tends to be 90^0 out of phase with the beam current. These factors are included for convention only.

Inverting the Fourier transforms (1.45) and (1.47) allows us to construct the wake functions from the impedances:

$$W'_m(z) = \frac{1}{2\pi}\int_{-\infty}^{\infty} d\omega\, e^{-i\omega z/c}\, Z_m''(\omega)/L$$
$$W_m(z) = \frac{1}{2\pi}\int_{-\infty}^{\infty} d\omega\, e^{-i\omega z/c}\, iZ_m^{\perp}(\omega)/L \qquad (1.48)$$

Equation (1.37), which relates the longitudinal wake to the derivative of the transverse wake also gives a relationship between the longitudinal and transverse impedances for a given m:

$$Z_m''(\omega) = \frac{\omega}{c} Z_m^{\perp}(\omega) \quad . \qquad (1.49)$$

For a resistive wall, the impedance that corresponds to the wake (1.38) is

$$Z_m''(\omega)/L = \frac{\omega}{c} Z_m^{\perp}(\omega)/L$$
$$= \sqrt{\frac{2}{\pi\sigma}}\,\frac{1}{p_m\, b^{2m+1}\, c}\,|\omega|^{1/2}\,[1 - \mathrm{sgn}(\omega)i] \quad . \qquad (1.50)$$

As we mentioned before, in reality the resistive wall constitutes only a small part of the total impedance in an accelerator. In the SLAC linac, for example, the impedance per cavity corresponding to the wake W'_0 shown in Fig. 8 is plotted in Fig. 10.

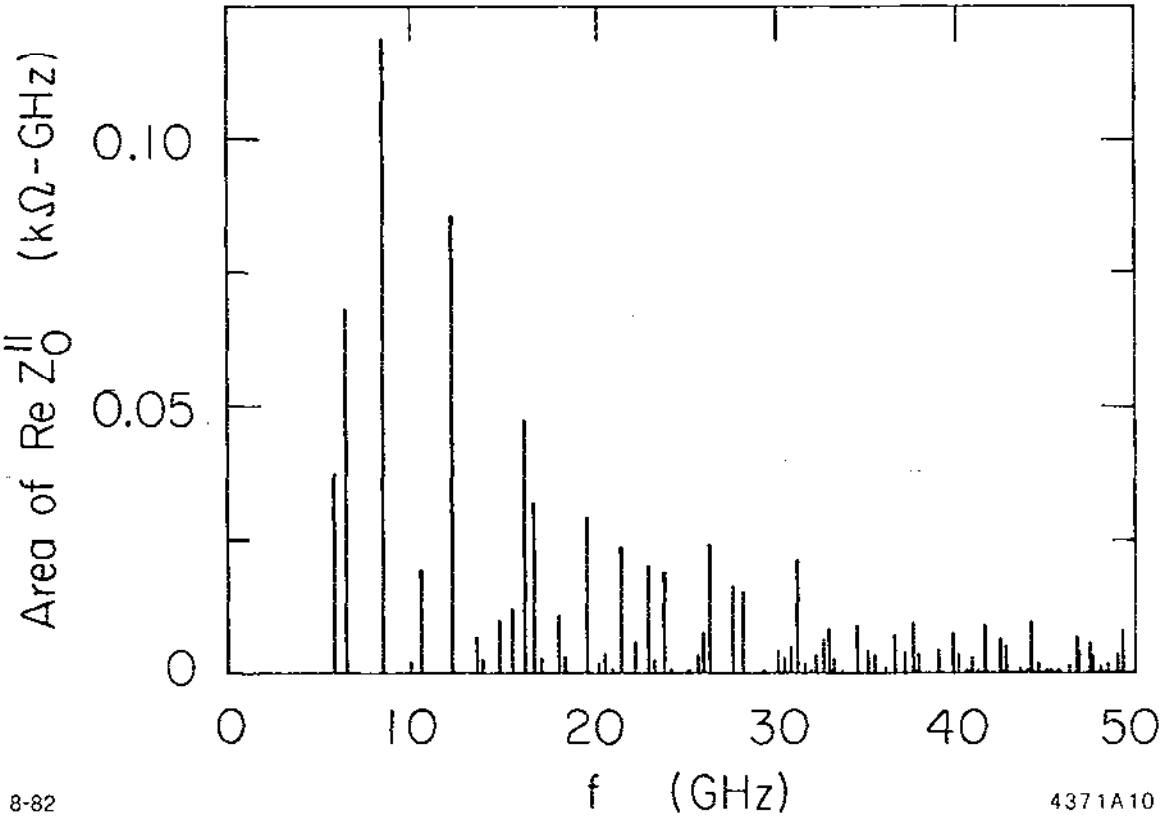

Fig. 10. Real part of the longitudinal impedance (m = 0) for the SLAC linac versus frequency $f = \omega/2\pi$, up to f = 50 GHz. The impedance consists of a large number of δ-function spikes. The height of each spike represents the area under the δ-function. The spike corresponding to the fundamental accelerating frequency at 2.84 GHz is not plotted.

The impedance shown in Fig. 10 consists of a large number of δ-function spikes, each corresponding to a mode of wake field that can be excited in the SLAC linac structure and all these wake field modes have m = 0. Note that it is only the real part of the impedance that contains δ-function spikes. The imaginary part is a continuum; for each δ-function peak of Re Z located at ω_R, there is an imaginary part Im Z that has a long $(\omega - \omega_R)^{-1}$ tail around it. See problem 4(d) and Eq. (1.53) later.

The fact that the impedance consists strictly of δ-functions is due to the assumptions that the vacuum chamber wall is infinitely conducting and that the cavity structure is infinitely periodic. In case there is only a small number of cavity structures in the entire pipe, the impedance actually looks like that sketched in Fig. 11. For modes whose frequencies are below a certain cut-off frequency ~c/b, where b is the pipe radius, the wake fields are trapped by the cavity and ring in the cavity after the beam has left. The widths of these modes are determined by the resistance on the cavity wall and are described by $\Delta\omega/\omega \approx 1/2Q$ where Q is the quality factor, typically of the order of 10^4. Above the frequency c/b, the wake field leaks out of the cavity and propagates in the pipe. The impedance in this region forms a continuum. Roughly, one can obtain this part of impedance from that of Fig. 10 by spreading each impedance peak into a width of $\Delta\omega/\omega \sim 1/N$, where N is the number of cavities in series. For this reason, the impedances are often either sharply peaked (below cut-off) or "broad-banded" (above cut-off) and not too often in between. The corresponding wakes either ring for a long time or decay quickly after being excited.

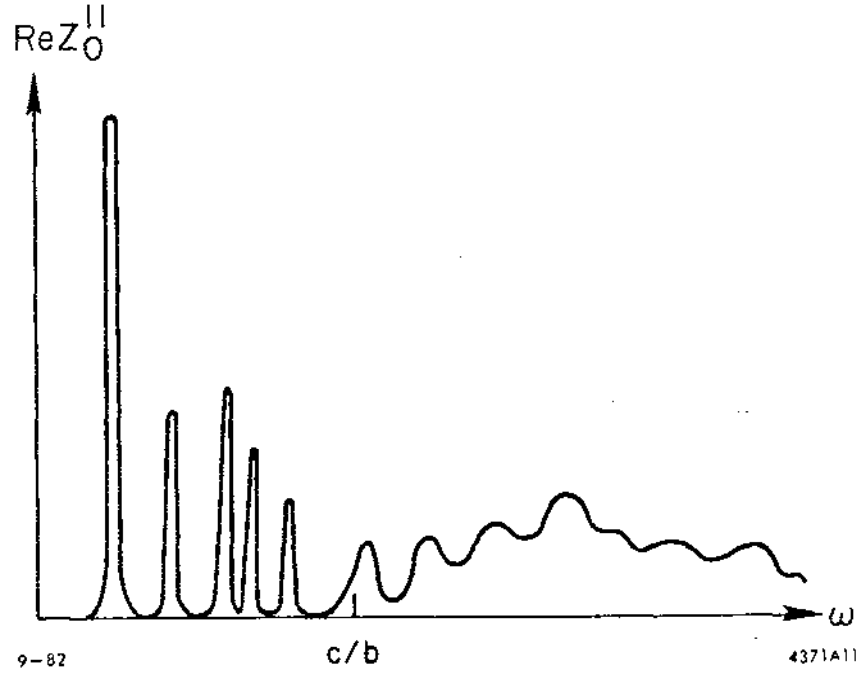

Fig. 11. Sketch of the real part of the impedance for a small number of cavities in series.

In addition to (1.49) there are a few other properties of impedances that we will now describe:

(i) Since the wake functions are real, Eqs. (1.45) and (1.47) imply

$$\begin{aligned} Z_m^{\parallel *}(\omega) &= Z_m^{\parallel}(-\omega) \\ Z_m^{\perp *}(\omega) &= -Z_m^{\perp}(-\omega) \end{aligned} \tag{1.51}$$

i.e., Re $Z_m^{\parallel}$ and Im $Z_m^{\perp}$ are even functions of ω while Im $Z_m^{\parallel}$ and Re $Z_m^{\perp}$ are odd functions.

(ii) The fact that the transverse wake satisfies $W_m(0) = 0$ gives

$$\begin{aligned} &\int_0^{\infty} d\omega \ \mathrm{Im}\, Z_m^{\perp}(\omega) = 0 \\ &\int_0^{\infty} d\omega \ \frac{\mathrm{Im}\, Z_m^{\parallel}(\omega)}{\omega} = 0 \quad . \end{aligned} \tag{1.52}$$

(iii) The real and the imaginary parts of $Z_m^{\parallel}(\omega)$ must be related to each other in such a way that they, together, guarantees the causality of the wake functions. The relationship is given by the Hilbert transforms:[25]

$$\begin{aligned} \mathrm{Re}\, Z_m^{\parallel}(\omega) &= \frac{1}{\pi} \mathrm{P.V.} \int_{-\infty}^{\infty} d\omega' \ \frac{\mathrm{Im}\, Z_m^{\parallel}(\omega')}{\omega' - \omega} \\ \mathrm{Im}\, Z_m^{\parallel}(\omega) &= -\frac{1}{\pi} \mathrm{P.V.} \int_{-\infty}^{\infty} d\omega' \ \frac{\mathrm{Re}\, Z_m^{\parallel}(\omega')}{\omega' - \omega} \end{aligned} \tag{1.53}$$

where P.V. means taking the principal value.* The same expressions apply to $Z_m^{\perp}$. The proof of (1.53) can be found in Ref. 25.

The point of (1.53) is that, at least in principle, knowing either the real or the imaginary part of the impedance, one can construct the whole impedance as well as the wake function.

Problem 4. (a) Show that the circuit shown in Fig. 12(a) has an impedance

$$Z = \frac{R}{1 + iQ\left(\frac{\omega_R}{\omega} - \frac{\omega}{\omega_R}\right)}$$

where $Q = R\sqrt{C/L}$ is the quality factor and $\omega_R = 1/\sqrt{CL}$ is the resonant frequency. This impedance is drawn in Fig. 12(b). The width of the resonance peak is about $\Delta\omega \approx \omega_R/2Q$ if $Q \gg 1$.

(b) Make a Fourier transform on the impedance to obtain the wake function

$$W(z) = \begin{cases} 0 & \text{if } z < 0 \\ W_0\, e^{-\alpha\tau}\left[\cos\bar{\omega}\tau - \frac{\alpha}{\bar{\omega}}\sin\bar{\omega}\tau\right] & \text{if } z > 0 \end{cases}$$

---

* The integrals (1.53) are undefined without specifying P.V. because of the divergence at $\omega' = \omega$. The trick of P.V. is to utilize the property that the divergences on the side $\omega' < \omega$ and the side $\omega' > \omega$ are of opposite signs and, if the integration is taken in such a way that the divergences on the two sides cancel each other, the integrals can actually be well-defined.

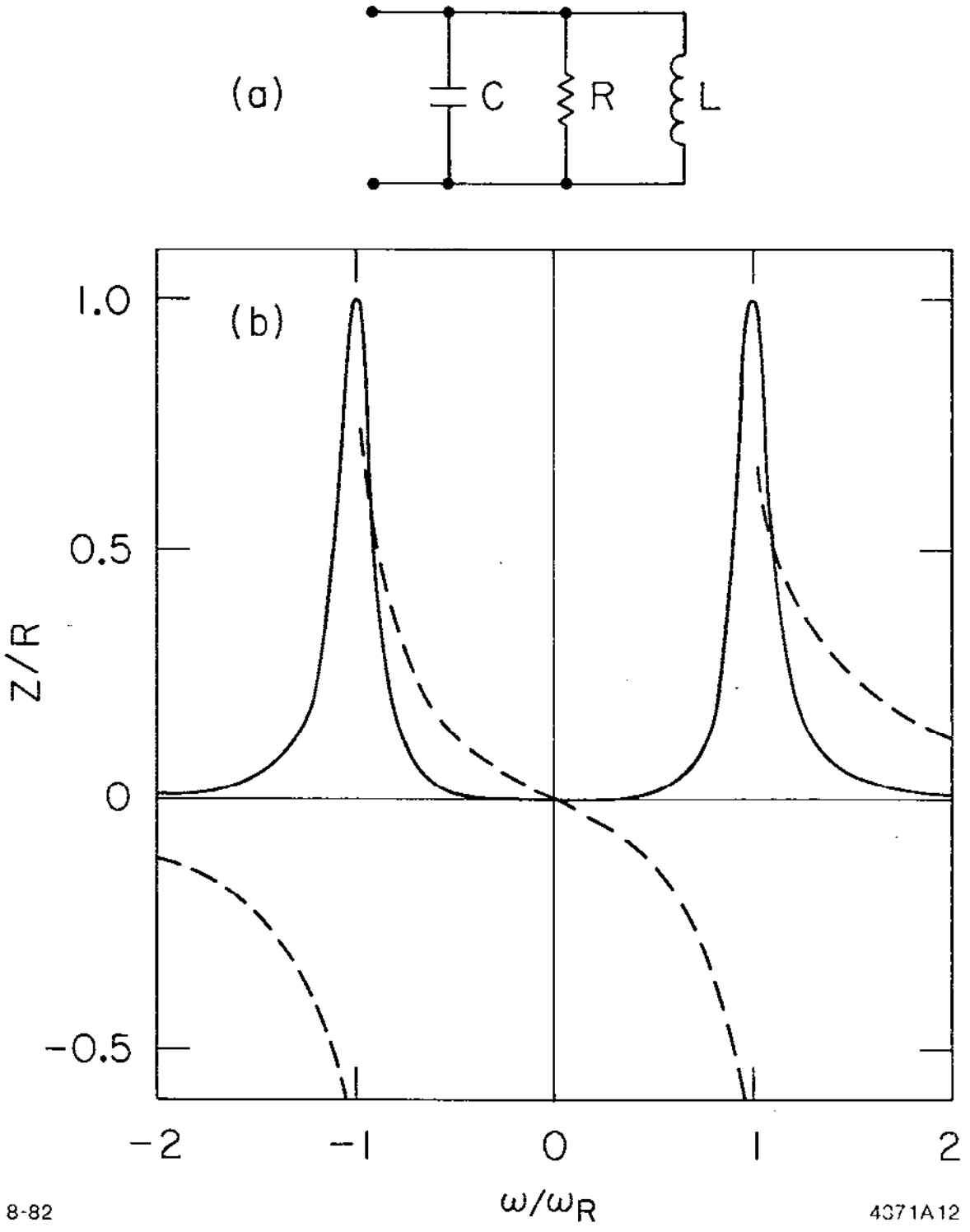

Fig. 12. (a) An LRC circuit. (b) The impedance of the LRC circuit. The solid curve gives the real part and the dashed curve gives the imaginary part of the impedance. The quality factor Q is typically either ~1 for a "broad-band" impedance or ~10^4 for a fine-tuned sharp impedance. We have drawn the case for Q = 5.

where $\tau = z/c$, $\alpha = \omega_R/2Q$, $\tilde{\omega} = \sqrt{\omega_R^2 - \alpha^2}$ and W_0 integrated through the impedance section is equal to $2\alpha R$.

(c) Show that the real and imaginary parts of the impedance satisfy the Hilbert transform relationship (1.53).

(d) Show that in the limit $Q \to \infty$ and $R \to \infty$ while keeping R/Q fixed, the impedance becomes

$$\text{Re } Z = \frac{\pi}{2}\frac{R}{Q}\omega_R \left[\delta(\omega-\omega_R) + \delta(\omega+\omega_R) \right]$$

$$\text{Im } Z = \frac{R\,\omega_R}{2Q}\left[\frac{1}{\omega+\omega_R} + \frac{1}{\omega-\omega_R} \right]$$

The corresponding wake function is $W(z) = W_0\cos(\omega_R z/c)$ for $z > 0$.

(iv) Energy loss consideration gives another general condition on impedance. Consider a beam whose m-th moment has a longitudinal distribution $\rho(z-ct)$. As this beam travels down the pipe, it loses energy at a rate [compare Eq. (1.23)]

$$\frac{d\epsilon}{dt} = c\int_{-\infty}^{\infty} dz\ \rho(z) \int_{z}^{\infty} dz'\ \rho(z')\ W'_m(z'-z) \quad . \tag{1.54}$$

This result can also be written in terms of the Fourier transformed quantities:

$$\frac{d\epsilon}{dt} = 2\pi c^3 \int_{-\infty}^{\infty} d\omega\ |\tilde{\rho}(\omega)|^2\ \text{Re}\ Z_m''(\omega)/L \tag{1.55}$$

where

$$\tilde{\rho}(\omega) = \frac{1}{2\pi}\int_{-\infty}^{\infty}\frac{dz}{c}\, e^{-i\omega z/c}\,\rho(z) \quad . \tag{1.56}$$

Since the beam as a whole can never gain energy from the pipe structure, and this must be valid for arbitrary ρ and $\tilde{\rho}$, we conclude that

$$\text{Re } Z_m''(\omega) \geq 0 \qquad \text{for all } \omega \quad . \tag{1.57}$$

This is the complete condition that is only partially studied in Problem 3. It follows from (1.57) and (1.49) that the real part of the transverse impedance $Z_m^{\perp}$ is positive in the region $\omega > 0$ and negative in the region $\omega < 0$.

(v) The relationship (1.49) holds for a given m. There is no a priori connection between the impedances of different m's. On the other hand, a rough connection between Z_0'' and $Z_1^{\perp}$ can be very useful if one knows Z_0'' and wants to have some idea of $Z_1^{\perp}$. From a simple dimensionality argument, one expects $Z_1'' \sim Z_0''/b^2$ and therefore[26]

$$Z_1^{\perp} \sim \frac{2c}{b^2\omega} Z_0'' \quad , \tag{1.58}$$

where b is a length characterizing the vacuum chamber structure and is most likely given by the radius of the chamber pipe. A factor of two is included so that this expression is strictly valid for the resistive wall case. In general, the relation (1.58) describes only a gross averaged behavior; it applies more or less to frequencies above the cut-off frequency c/b and is not to be confused with the exact relationship (1.49).

1.6. Parasitic Loss

The energy loss (1.54) or (1.55) is referred to as the parasitic energy loss of the beam. It is valid for a beam traversing the impedance once. In a circular accelerator, the situation is somewhat different. As the beam traverses the impedance region, it not only sees the wake field generated in this traversal but also all traversals made in previous revolutions. The energy loss can then be written as (take m = 0)

$$\frac{d\epsilon}{dt} = c \int_{-\infty}^{\infty} dz\, \rho(z) \int_{-\infty}^{\infty} dz'\, \rho(z') \sum_{k=-\infty}^{\infty} W'_0(kC+z'-z) \qquad (1.59)$$

where C is the circumference of the accelerator, k sums over revolutions and we have used the fact that $W'_0(z) = 0$ if $z < 0$.

It is more convenient to express (1.59) in terms of impedance. To do so, we will use the following identity (the Poisson sum formula):

$$\sum_{k=-\infty}^{\infty} F(kC) = \frac{2\pi}{C} \sum_{p=-\infty}^{\infty} \tilde{F}(2\pi p/C) \qquad (1.60)$$

where $F(z)$, $\tilde{F}(k)$ are arbitrary Fourier transform pairs. In other words, summing a function at a regular interval C is equal to summing over its Fourier transform at the regular intervals $2\pi/C$. Using (1.60), the summation over W'_0 in (1.59) becomes a summation over the impedance Z_0''.

Problem 5. Prove (1.60). As a special case show

$$\sum_{k=-\infty}^{\infty} e^{-ikx} = 2\pi \sum_{p=-\infty}^{\infty} \delta(x + 2\pi p) \quad .$$

Let the total impedance in a circular accelerator be Z_0''. The energy loss of a beam per revolution then becomes

$$U_{\substack{\text{parasitic} \\ \text{loss}}} = 2\pi c^2 \omega_0 \sum_{p=-\infty}^{\infty} |\tilde{\rho}(p\omega_0)|^2 \, \text{Re}\, Z_0''(p\omega_0) \qquad (1.61)$$

where $\omega_0 = 2\pi c/C$ is the revolution frequency. Here we see one example of the usefulness of the impedance concept; Eq. (1.61) contains a summation, while Eq. (1.59) involves a summation and a double integral.

The parasitic energy lost by the beam goes into the wake fields. Under unfavorable conditions, this energy stored in the wake fields will be transferred systematically back to beam motion, causing beam instabilities. This is the subject to which we will devote the rest of these lectures. The parasitic energy loss, of course, will have to be supplied back to the beam by an rf accelerating voltage.

II. ONE-PARTICLE AND TWO-PARTICLE MODELS

In Section I, we studied the wake fields generated by a beam in an accelerator environment. We assumed that the particle distribution within the beam is rigid and that the beam is unperturbed by the wake fields in its motion other than the parasitic energy losses. In this Section II, we will study the effect of the wake fields acting back upon the beam, except that the beam is allowed only to have center of charge motions and not internal motions. For this purpose, the beam will be represented simply as a point charge -- a single macroparticle without internal structure. A few of these one-particle models, leading to longitudinal and transverse beam instabilities, will be studied.

The advantage of introducing the one-particle models is obvious; it offers an intuitive picture of some of the instability mechanisms. In fact this simplified description is so beneficial that we will extend it and introduce a two-particle picture, in which the beam is represented as two macroparticles interacting with each other through the wake fields. This picture offers the opportunity of looking into the instability mechanisms associated with the internal degrees of freedom in the beam distribution. A few of these two-particle models will be included in this section. A full account of the internal beam motions will be postponed until Section III, where most of the results obtained in Section II will be rederived systematically.

The seven one-particle and two-particle models included in Sections 2.1 to 2.7 are not meant to be exhaustive. A two-particle model for the longitudinal instability, for instance, is missing from our list. Hopefully, the reader will venture along these lines to make a more complete list.

2.1. Robinson Instability

The rf accelerating cavities in a circular accelerator are tuned so that the fundamental mode* has its resonant frequency ω_R very close to an integral multiple of the revolution frequency ω_0 of the beam. This necessarily means that the wake field excited by the beam contains a major frequency component near $\omega_R \approx h\omega_0$, or equivalently, the impedance Z_0'' has a sharp peak at $\omega_R \approx h\omega_0$, where h is an integer called the harmonic number.

As we will soon show, the exact value of ω_R relative to $h\omega_0$ is of critical importance for the stability of the beam. Above the transition energy, the beam will be unstable is ω_R is slightly above $h\omega_0$ and stable if slightly below. This instability mechanism was first analyzed by Robinson.[27] Since then, various approaches have been taken to describe the mechanism of this instability.[7,28-30]

We will begin with the longitudinal motion of our macroparticle beam. Let τ_n be the arrival time displacement of the beam at the accelerating

---

* i.e., the lowest m = 0 cavity mode. In Fig. 11, it corresponds to the peak with the lowest resonant frequency.

cavity in the n-th revolution, measured relative to a fictitious reference beam that circulates around the accelerator without executing synchrotron motions. The rate of change of τ_n is related to the relative energy error $\delta_n = \Delta E/E$ of the beam in the same n-th revolution[31]

$$\frac{d}{dn}\tau_n = -\alpha T_0 \delta_n \qquad (2.1)$$

where α is a positive constant called the momentum compaction factor and T_0 is the revolution period of the beam. A positive τ_n means the beam arrives earlier than the reference beam. Equation (2.1) is valid when the beam energy E is above transition energy so that $\delta_n > 0$ means τ_n tends to decrease.

The applied voltage at the accelerating cavity is such that the beam receives more energy if it arrives early and receives less energy if it arrives late. Again from Ref. 31, this gives

$$\frac{d}{dn}\delta_n = \frac{T_0 \omega_s^2}{\alpha}\tau_n \qquad (2.2)$$

where ω_s is the synchrotron oscillation frequency. Equations (2.1) and (2.2), of course, define the unperturbed synchrotron oscillation of the beam. Typically, ω_s is much less than the revolution frequency $\omega_0 = 2\pi/T_0$.

Equation (2.2) is valid when the beam intensity is vanishingly small. For an intense beam, the energy variation also depends on the wake field generated by the beam. Let Ne be the total charge of the beam, the $d\delta/dn$

equation then acquires an additional term:

$$\frac{d}{dn}\delta_n = \frac{T_0\omega_s^2}{\alpha}\tau_n - \frac{Ne^2L}{E}\sum_{k=-\infty}^{n} W(nT_0 - kT_0 - \tau_n + \tau_k) \qquad (2.3)$$

where L is the total length of the rf cavity, W is an abbreviation of the wake function W'_0 studied before and we have changed freely the argument of W from a distance unit to a time unit. The summation over k sums over the wake fields left over from all revolutions previous to n. The argument in the wake function is the time separation of beam positions in the n-th and the k-th revolutions. Combining the two Eqs. (2.1) and (2.3) yields the equation of motion

$$\frac{d^2\tau_n}{dn^2} + (\omega_s T_0)^2\tau_n = \frac{\alpha T_0\, Ne^2L}{E}\sum_{k} W(nT_0 - kT_0 - \tau_n + \tau_k)\ . \qquad (2.4)$$

In case the beam bunch has an oscillation amplitude much shorter than the wave length of the fundamental cavity mode, one can expand the wake function

$$\sum_k W(nT_0 - kT_0 - \tau_n + \tau_k) \approx \sum_k W(nT_0 - kT_0) - \sum_k (\tau_n - \tau_k)\, W'(nT_0 - kT_0)\ . \qquad (2.5)$$

The first term on the right hand side of (2.5) is a static term independent of the motion of the beam. It describes the parasitic loss already discussed before and can be taken care of by a constant shift in the arrival time. We will drop this term altogether. The second term, on the other hand, does involve the dynamics of the beam. The quantity

$\tau_n - \tau_k$, is the difference of τ's and -- although we will not make such an approximation -- resembles a time derivative $d\tau/dn$. An inspection of Eq. (2.4) then immediately gives the expectation of instabilities since a $d\tau/dn$ term in a $d^2\tau/dn^2$ equation indicates a possible exponential growth of τ.

Substituting (2.5) into (2.4), one gets a linear equation for τ_n. Obviously one can try to solve it staying in the time domain, but it turns out that transforming to the frequency domain makes the mathematics much easier. In the frequency domain, τ_n as a function of n behaves like

$$\tau_n \propto e^{-in\Omega T_0} \tag{2.6}$$

where Ω is the mode frequency of the beam oscillation and is a key quantity yet to be determined. An ansatz of the form (2.6) works only if the equation of motion is linear in τ. By writing down (2.6), the problem of solving the equation of motion becomes the problem of solving for Ω. Equation (2.4) for τ_n becomes

$$\Omega^2 - \omega_s^2 = \frac{\alpha\, Ne^2\, L}{ET_0} \sum_{k=-\infty}^{\infty} (1 - e^{ik\Omega T_0})\, W'(kT_0) \ .$$

The wake function is then expressed in terms of the longitudinal impedance of the rf cavity using (1.48). An application of the identity (1.60) gives

$$\Omega^2 - \omega_s^2 = -i \frac{\alpha\, Ne^2}{ET_0^2} \sum_{p=-\infty}^{\infty} [p\omega_0 Z(p\omega_0) - (p\omega_0+\Omega)Z(p\omega_0+\Omega)] \tag{2.7}$$

where $\omega_0 = 2\pi/T_0$ is the revolution frequency.

Given the impedance, Eq. (2.7) can in principle be solved for Ω. Here we will take a perturbative approach and assume Ω does not deviate much from ω_s due to the wake fields. We thus replace Ω by ω_s on the right hand side of Eq. (2.7).

In general, Ω is complex. The real part of Ω is the perturbed synchrotron oscillation of the beam motion, while the imaginary part gives the growth rate (or damping rate if negative) of the motion. Equation (2.7) then gives

$$\text{frequency shift } \Delta\Omega = \mathrm{Re}(\Omega - \omega_s)$$

$$= \frac{\alpha\, Ne^2}{2ET_0{}^2\omega_s} \sum_{p=-\infty}^{\infty} [p\omega_0\ \mathrm{Im}\ Z(p\omega_0) - (p\omega_0+\omega_s)\ \mathrm{Im}\ Z(p\omega_0+\omega_s)] \qquad (2.8)$$

and

$$\text{growth rate } \tau^{-1} = \mathrm{Im}(\Omega - \omega_s)$$

$$= \frac{\alpha\, Ne^2}{2ET_0{}^2\omega_s} \sum_{p=-\infty}^{\infty} (p\omega_0+\omega_s)\ \mathrm{Re}\ Z(p\omega_0+\omega_s)\ . \qquad (2.9)$$

Note that the imaginary part of the impedance contributes to a mode frequency shift and the real part of the impedance contributes to instability growth rate.

There are two terms under the summation for $\Delta\Omega$. As we will show later in Sections 3.2 and 3.4, the first term comes from a static phenomenon called potential-well distortion, while the origin of the second term is dynamics. Note that the growth rate τ^{-1} does not have a term due to the

static potential-well distortion; mathematically, this term vanishes because Re Z is an even function of ω.

If we consider the impedance due to the fundamental cavity mode, the only significant contribution to the growth rate (2.9) comes from two terms in the summation: $n = h$ and $n = -h$. Assuming $h\omega_0 \gg \omega_s$, we obtain

$$\tau^{-1} = \frac{\alpha N e^2 \, h\omega_0}{2ET_0^2 \, \omega_s} [\text{Re } Z(h\omega_0+\omega_s) - \text{Re } Z(h\omega_0-\omega_s)] \, . \qquad (2.10)$$

Beam stability requires $\tau^{-1} < 0$. That is, the real part of the impedance must be lower at frequency $h\omega_0+\omega_s$ than at frequency $h\omega_0-\omega_s$. This condition implies that the resonant frequency ω_R of the fundamental cavity mode should be slightly detuned downwards from an exact integral multiple of ω_0. The situation is sketched in Fig. 13. When this is done, the synchrotron oscillation of the beam is actually "Robinson damped."

2.2. Rigid-Beam Transverse Instability

We now consider a macroparticle beam executing a transverse betatron oscillation, say in the vertical (y) direction. The beam possesses an instantaneous dipole moment $Ne\ y(t)$. A particle that follows the beam at a distance Z behind sees, at time $t + Z/c$, according to Table II, a transverse wake force $Ne^2\ y(t)\ W(Z)$ in the vertical direction. The equation of motion of the beam is therefore

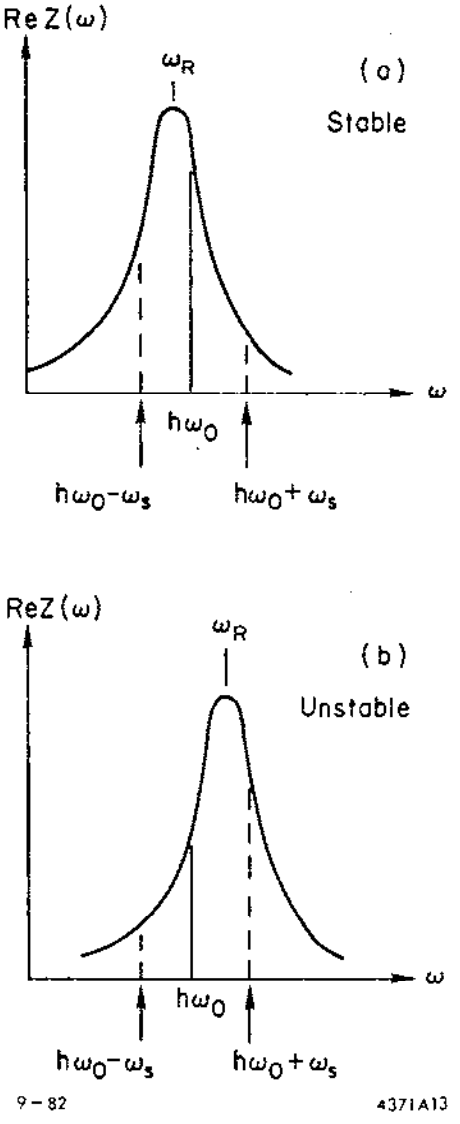

Fig. 13. Illustration of the Robinson instability. The resonant frequency ω_R of the fundamental mode of the rf cavity must be slightly lower than $h\omega_0$ for beam stability.

$$\frac{d^2y(t)}{dt^2} + \omega_\beta^2\, y(t) = \frac{Ne^2}{m_0\gamma} \sum_{k=1}^{\infty} y(t-kT_0)\, W(kT_0) \qquad (2.11)$$

where m_0 is the rest mass of a particle (not the macroparticle), ω_β is the free betatron oscillation frequency, T_0 is the revolution period and the summation over k sums the wake field over all previous revolutions. This model was first suggested by Courant and Sessler[32] and also by Pellegrini.[33,34]

Of course, an off-axis beam also possesses distribution moments other than the dipole moment. For instance, it possesses a monopole moment (i.e., the total beam charge) and also higher moments such as the quadrupole moment. The effect of the monopole moment has been considered in Section 2.1 and does not give rise to a transverse wake force. Effects due to the higher moments will be ignored as compared with the dipole wake since the beam displacement y is considered to be much smaller than the vacuum chamber pipe radius.

One may still object since a dipole moment also generates a longitudinal wake, which is not considered in Eq. (2.11). Indeed, strictly speaking, a rigorous treatment of the problem must also include the longitudinal motion of the beam. Thus, the wake function in the betatron equation of motion (2.11) should be modulated by the arrival time of the beam while the synchrotron motion should be perturbed by the longitudinal wake associated with the betatron motion. Only when this coupled betatron and synchrotron motion is considered does the system strictly satisfy the Maxwell equations and becomes Hamiltonian. However,

for practical purposes, as long as the synchrotron and betatron frequencies are not close to a resonance condition $\omega_\beta \pm \omega_s = n\omega_0$ and the transverse displacements are small, Eq. (2.11) still accurately describes the transverse motion of the beam. This point will be discussed further following Eq. (3.47).

We will again solve Eq. (2.11) in the frequency domain. Let $y \propto \exp(-i\Omega t)$ and transform the wake function into the transverse impedance according to Eq. (1.48), we obtain the following equation for Ω:

$$\Omega^2 - \omega_\beta^2 = -i \frac{Ne^2c}{ET_0^2} \sum_{p=-\infty}^{\infty} Z(p\omega_0+\Omega) \qquad (2.12)$$

where $\omega_0 = 2\pi/T_0$. Assuming Ω does not deviate much from ω_β, we have

$$\text{frequency shift } \Delta\Omega = \text{Re}\,(\Omega - \omega_\beta)$$

$$\approx \frac{Ne^2c}{2E\,\omega_\beta\,T_0^2} \sum_{p=-\infty}^{\infty} \text{Im}\, Z(p\omega_0 + \omega_\beta) \qquad (2.13)$$

and

$$\text{growth rate } \tau^{-1} = \text{Im}\,(\Omega - \omega_\beta)$$

$$\approx -\frac{Ne^2c}{2E\,\omega_\beta\,T_0^2} \sum_{p=-\infty}^{\infty} \text{Re}\, Z(p\omega_0 + \omega_\beta) \quad . \qquad (2.14)$$

Given the transverse impedance, Eqs. (2.13) and (2.14) are our final expressions. We first note that if the real part of $Z(\omega)$ contains sharp resonant peaks, there can be a transverse counterpart of the Robinson effect. More explicitly, if a resonant frequency ω_R is close to $h\omega_0$, an integral multiple of ω_0, then

$$\tau^{-1} \approx -\frac{Ne^2c}{2E\,\omega_\beta\,T_0^2}\,[\mathrm{Re}\,Z(h\omega_0 + \Delta_\beta\omega_0) - \mathrm{Re}\,Z(h\omega_0 - \Delta_\beta\omega_0)] \qquad (2.15)$$

where Δ_β is the non-integer part of the betatron tune $\nu_\beta = \omega_\beta/\omega_0$ and we have chosen $-1/2 < \Delta_\beta < 1/2$. For stability, ω_β should be slightly above $h\omega_0$ if $\Delta_\beta > 0$ and below $h\omega_0$ if $\Delta_\beta < 0$.

Problem 6. Using (2.14), show that the instability growth rate $\tau^{-1} = 0$ if ν_β = integer or if ν_β = integer + 1/2.[33] This is true for arbitrary impedance.

As another application of Eq. (2.14), let us find the instability growth rate for an accelerator with resistive wall. Substituting the transverse impedance (1.50), i.e.,

$$Z(\omega) = \sqrt{\frac{2}{\pi\sigma}}\,\frac{cT_0}{b^3}\,|\omega|^{-1/2}\,[\mathrm{sgn}(\omega) - i]\,, \qquad (2.16)$$

into (2.14), we obtain the result*

---

* Applying (2.16) to the frequency shift (2.13) is more subtle; the result will diverge or converge depending on how the summation is performed.[32] The subtlety comes from the fact that the transverse wake force should vanish at $Z = 0$ while the wake force corresponding to the impedance (2.16) diverges for $Z \to 0^+$ and vanishes for $Z \to 0^-$. We will not explore this point here since it is the growth rate, not the frequency shift, that concerns us. Suffice it to say that after the subtlety is removed, the frequency shift is finite.

$$\tau^{-1} \approx -\frac{Ne^2 c^2}{b^3 E \omega_\beta T_0 \sqrt{\pi\sigma\omega_0}} G(\Delta_\beta) \tag{2.17}$$

where we have defined[32]

$$G(\Delta_\beta) = \frac{1}{\sqrt{2}} \sum_{p=-\infty}^{\infty} \frac{\mathrm{sgn}(p+\Delta_\beta)}{|p+\Delta_\beta|^{1/2}} \quad . \tag{2.18}$$

The function $G(\Delta_\beta)$ is plotted in Fig. 14. We see that $G(\Delta_\beta)$ is positive (so that $\tau^{-1} < 0$ and the beam is stable) if $0 < \Delta_\beta < 1/2$, and negative if $-1/2 < \Delta_\beta < 0$. This means one should choose the betatron tune below a half-integer. However, this conclusion is valid only for the resistive wall case and for a different impedance the conclusion may very well be reversed.

Note that the stability criterion invariably involves the sign of Δ_β. This is because the beam oscillation is damped or antidamped depending on the relative phase between the wake force and the oscillation (damped if the wake force leads the oscillation and antidamped if the reverse is true) and the relative phase is determined by Δ_β.

2.3. Beam Break-Up in Linacs

In linear accelerators, wake field effects impose an important limitation on the maximum beam intensity that can be accelerated. Although we are mainly interested in coherent instabilities in circular accelerators, the instabilities -- or beam break-ups as they are called -- in a linac are actually the basic mechanisms underlying many of the instabilities in the circular accelerators and deserve to be looked into.

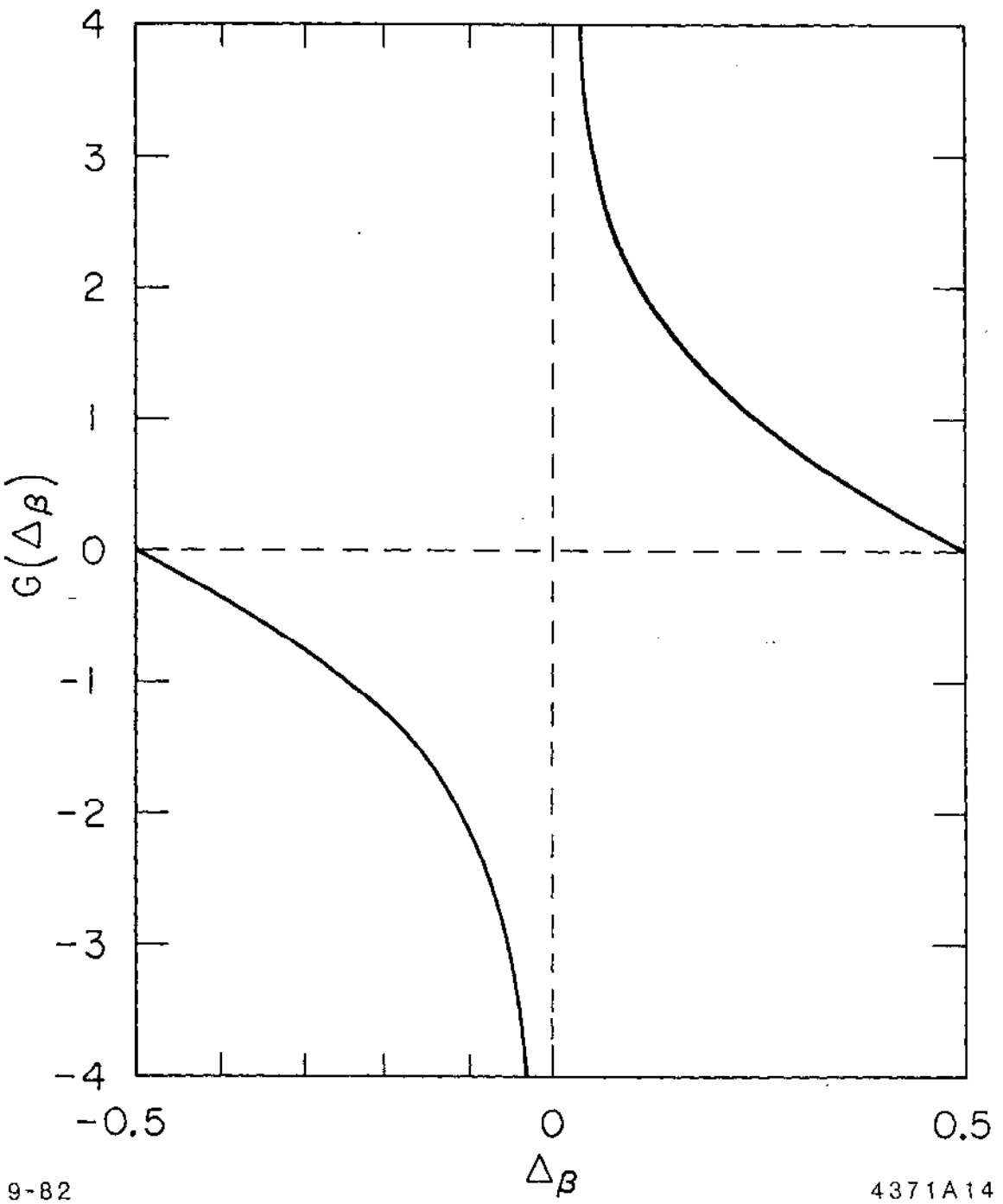

Fig. 14. The function $G(\Delta_\beta)$.

In this section we will discuss three wake field effects in a linac, using a model in which the beam is represented as two macroparticles each containing N/2 particles, separated by a distance Z. The three effects are due to the m = 0, 1, and 2 components of the wake field, respectively. In a linac, the separation of the two macroparticles does not change in time.

First the m = 0 wake. The particles in the trailing macroparticle see a longitudinal electric field left behind by the leading macroparticle and lose energy at a rate

$$\frac{d\epsilon}{dt} = \frac{c\, Ne^2\, W'_0(Z)}{2} \quad . \tag{2.19}$$

Because of this loss, the beam acquires a spread of energy among its particles. Take for instance the SLAC linac with $N = 5 \times 10^{10}$, $Z = 2$ mm, accelerator length $L = 3000$ m and, from Fig. 8(a), $W'_0(Z) = 0.9$ cm^{-2}, we find this energy spread is roughly 1.0 GeV, which is not negligible. As pointed out in Loew's Lecture,[35] most of this spread can be removed by properly phasing the accelerating rf voltage relative to the beam so that the energy spread is more like 1/4 GeV or so at the end of linac.

The second effect we will study is the transverse dipole beam break-up instability (m = 1). In our two-particle model, the leading macroparticle executes a free betatron oscillation

$$y_1(t) = \hat{y} \cos \omega_\beta t \quad , \tag{2.20}$$

while the trailing macroparticle sees a deflecting wake field left behind by the leading macroparticle. Thus

$$\ddot{y}_2 + \omega_\beta^2 y_2 = \frac{Ne^2 W_1(Z)}{2m_0\gamma} y_1$$

$$= \frac{Ne^2 W_1(Z)}{2m_0\gamma} \hat{y} \cos \omega_\beta t \quad . \qquad (2.21)$$

In writing down this equation, we have assumed that $\omega_\beta Z/c \ll 1$ so that one can ignore the betatron phase slip from bunch head to tail due to the difference in their times of arrival.

Equation (2.21) shows that the mechanism of beam break-up is that particles in the tail of the beam are driven exactly on resonance by the oscillating wake left by the head of the beam. The solution to (2.21) is

$$y_2(t) = \hat{y} \left[\cos \omega_\beta t + \frac{Ne^2 W_1(Z)}{4\omega_\beta m_0\gamma} t \sin \omega_\beta t \right] \qquad (2.22)$$

in which the first term describes the free oscillation and the second term is the resonant response to the driving term. Note that the amplitude of the second term grows linearly with time. At the end of the linac, the oscillation amplitude of the tail macroparticle has grown a factor of

$$\eta_1 = \frac{Ne^2 W_1(Z) L}{4\omega_\beta m_0\gamma c} \quad . \qquad (2.23)$$

For a beam bunch with realistic distribution, the off-axis motion of the head of the bunch deflects the tail of the bunch so that the bunch is distorted into a banana shape as sketched in Fig. 15(a). Obviously, if the beam intensity is too high, the tail particles may acquire too large an amplitude and be lost from the beam.

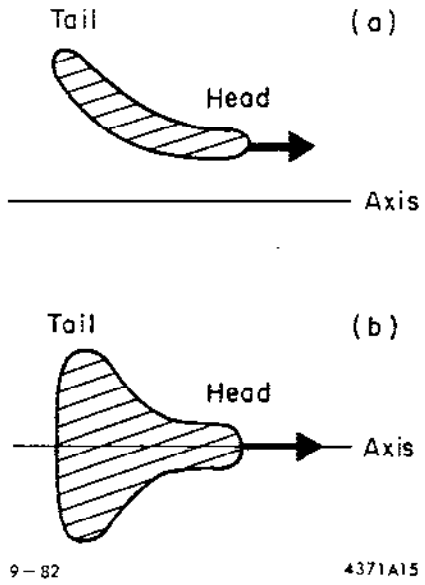

Fig. 15. Sketches of the beam shape when the bunch is undergoing (a) dipole beam break up and (b) quadrupole beam break up.

The third coherent effect we want to study is the transverse quadrupole beam break-up instability (m = 2). What happens here is that the quadrupole wake field generated by the bunch head perturbs the focusing force that acts on the bunch tail, leading to an instability.

To describe the quadrupole wake, it is better to imagine that the leading macroparticle is actually an elliptical-shaped slice of charge possessing a quadrupole moment but no dipole moment. The quadrupole moment executes a free betatron oscillation with frequency $2\omega_\beta$, i.e., $\langle y_1^2 \rangle = \hat{I}_2 \cos 2\omega_\beta t$.

Just like the dipole beam break-up, the quadrupole instability is also a result of a resonant excitation. The equation of motion of the trailing particle is

$$\ddot{y}_2 + \omega_\beta^2 y_2 = \frac{Ne^2 W_2(Z)}{m_0\gamma} \hat{I}_2 \cos(2\omega_\beta t) y_2 \quad . \tag{2.24}$$

The driving term on the right hand side is obtained from Table II. Equations of the type (2.24) are unstable just like equation (2.21) is. If we let $y_2 = \hat{y} \cos \omega_\beta t$ be the unperturbed zeroth order solution, one finds by a first-order perturbation calculation that*

$$y_2 \approx \hat{y} \left[\cos \omega_\beta t + \frac{Ne^2 W_2(Z) \hat{I}_2}{4\omega_\beta m_0\gamma} t \sin \omega_\beta t \right] \quad . \tag{2.25}$$

---

* A perturbation calculation applied to equations of the type (2.24) -- the Mathieu equation -- can be misleading; a simple frequency shift can be mistaken as a behavior of the type (2.25). Here, however, since the driving term is exactly on resonance, the perturbation calculation does apply. See Ref. 36.

Note the similarity between Eqs. (2.25) and (2.22). The oscillation amplitude of the tail particle therefore grows by a factor

$$\eta_2 = \frac{Ne^2 W_2(Z) \hat{I}_2 L}{4\omega_\beta m_0 \gamma c} \quad . \tag{2.26}$$

Fig. 15(b) is a sketch of the beam shape when the quadrupole beam break up is taking place.

We have now discussed the wake effects in a linac in terms of a highly simplified beam model. Generalization to realistic beams is straightforward although often not trivial. Interested readers should read Refs. 37 to 42 and the references quoted therein.

Analysis similar to the above can be applied to higher values of m. For instance, m = 3 requires the consideration of two triangular charge slices. We then obtain a strength parameter η_m that resembles Eqs. (2.23) and (2.26). As m increases, the strength parameter decreases roughly with $(a/b)^{2m}$, where a is the transverse beam size and b is the pipe radius.

2.4. Strong Head-Tail Instability

There is also a dipole beam break-up mechanism in a circular accelerator. It will be called the strong head-tail instability here for reasons to be discussed in Section 2.6 and also in the paragraph preceding Eq. (3.71). The difference from the linac case is that now the

two macroparticles are no longer frozen in their relative longitudinal positions. Instead, both macroparticles, each containing a charge Ne/2, execute synchrotron oscillations with a slow frequency ω_s.

We assume the synchrotron oscillations of the two particles have equal amplitude but opposite phases. During time $0 < t < T_s/2$, where $T_s = 2\pi/\omega_s$, particle 1 leads particle 2; the equations of motion for the two particles are

$$\begin{aligned} \ddot{y}_1 + \omega_\beta^2 \, y_1 &= 0 \\ \ddot{y}_2 + \omega_\beta^2 \, y_2 &= \frac{Ne^2 \, W_0}{2m_0\gamma} \, y_1 \end{aligned} \qquad . \tag{2.27}$$

Similarly, during $T_s/2 < t < T_s$, we have the same equations with indices 1 and 2 switched. Then during $T_s < t < 3T_s/2$, Eq. (2.27) applies again, etc. This model was first suggested by Kohaupt[93] and Talman.[94,95]

In writing down (2.27), we have assumed for simplicity that the wake function W is a constant, and yet it vanishes before the beam completes one revolution, i.e.

$$W_1(Z) = \begin{cases} 0 & \text{if } Z \leq 0 \\ W_0 & \text{if } 0 < Z < \text{beam length} \\ 0 & \text{if } Z > \text{beam length} \end{cases} \qquad . \tag{2.28}$$

We will now analyze the stability condition of the system. We start with (2.27); the solution for y_1 is simply a free betatron oscillation:

$$\bar{y}_1(t) = e^{-i\omega_\beta t}\,\bar{y}_1(0) \tag{2.29}$$

where

$$\bar{y}_1 = y_1 + \frac{i}{\omega_\beta}\,\dot{y}_1 \quad . \tag{2.30}$$

Substituting (2.29) into the equation for y_2 yields the solution

$$y_2(t) = \mathrm{Re}\left[B e^{-i\omega_\beta t} + i\,\frac{Ne^2 W_0}{4\omega_\beta m_0 \gamma}\,\bar{y}_1(0)\, t e^{-i\omega_\beta t} \right] \quad . \tag{2.31}$$

The first term describes the free betatron oscillation, while the second term is the resonantly driven response. Equation (2.31), of course, has its linac counterpart given by Eq. (2.22). The coefficient B depends on the initial conditions $y_2(0)$ and $\dot{y}_2(0)$.

Equation (2.31) can also be written in terms of the phasor $\bar{y}_2$ if $\omega_\beta T_s/2 \gg 1$, or equivalently, $\omega_\beta \gg \omega_s$. The result is

$$\bar{y}_2(t) = \bar{y}_2(0)\, e^{-i\omega_\beta t} + i\,\frac{Ne^2 W_0}{4\omega_\beta m_0 \gamma}\,\bar{y}_1(0)\, t e^{-i\omega_\beta t} \quad . \tag{2.32}$$

We have thus solved the equations of motion during the period $0 < t < T_s/2$. Written in matrix form, we have

$$\begin{bmatrix} \bar{y}_1 \\ \bar{y}_2 \end{bmatrix}_{t=T_s/2} = e^{-i\omega_\beta T_s/2} \begin{bmatrix} 1 & 0 \\ i\eta_1 & 1 \end{bmatrix} \begin{bmatrix} \bar{y}_1 \\ \bar{y}_2 \end{bmatrix}_0 \quad , \tag{2.33}$$

where [cf., Eq. (2.23)] we have define the dimensionless parameter

$$\eta_1 = \frac{Ne^2 W_0 T_s}{8\omega_\beta m_0 \gamma} \quad . \tag{2.34}$$

From the properties of wake functions, we know η_1 is positive.

The time evolution during $T_s/2 < t < T_s$ can be obtained by interchanging indices 1 and 2 in the above analysis. The total transformation for one full synchrotron period is therefore

$$\begin{bmatrix} \bar{y}_1 \\ \bar{y}_2 \end{bmatrix}_{T_s} = e^{-i\omega_\beta T_s} \begin{bmatrix} 1 & i\eta_1 \\ 0 & 1 \end{bmatrix} \begin{bmatrix} 1 & 0 \\ i\eta_1 & 1 \end{bmatrix} \begin{bmatrix} \bar{y}_1 \\ \bar{y}_2 \end{bmatrix}_0$$

$$= e^{-i\omega_\beta T_s} \begin{bmatrix} 1-\eta_1^2 & i\eta_1 \\ i\eta_1 & 1 \end{bmatrix} \begin{bmatrix} \bar{y}_1 \\ \bar{y}_2 \end{bmatrix}_0 \quad . \tag{2.35}$$

As time evolves, the vector formed by the phasors $\bar{y}_1$ and $\bar{y}_2$ is repeatedly transformed by the 2 × 2 matrix in (2.35). Stability of the system is thus determined by the eigenvalues of this matrix. The two eigenvalues for the two modes -- a + mode and a - mode -- are

$$\lambda_\pm = e^{\pm i\mu} \quad , \quad \cos\mu = 1 - \frac{1}{2}\eta_1^2 \quad . \tag{2.36}$$

Stability requires μ = real, which is fulfilled if $|\cos\mu| \leq 1$, or

$$\eta_1 \leq 2 \quad . \tag{2.37}$$

For weak beams, the growths made during the half synchrotron periods when the particle is trailing do not accumulate and the beam is stable. As the beam intensity increases, η_1 exceeds 2, the growths of the particles then do accumulate and bootstrap into an instability. This threshold behavior is very different from the linac case in which the beam -- at least the tail of it -- is always unstable. One can imagine that, by periodically switching the roles of being the leading and the trailing particles, the two-particle beam is made more stable. The more frequently they are switched, the more stable is the beam. This shows up in that η_1 is proportional to T_s. Synchrotron oscillation is thus an effective stablizing mechanism. The fact that η_1 is inversely proportional to γ is because high energy particles are more rigid in their motion against perturbations.

It would be interesting to Fourier analyze the center-of-mass signal y_1+y_2 to examine its frequency spectrum since the center-of-mass signal is easily observed experimentally. This is straightforward to do and here we give the result. In the stable region, the ± modes contain the following frequencies:[46]

$$\begin{aligned} &+ \text{ mode} \quad : \quad \omega_\beta + \ell\omega_s - \frac{\mu}{2\pi}\omega_s \quad , \quad \ell = \text{even} \\ &- \text{ mode} \quad : \quad \omega_\beta + \ell\omega_s + \frac{\mu}{2\pi}\omega_s \quad , \quad \ell = \text{odd} \quad . \end{aligned} \tag{2.38}$$

Note that each mode contains a multiple of frequencies when observed continuously in time. Figure 16 shows the spectrum.

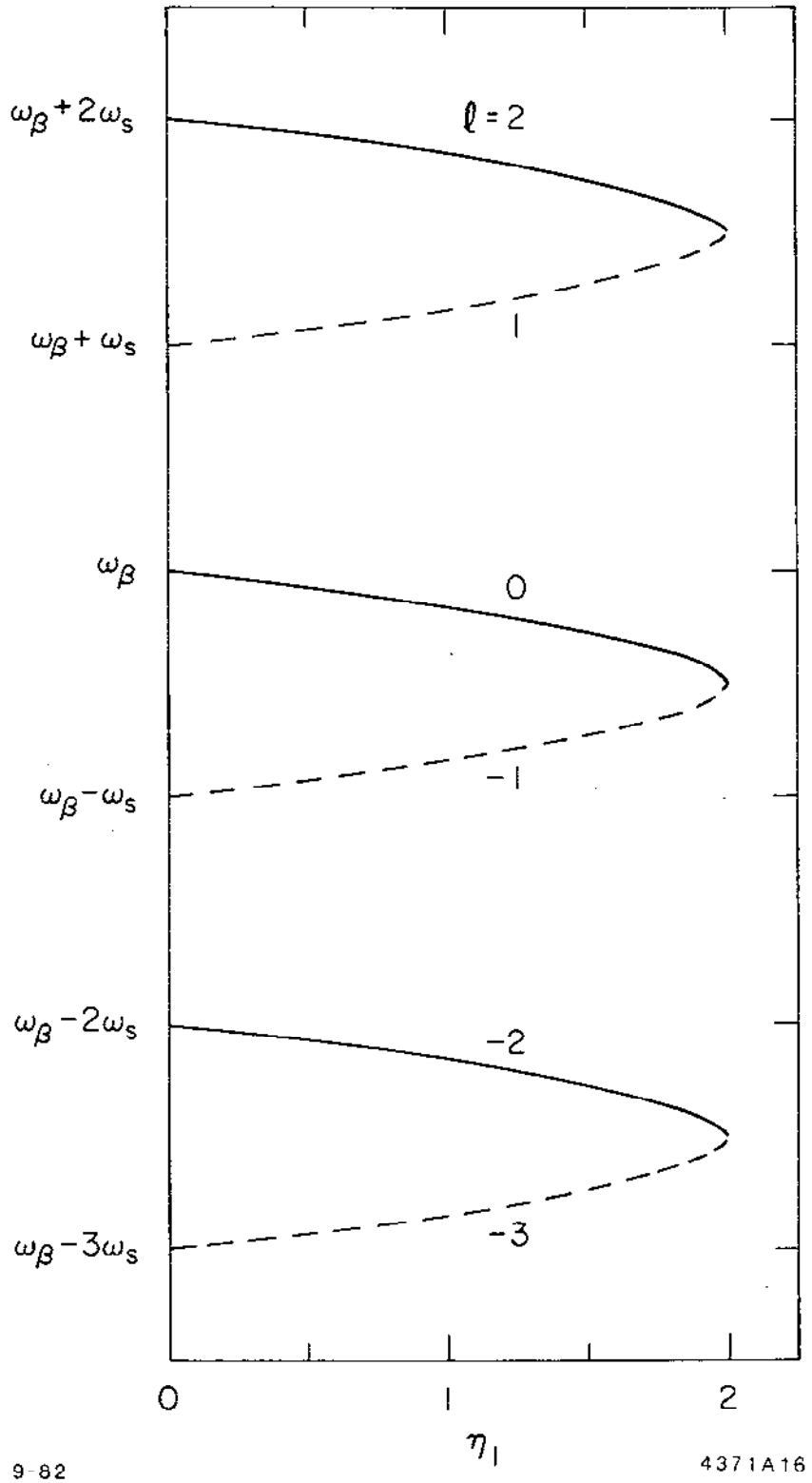

Fig. 16. Frequency spectrum of the center-of-mass signal of the beam in the stable region $\eta_1 < 2$. The solid lines are the sprectrum of the + mode and the dashed lines are that for the - mode.

For weak beams (i.e., small η_1), the two macroparticles move up and down with the same phase in the + mode and out of phase in the - mode. As η_1 increases, the mode frequencies shift and the particle motions become more complicated; each mode then contains a combination of in-phase and out-of-phase motions. At the stability limit $\eta_1 = 2$, the frequencies of the two modes merge into each other and become imaginary, which means the beam is unstable.

Figure 16 shows the result obtained for a two-particle beam assuming the wake (2.28). We will show later (see Fig. 35) the result of a more sophisticated calculation assuming the same wake but taking fully into account the internal motions of the beam. We will then find that Fig. 16 does offer a qualitative description of the beam spectrum for $\ell = 0$ and $\ell = -1$ modes. It is not surprising that the two-particle model fails to describe the behavior of the higher modes.

One might want to have an idea of what happens in the unstable region. Suppose we are slightly above the instability threshold so that $\eta_1 = 2+\epsilon$ with $\epsilon \ll 1$. Equation (2.36) can be used to find the instability growth rate: $\tau^{-1} = 2\sqrt{\epsilon}/T_s$. Note the square root dependence of τ^{-1} on ϵ. This means a small ϵ can give rise to a sharp growth rate; for instance, 10% above threshold gives $\tau \cong T_s$. One consequence is that feedback systems are not very effective to bring the beam intensity substantially beyond the threshold unless the feedback damping rate is at least comparable to ω_s.

2.5. Transverse Quadrupole Instability

It does not require too much stretching of the imagination to suspect that there is also an instability which is the circular accelerator's counterpart of the quadrupole beam break-up in linacs. By observing the similarity between (2.25) and (2.22), we expect to find a stability condition that assumes the form

$$\eta_2 \leq 2 \tag{2.39}$$

where, with W_0 the constant quadrupole wake function and $\underline{a}$ the rms radius of the unperturbed beam cross-section,

$$\eta_2 = \frac{Ne^2 W_0 a^2 T_s}{4\omega_B m_0 \gamma} \quad . \tag{2.40}$$

What happens here is that the throbbing motions of the two charge slices couple through the quadrupole wake force, leading to instability. At this point, the reader may want to read Ref. 4, in which the various throbbing beam instabilities are discussed under the assumption that synchrotron motions can be ignored.

We will now show the stability criterion (2.39) somewhat more elaborately. For this purpose, we represent the beam by two elliptically shaped charge slices, each slice is described by a symmetric 4×4 Σ-matrix whose elements are the second moments of distribution, i.e.

$$\Sigma_i = \begin{bmatrix} \langle x^2 \rangle_i & \langle x\dot{x} \rangle_i & 0 & 0 \\ \langle x\dot{x} \rangle_i & \langle \dot{x}^2 \rangle_i & 0 & 0 \\ 0 & 0 & \langle y^2 \rangle_i & \langle y\dot{y} \rangle_i \\ 0 & 0 & \langle y\dot{y} \rangle_i & \langle \dot{y}^2 \rangle_i \end{bmatrix} , \quad i = 1,2 . \qquad (2.41)$$

We have assumed the ellipses are upright in the x-y plane.

We first concentrate on the leading slice. The moments of the slice execute free betatron oscillations. The equation of motion is

$$\dot{\Sigma}_1 = \Omega\Sigma_1 + \Sigma_1\tilde{\Omega} \qquad (2.42)$$

where a tilde means taking the transpose of a matrix, and

$$\Omega = \begin{bmatrix} 0 & 1 & 0 & 0 \\ -\omega_x^2 & 0 & 0 & 0 \\ 0 & 0 & 0 & 1 \\ 0 & 0 & -\omega_y^2 & 0 \end{bmatrix}$$

with ω_x and ω_y the betatron frequencies. Eq. (2.42) has the solution

$$\Sigma_1(t) = T\,\Sigma_1(0)\,\tilde{T} \qquad (2.43)$$

where

$$T = \begin{bmatrix} \cos \omega_x t & \frac{1}{\omega_x} \sin \omega_x t & 0 & 0 \\ -\omega_x \sin \omega_x t & \cos \omega_x t & 0 & 0 \\ 0 & 0 & \cos \omega_y t & \frac{1}{\omega_y} \sin \omega_y t \\ 0 & 0 & -\omega_y \sin \omega_y t & \cos \omega_y t \end{bmatrix} .$$

In the following we will do a perturbation calculation. Let

$$\begin{aligned} \langle x^2 \rangle_i &= a^2 + A_{xi} \\ \langle x\dot{x} \rangle_i &= 0 + B_{xi} \\ \langle \dot{x} \rangle_i &= \omega_x^2 a^2 + C_{xi} \\ \langle y^2 \rangle_i &= a^2 + A_{yi} \\ \langle y\dot{y} \rangle_i &= 0 + B_{yi} \\ \langle \dot{y} \rangle_i &= \omega_y^2 a^2 + C_{yi} \quad , \quad i = 1,2 \quad . \end{aligned} \tag{2.44}$$

The first terms on the right hand sides are the unperturbed values and the second terms are small, time-dependent perturbations. We have assumed that the unperturbed beam is round with rms radius $\underline{a}$.

Since the beam emittances $(\langle x^2 \rangle_i \langle \dot{x}^2 \rangle_i - \langle x\dot{x} \rangle_i^2)^{1/2}$ and $(\langle y^2 \rangle_i \langle \dot{y}^2 \rangle_i - \langle y\dot{y} \rangle_i^2)^{1/2}$ are constants of the motion, it follows that $\omega_x^2 A_{xi} + C_{xi}$ and $\omega_y^2 A_{yi} + C_{yi}$ are invariants. Without losing any beam stability information, we are therefore free to choose the constraints

$$C_{xi} = -\omega_x^2 A_{xi}$$

$$C_{yi} = -\omega_y^2 A_{yi} \quad , \quad i = 1,2 \quad .$$

In terms of the perturbation moments, Eq. (2.43) can be written explicitly as

$$A_{\beta 1}(t) = A_{\beta 1}(0) \cos 2\omega_\beta t + \frac{B_{\beta 1}(0)}{\omega_\beta} \sin 2\omega_\beta t$$

$$B_{\beta 1}(t) = -\omega_\beta A_{\beta 1}(0) \sin 2\omega_\beta t + B_{\beta 1}(0) \cos 2\omega_\beta t \ , \ \beta = x,y \ . \tag{2.45}$$

Equation (2.45) describes the free quadrupole oscillation of the first slice. The oscillation frequency is $2\omega_\beta$.

Slice 1 leaves behind a quadrupole wake force that, according to Table II, is equivalent to the force due to a quadrupole magnet with a gradient $\partial B_y/\partial x = -NeW_0(\langle x^2\rangle_1 - \langle y^2\rangle_1) = -NeW_0(A_{x1} - A_{y1})$. This wake contributes an additional term to the equation of motion for Σ_2, i.e.

$$\dot{\Sigma}_2 = \Omega\Sigma_2 + \Sigma_2\tilde{\Omega} + \frac{Ne^2 W_0 a^2}{m_0\gamma}(A_{x1} - A_{y1}) \begin{bmatrix} 0 & 1 & 0 & 0 \\ 1 & 0 & 0 & 0 \\ 0 & 0 & 0 & -1 \\ 0 & 0 & -1 & 0 \end{bmatrix} . \tag{2.46}$$

This equation can be integrated exactly, but we will keep only the resonant terms, yielding the result

$$\Sigma_2 = T S \tilde{T} \tag{2.47}$$

where

$$S(t) = \Sigma_2(0) + \frac{Ne^2 W_0 a^2 t}{2m_0\gamma}$$

$$\times \begin{bmatrix} -\frac{1}{\omega_x^2} B_{x1}(0) & A_{x1}(0) & 0 & 0 \\ A_{x1}(0) & B_{x1}(0) & 0 & 0 \\ 0 & 0 & -\frac{1}{\omega_y^2} B_{y1}(0) & A_{y1}(0) \\ 0 & 0 & A_{y1}(0) & B_{y1}(0) \end{bmatrix}$$

We have assumed ω_x and ω_y are different so that there is no resonant coupling between the two dimensions. The x and y motions thus decouple and we need only to consider one of the two dimensions. Note that the second term in S is proportional to t.

The solution (2.47), written in terms of the perturbation moments, is

$$\begin{aligned} A_2(t) &= A_2(0) \cos 2\omega_\beta t + \frac{B_2(0)}{\omega_\beta} \sin 2\omega_\beta t \\ &\quad + \frac{Ne^2 W_0 a^2 t}{2m_0\gamma\,\omega_\beta} \left[-\frac{B_1(0)}{\omega_\beta} \cos 2\omega_\beta t + A_1(0) \sin 2\omega_\beta t \right] \\ B_2(t) &= -\omega_\beta A_2(0) \sin 2\omega_\beta t + B_2(0) \cos 2\omega_\beta t \\ &\quad + \frac{Ne^2 W_0 a^2 t}{2m_0\gamma} \left[\frac{B_1(0)}{\omega_\beta} \sin 2\omega_\beta t + A_1(0) \cos 2\omega_\beta t \right] . \end{aligned} \tag{2.48}$$

We have dropped the subscripts x and y on A's and B's, and ω_β is either ω_x or ω_y depending on which dimension is being considered. Equations (2.45) and (2.48) are our solutions during the time $0 < t < T_s/2$. If we now form two phasors

$$\tilde{Q}_1 = A_1 + i\frac{B_1}{\omega_\beta}$$
$$\tilde{Q}_2 = A_2 + i\frac{B_2}{\omega_\beta} \quad , \tag{2.49}$$

the transformation from $t = 0$ to $t = T_s/2$ is found to be

$$\begin{bmatrix} \tilde{Q}_1 \\ \tilde{Q}_2 \end{bmatrix}_{t=T_s/2} = e^{-i\omega_\beta T_s} \begin{bmatrix} 1 & 0 \\ i\eta_2 & 1 \end{bmatrix} \begin{bmatrix} \tilde{Q}_1 \\ \tilde{Q}_2 \end{bmatrix}_0 \tag{2.50}$$

where η_2 is the parameter defined in (2.40).

Equation (2.50) looks almost identical to the dipole result, Eq. (2.33). The same analysis of the previous section then leads to the stability criterion (2.39). The frequency spectrum of the quadrupole oscillation, of course, clusters around $2\omega_\beta$.

2.6. Head-Tail Instability

In our analysis of the strong head-tail instability in Section 2.4, we have assumed that the betatron and the synchrotron motions are decoupled from each other. By doing so, we have ignored an important source of

instability known as the head-tail instability,[26,44,45,47-49] to which we now turn. This instability is one of the cleanest to be observed experimentally.[50,51]

The betatron oscillation frequency of a particle in a circular accelerator depends on the energy error $\delta = \Delta E/E$ of the particle. If we denote that betatron frequency of an on-momentum particle as ω_β, the betatron frequency for an off-momentum particle can be written as

$$\omega_\beta(\delta) = \omega_\beta + \omega_0 \xi \delta \quad , \tag{2.51}$$

where ω_0 is the revolution frequency, ξ is the chromaticity parameter determined by the accelerator lattice.

In Section 2.4, we have used the time of an external clock as the independent variable. This is no longer convenient here because now we have to consider synchrotron motions and the varying time-of-arrival complicates the analysis. We will therefore choose the longitudinal coordinate along the accelerator, s, as the independent variable.

Let us first examine the free betatron oscillation in the absence of the wake field. The accumulated betatron phase is given by an integration of (2.51), i.e.

$$\int \omega_\beta(\delta)\, ds/c = \omega_\beta s/c + \omega_0 \xi \int \delta\, ds/c$$

$$= \omega_\beta s/c - \frac{\xi \omega_0}{\alpha} \tau(s) \tag{2.52}$$

where α is the momentum compaction, τ is the time displacement and use has been made of Eq. (2.1). This is already a remarkable result; the modulation of betatron phase due to the chromatic effect depends only on τ and not on other dynamical variables such as δ. The modulation, of course, is slow and weak.

We now consider two macroparticles whose synchrotron oscillations are given by

$$\tau_1 = \hat{\tau} \sin(\omega_s s/c) \quad \text{and} \quad \tau_2 = -\tau_1 \ , \tag{2.53}$$

where ω_s is the synchrotron oscillation frequency. Particle 1 leads particle 2 during $0 < s/c < \pi/\omega_s$ and trails during $\pi/\omega_s < s/c < 2\pi/\omega_s$. The free betatron oscillations of the two particles are described by

$$\begin{aligned} y_1(s) &= \bar{y}_1 \exp\left[-i\omega_\beta s/c + i \frac{\xi\omega_0}{\alpha} \hat{\tau} \sin \frac{\omega_s s}{c} \right] \\ y_2(s) &= \bar{y}_2 \exp\left[-i\omega_\beta s/c - i \frac{\xi\omega_0}{\alpha} \hat{\tau} \sin \frac{\omega_s s}{c} \right] \ . \end{aligned} \tag{2.54}$$

As the particles exchange their roles of being a leading particle and a trailing particle, the betatron phases are such that the leading particle always lags in phase behind the trailing particle if $\xi > 0$ and the situation reverses if $\xi < 0$, as shown in Fig. 17. The factor $\xi\omega_0\hat{\tau}/\alpha$ is called the "head-tail phase."

The quantities $y_1(s)$ and $y_2(s)$ are the displacements of the two macroparticles as observed at a fixed location s. One revolution later, their

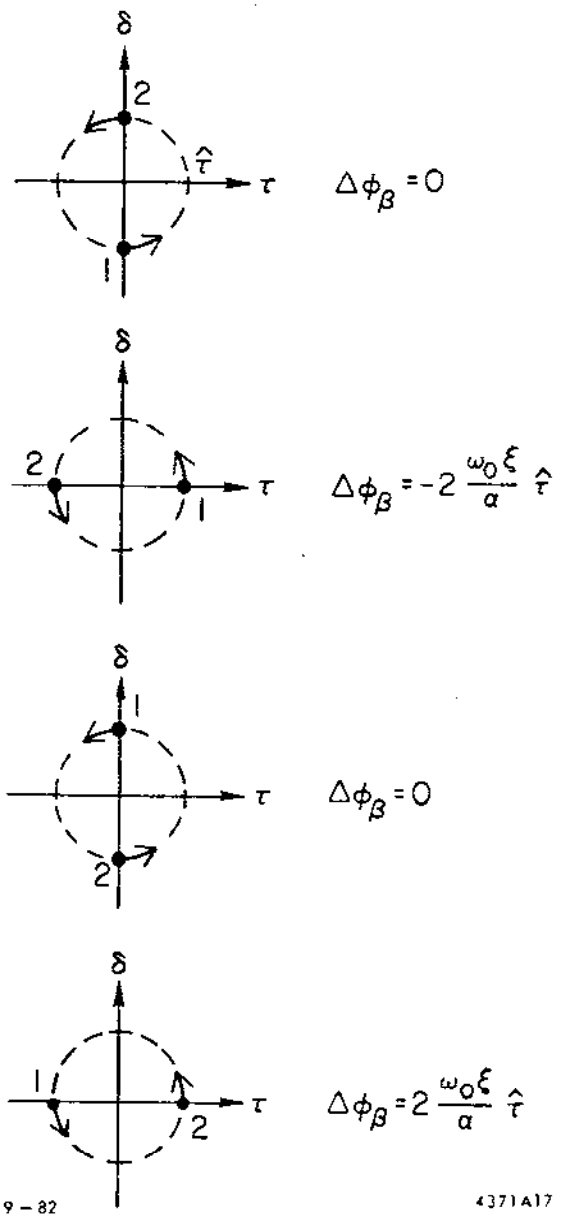

Fig. 17. The synchrotron oscillations of a two-particle beam; $\Delta\phi_\beta = \phi_\beta(1) - \phi_\beta(2)$ is the difference of the betatron phases of the two particles.

displacements observed at the same location will be $y_1(s+C)$ and $y_2(s+C)$, where C is the accelerator circumference.

Recalling the strong head-tail instability studied before, the trailing particle is always unstable due to the resonant driving by the wake generated by the leading particle; the growths of the tail particle during the half-synchrotron-periods are strong, but below a certain threshold, the synchrotron oscillation washes away the growths and the net result is that the beam becomes stable. The additional chromatic term that we are studying now does not have this fortunate property. As we shall see, the weak growths associated with chromaticity do accumulate persistently from one half-synchrotron-period to the next, thus slowly build up an instability. We shall also see that there is no threshold behavior in this instability.

Let us look at the motion of particle 2 during $0 < s/c < \pi/\omega_s$ in the presence of the wake field. The wake function, we assume, is that given by (2.28). The equation of motion is

$$c^2 \frac{d^2y_2}{ds^2} + \left(\omega_\beta + \frac{\xi\omega_0\hat{\tau}\omega_s}{\alpha} \cos\frac{\omega_s s}{c} \right)^2 y_2 = \frac{Ne^2 W_0}{2m_0\gamma} y_1 \quad . \qquad (2.55)$$

The y_1 on the right hand side is given by the free oscillation result (2.54). If we let y_2 also be given by (2.54), but allowing $\bar{y}_2$ to be slowly varying in time, Eq. (2.55) leads to an equation for $\bar{y}_2$:

$$\frac{d}{ds}\bar{y}_2(s) \approx \frac{iNe^2 W_0}{4m_0\gamma\omega_\beta c} \bar{y}_1(0) \exp\left(2i \frac{\xi\omega_0}{\alpha} \hat{\tau} \sin\frac{\omega_s s}{c} \right) . \qquad (2.56)$$

For most practical cases, the head-tail phase $\xi\omega_0\hat{\tau}/\alpha$ is much less than unity, the exponential in (2.56) can be Taylor expanded and y_2 can be integrated to yield

$$\tilde{y}_2(s) = \tilde{y}_2(0) + \frac{iNe^2 W_0}{4m_0\gamma\omega_\beta c}\tilde{y}_1(0)\left[s + \frac{2i\xi\omega_0\hat{\tau}c}{\alpha\omega_s}\left[1 - \cos\frac{\omega_s s}{c}\right]\right] . \tag{2.57}$$

The first term in the brackets is the resonant response already studied in Section 2.4. The second chromatic term is small because it is proportional to the head-tail phase and also because it is not a resonant response. Note that the chromatic term is 90° out of phase from the resonant term; this result follows from the fact that the chromatic effect modulates the phase, rather than the amplitude, of the free betatron oscillations.

The transformation from $s/c = 0$ to $s/c = \pi/\omega_s$ is thus given by

$$\begin{bmatrix} \tilde{y}_1 \\ \tilde{y}_2 \end{bmatrix}_{\pi/\omega_s} = \begin{bmatrix} 1 & 0 \\ i\eta_1 & 1 \end{bmatrix}\begin{bmatrix} \tilde{y}_1 \\ \tilde{y}_2 \end{bmatrix}_0 \tag{2.58}$$

where

$$\eta_1 = \frac{\pi Ne^2 W_0}{4m_0\gamma\,\omega_\beta\omega_s}\left[1 + i\frac{4\xi\omega_0\hat{\tau}}{\pi\alpha}\right] . \tag{2.59}$$

This η_1, of course, reduces to (2.34) if $\xi = 0$. Note that now η_1 is complex.

A similar procedure applied to the period $\pi/\omega_s < s/c < 2\pi/\omega_s$ leads to the transformation

$$\begin{bmatrix} \tilde{y}_1 \\ \tilde{y}_2 \end{bmatrix}_{2\pi/\omega_s} = \begin{bmatrix} 1 & i\eta_1 \\ 0 & 1 \end{bmatrix} \begin{bmatrix} \tilde{y}_1 \\ \tilde{y}_2 \end{bmatrix}_{\pi/\omega_s} . \qquad (2.60)$$

As we did before, the stability of the system is determined by the total transformation matrix

$$\begin{bmatrix} 1 & i\eta_1 \\ 0 & 1 \end{bmatrix} \begin{bmatrix} 1 & 0 \\ i\eta_1 & 1 \end{bmatrix} = \begin{bmatrix} 1-\eta_1^2 & i\eta_1 \\ i\eta_1 & 1 \end{bmatrix} .$$

The eigenvalues of this matrix have been obtained before in Eq. (2.36). For a weak beam intensity, $|\eta_1| \ll 1$, the two eigenvalues are

$$\lambda_\pm \approx e^{\pm i\eta_1} . \qquad (2.61)$$

The + mode (- mode) is the mode when the two macroparticles oscillate in phase (out of phase) in the limit of weak beam intensity. The imaginary part of η_1 thus gives a growth rate of the betatron oscillations. We find

$$\tau_\pm^{-1} = \mp \frac{Ne^2 W_0}{2\pi m_0 \gamma \omega_\beta} \cdot \frac{\xi \hat{\tau} \omega_0}{\alpha} . \qquad (2.62)$$

The + mode is damped if $\xi > 0$ and antidamped when $\xi < 0$. The - mode is damped if $\xi < 0$ and antidamped when $\xi > 0$. We conclude from this result that the only value of ξ that assures a stable beam is $\xi = 0$. On the other hand, as we will see much later using a Vlasov equation

technique, the two-particle model has over-estimated the growth rate of the - mode. This consideration, together with the presence of some stabilizing mechanisms such as the radiation damping in electron storage rings, leads us to choose slightly positive values for ξ for rings above transition.

2.7. Coupling of Multiple Bunches

So far we have treated a beam that has only one bunch of particles. In this section, we will consider a beam that has two bunches circulating in the same direction in the accelerator. Each bunch is represented as a point charge Ne and the two bunches are separated by half the accelerator circumference. We will specify the two bunches by indices 0 and 1.

We assume that a transverse m = 1 wake force is functioning. The equations of motion for the two point particles are

$$\ddot{y}_0(t) + \omega_\beta^2\, y_0(t) = \frac{Ne^2}{m_0\gamma}$$

$$\times \sum_k \left[W(kT_0 + T_0/2)\, y_1(t - kT_0 - T_0/2) + W(kT_0)\, y_0(t-kT_0) \right] . \quad (2.63)$$

and another equation with y_0 and y_1 exchanged. The index k sums over all previous revolutions.

Let the two bunches be executing transverse motion in a mode with frequency Ω, i.e.,

$$y_{0,1}(t) = \tilde{y}_{0,1}\, e^{-i\Omega t} \quad . \quad (2.64)$$

The complex quantities $\tilde{y}_{0,1}$ give the amplitudes and phases at a fixed time t, i.e., they are the "snap-shot" quantities rather than quantities observed at a fixed location.

Substituting (2.64) into (2.63) and assuming Ω is close to ω_β, we obtain

$$\begin{aligned}(\Omega - \omega_\beta + \omega_\beta\eta_A)\tilde{y}_0 + \omega_\beta\,\eta_B\,\tilde{y}_1 &= 0\\ \omega_\beta\,\eta_B\,\tilde{y}_0 + (\Omega - \omega_\beta + \omega_\beta\eta_A)\tilde{y}_1 &= 0\end{aligned} \tag{3.65}$$

where we have introduced two dimensionless quantities

$$\begin{aligned}\eta_A &= \frac{Ne^2}{2\omega_\beta{}^2 m_0\gamma}\sum_k W(kT_0)\, e^{i\omega_\beta k T_0}\\ \eta_B &= \frac{Ne^2}{2\omega_\beta{}^2 m_0\gamma}\sum_k W(kT_0 + T_0/2)\, e^{i\omega_\beta (k+1/2)T_0}\end{aligned} \tag{3.66}$$

The only solution to the above pair of equations is the trivial solution $\tilde{y}_0 = \tilde{y}_1 = 0$, unless

$$\det\begin{bmatrix}\Omega-\omega_\beta+\omega_\beta\eta_A & \omega_\beta\,\eta_B\\ \omega_\beta\,\eta_B & \Omega-\omega_\beta+\omega_\beta\eta_A\end{bmatrix} = 0 \quad . \tag{2.67}$$

In other words, in order for a mode to exist at all, Ω must satisfy Eq. (2.67). Solving Eq. (2.67) gives two values for Ω:

$$\Omega_\pm = \omega_\beta(1 - \eta_A \mp \eta_B) \quad . \tag{2.68}$$

Expressed in terms of the transverse impedance, Eq. (2.68) reads

$$\Omega_{\pm} - \omega_{\beta} = - \frac{iNe^2c}{2\omega_{\beta}ET_0^2} \sum_{p=-\infty}^{\infty} [1 \pm (-1)^p] Z(p\omega_0 + \omega_{\beta}) \quad . \qquad (2.69)$$

It follows that the + mode is affected only by the impedance sampled at $p\omega_0+\omega_{\beta}$ with even p's while the - mode is affected only by odd p's. Compared with Eq. (2.12) for a single one-particle bunch, the right hand side contains an extra factor of two but the summation over p is twice more sparse. Note that N is the number of particles per bunch.

Substituting (2.68) into (2.65), we find that the two bunches oscillate in phase for the + mode and out of phase for the - mode, i.e.,

$$\begin{aligned} \bar{y}_0 &= \bar{y}_1 \quad \text{for + mode} \\ \bar{y}_0 &= -\bar{y}_1 \quad \text{for - mdoe} \quad . \end{aligned} \qquad (2.70)$$

For this reason, the + mode is also called the 0 mode and the - mode is called the π mode.

The property (2.70) has a generalization to the case of M equally-spaced, equal-intensity bunches.[26,32] Then there will be M oscillation modes of the bunches; each mode is specified by an index μ which assumes the values $0,1,\ldots,M-1$. The amplitudes of the M bunches, as the whole beam is executing the μ-th mode, are given by

$$\bar{y}_n^{(\mu)} \propto e^{-2\pi i n\mu/M} \quad , \qquad (2.71)$$

where $n = 0,1,\ldots,M-1$ is the index specifying the bunch number. If $M = 2$, (2.71) reduces to (2.70). The oscillation amplitudes y_n in various modes are shown in Fig. 18 for $M = 4$.

Problem 7. Follow the procedure of this section to work out the case for a beam with M equal bunches. Show that the amplitudes of the bunches are given by Eq. (2.71).

Problem 8. Consider a beam with 100 bunches, each affecting only the next bunch through the wake field. Study the stability conditions on the coupled bunch modes. Show that 50 modes are stable and 50 modes are unstable. What happens to those modes and their stability if we remove one bunch from the beam so that the "loop" is broken?[52]

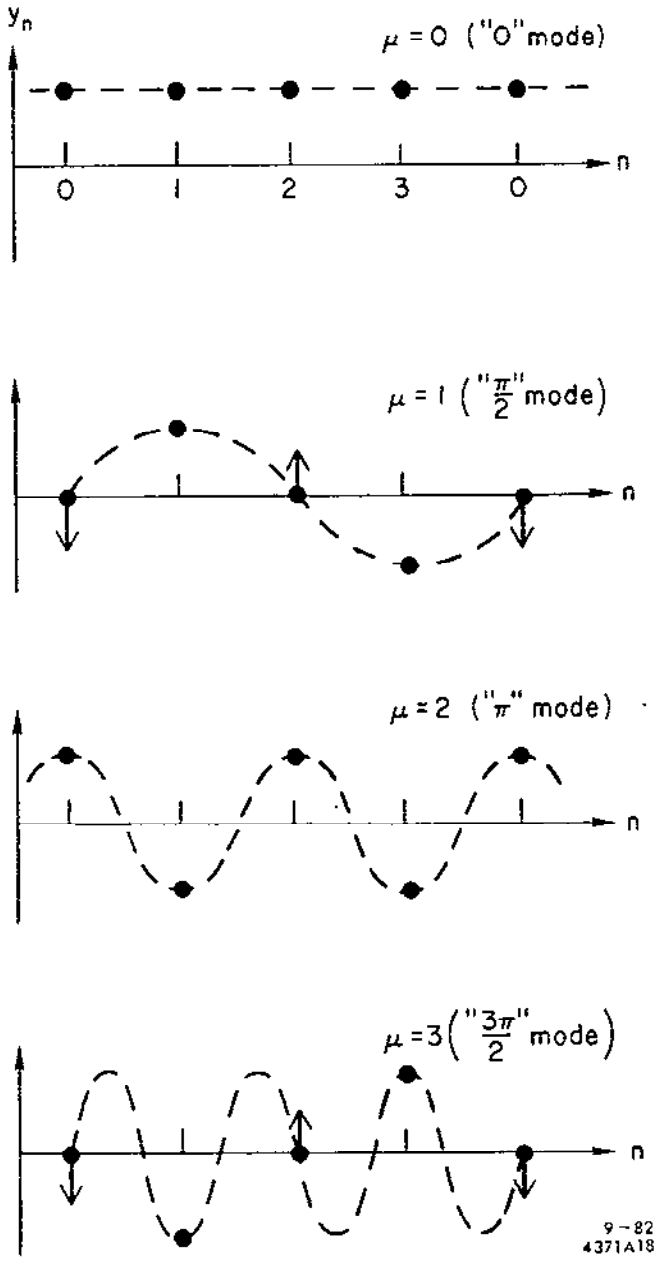

Fig. 18. Coupled bunch modes for a beam with four bunches.

III. PERTURBATION FORMALISM OF BUNCHED BEAM INSTABILITIES

In Section II, we have studied instability mechanisms using highly simplified models in which the particle beam is represented either as a single point charge without any internal structure, or as two point charges interacting with each other through wake fields. This approach offers intuitive pictures of the physics of several coherent instabilities encountered in high intensity accelerators.

However, these simplified models do have their limitations. One limitation is that the quantitative predictions of these models are rather crude.* Another is that the instabilities are treated one by one and it might be desirable to have a more formal treatment that puts these instabilities into one framework. Still another limitation, which is perhaps more serious, is the fact that many instabilities observed in circular accelerators involve higher oscillation modes in the longitudinal structure of the beam. A few of these modes are sketched in Figs. 19(a) and 19(b).[53] (We have used the symbol ℓ to denote the longitudinal mode number. This is not to be confused with the mode number m we have been using for the transverse modes.) Two-particle models clearly do not suffice to study any mode with mode number higher than $\ell = 2$.

---

* To have a more drastic example, substitute the LRC-circuit impedance given in Problem 4 into the frequency shift formula (2.8). The $1/\omega$ tail in the imaginary part of the impedance makes the summation divergent.

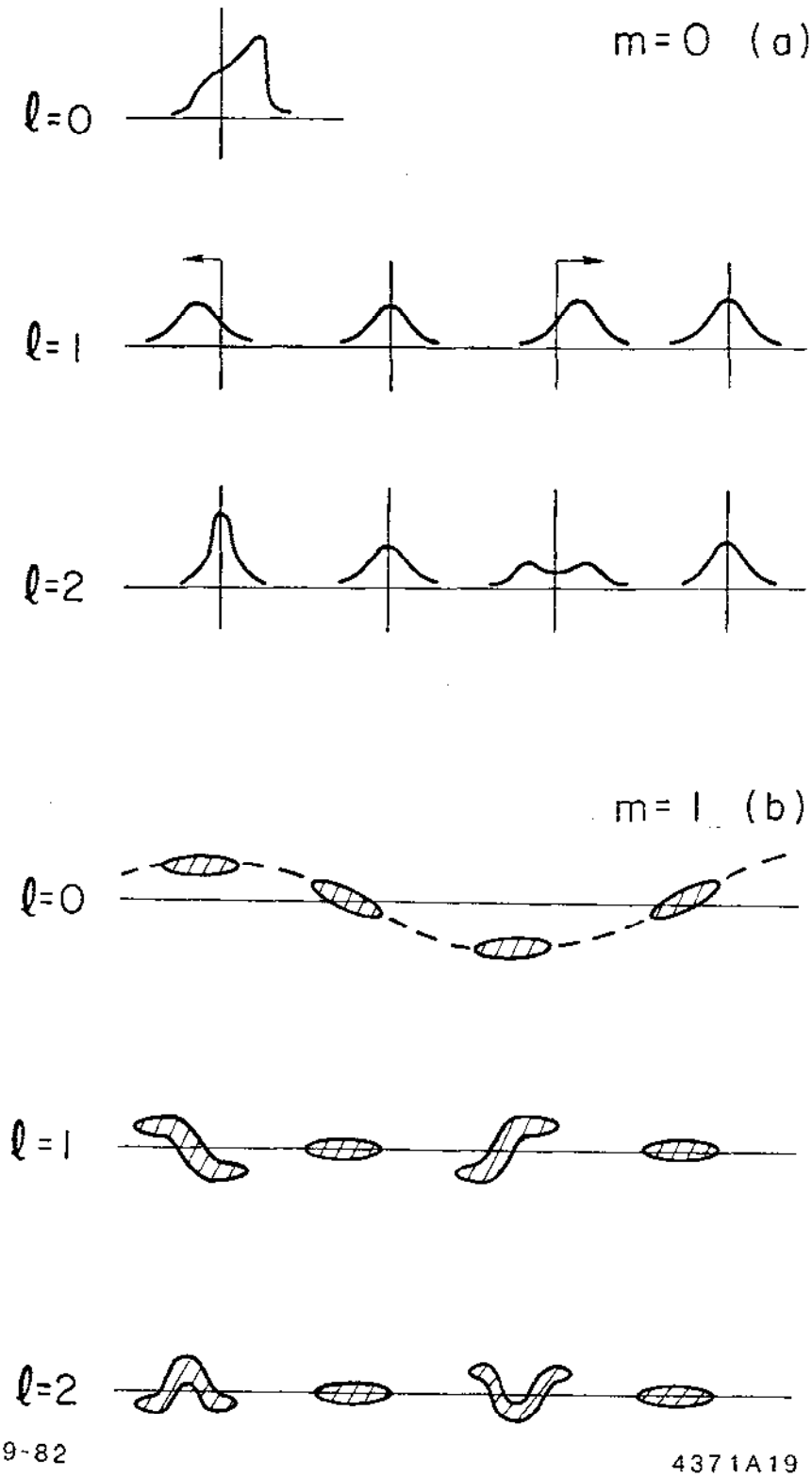

Fig. 19. Sketches of the lowest few modes in the longitudinal structure of the beam. Successive "snapshots" are taken for each mode as the beam executes collective (a) longitudinal (m = 0) and (b) transverse (m = 1) motions. These sketches represent the behavior at low beam intensities. The mode patterns become more complicated as the beam intensity increases. The mode with m = 0 and ℓ = 0 is static.

One could of course increase the number of macroparticles in the model, but as soon as there are more than two macroparticles in the system, the analysis along this line becomes cumbersome. A computer tracking program may be used to extend the model to anywhere from three to a few thousand macroparticles, but dealing with 10^{12} particles this way seems hopeless.

The solution to this difficulty is to go to the other extreme in which ideally one would have infinite number of particles, and then apply the result to our 10^{12}-particle system. In this approach, the motion of the beam is described by a superposition of modes rather than a collection of individual particles.

In principle, the "mode representation" and the "particle representation" of the beam motion are identical. To describe fully 10^{12} particles, one needs 10^{12} modes, and vice versa. The detailed methods of analysis in the two approaches are different -- the particle representation usually is conveniently treated in the time domain, while in the mode representation the frequency domain is more convenient -- but in principle they necessarily give the same final results.

In practice, the mode representation does offer a formalism which can be used systematically to treat the stability problem and, in many cases, be used to obtain analytic results for arbitrarily high mode numbers. The advantage over the particle representation in these respects will become obvious later.

In Section 3.1, the basic mathematical tool, namely the Vlasov equation,[54,55] used for the mode representation of the beam motion will be discussed. This Vlasov technique is applied in all following sections. In Section 3.2, we discuss a phenomenon in which the longitudinal wake field distorts the parabolic potential well formed by the accelerating rf voltage, and as a result, the longitudinal beam distribution gets deformed.[56,57] Such a phenomenon is depicted as the static mode with $m = 0$ and $\ell = 0$ in Fig. 19(a).

From Section 3.3 on, a perturbation treatment of the Vlasov equation that leads to the evaluation of the mode frequencies and mode distributions will be presented. The stability of the beam requires that all modes be stable; if any one of the modes has the potential of growing exponentially, the beam will not be stable. A critical analysis of the modes therefore leads to the stability criterion of the beam. The technique of mode analysis that we will follow was largely developed by Sacherer,[58,59] and supplemented and extended by a number of others.[60-73]

Strictly speaking, in a complete treatment of the beam-environment system, an oscillation mode λ is specified by the quantities

$$\psi^{(\lambda)}, \quad \vec{E}^{(\lambda)}, \quad \vec{B}^{(\lambda)}, \quad \text{and} \quad \Omega^{(\lambda)} \quad ,$$

where $\psi^{(\lambda)}$ is the beam distribution function, $\vec{E}^{(\lambda)}$ and $\vec{B}^{(\lambda)}$ are the electromagnetic wake fields and $\Omega^{(\lambda)}$ is the mode frequency that describes the time dependence. To study such a problem would require setting up and solving the "Vlasov-Maxwell" equations in which $\vec{E}^{(\lambda)}$ and $\vec{B}^{(\lambda)}$ appear in the Vlasov equation as the force terms and $\psi^{(\lambda)}$ appears in the Maxwell

equation as the source term.[55] This solution scheme is difficult to handle, but fortunately it is also not necessary. What we have done in the previous sections has allowed us to express $\vec{E}^{(\lambda)}$ and $\vec{B}^{(\lambda)}$ directly in terms of $\psi^{(\lambda)}$ through the wake functions. After doing so, the number of variables of the problem is greatly reduced and one needs then only to solve the Vlasov equation for $\psi^{(\lambda)}$ without having to pay attention to $\vec{E}^{(\lambda)}$ and $\vec{B}^{(\lambda)}$.

We need first to linearize the Vlasov equation; this will be done in Section 3.3. Modes will be found in Section 3.4. Stability conditions are then discussed in Section 3.5. It turns out that when the beam is unstable, particles will not be lost from the beam but the bunch length and the energy spread of the beam will increase; we will discuss why this occurs also in Section 3.5.

The three Sections 3.3 to 3.5 treat the longitudinal motions. The Sacherer formalism also applies to the transverse dipole motion of the beam. This motion will be treated in Sections 3.6 and 3.7.

3.1. The Vlasov Equation

The Vlasov equation is an equation that describes the collective behavior of a system consisting of a large number of particles under the influence of electromagnetic forces.[54,55] To construct the Vlasov equation, one invariably begins with the single particle equations of motion

$$\begin{aligned} \dot{x} &= f(x, p, t) \\ \dot{p} &= g(x, p, t) \quad . \end{aligned} \tag{3.1}$$

If the system is conservative, i.e., if the system is not influenced by any damping or diffusion due to external sources,* we have the conditions that $f = \partial H/\partial p$ and $g = -\partial H/\partial x$ where H is the Hamiltonian. Therefore,

$$\frac{\partial f}{\partial x} + \frac{\partial g}{\partial p} = 0 \quad . \tag{3.2}$$

The (x,p) plane is called the phase space. The state of a particle is represented as a point in the phase space. We sometimes do not distinguish between the representative point in phase space and the particle itself; although somewhat ambiguous, this should not cause any major confusion. As we will see, the construction of the Vlasov equation is pretty much a technique of drawing boxes in the phase space.

Particles move in phase space. For a particle executing a simple harmonic motion, for example, its representative point in phase space moves in a circle with angular speed ω. If a group of particles all execute simple harmonic motion with the same ω, the distribution of representative points rotate rigidly in phase space. If we arbitrarily draw a box in the phase space and let it rotates with the distribution, there will be no particles leaking into or out of the box.

---

* It is possible that the degrees of freedom of the system are coupled among themselves so that motions in some degrees of freedom grow exponentially at the expense of having some other motions damped. In fact, this possibility of damping and antidamping through internal couplings is the origin of beam instability we are studying. One way of telling whether the damping and antidamping come from an external source or an internal source is to sum over the growth rates of all modes (provided they can be found); the sum should vanish for an internal source. See Problem 13 later.

A similar situation happens for the general motion described by Eq. (3.1). In Fig. 20(a) we have drawn the distribution of a group of particles in the phase space at time t. A rectangular $\Delta x \Delta p$ box is then drawn:

$$A(x, p)$$

$$B(x+\Delta x, p)$$

$$C(x+\Delta x, p+\Delta p)$$

$$D(x, p+\Delta p) \quad .$$

The size of the box is small enough so that the number of particles contained in adjacent boxes -- if they are drawn -- are about equal. On the other hand, the box is large enough so that there are at least several particles inside of it.

Let the number of particles enclosed by the box be

$$\psi(x,p,t)\ \Delta x\ \Delta p \quad ,$$

with ψ the density depending on x, p and t. We will normalize ψ by

$$\int dx \int dp\ \psi(x,p,t) = N \qquad (3.3)$$

with N the total number of particles in the system.

At time t+dt, the box has moved to A'B'C'D' as shown in Fig. 20(b). Note we have used Δx and Δp (rather than dx and dp) to denote the dimensions of the box, and have used dt to denote the time increment.

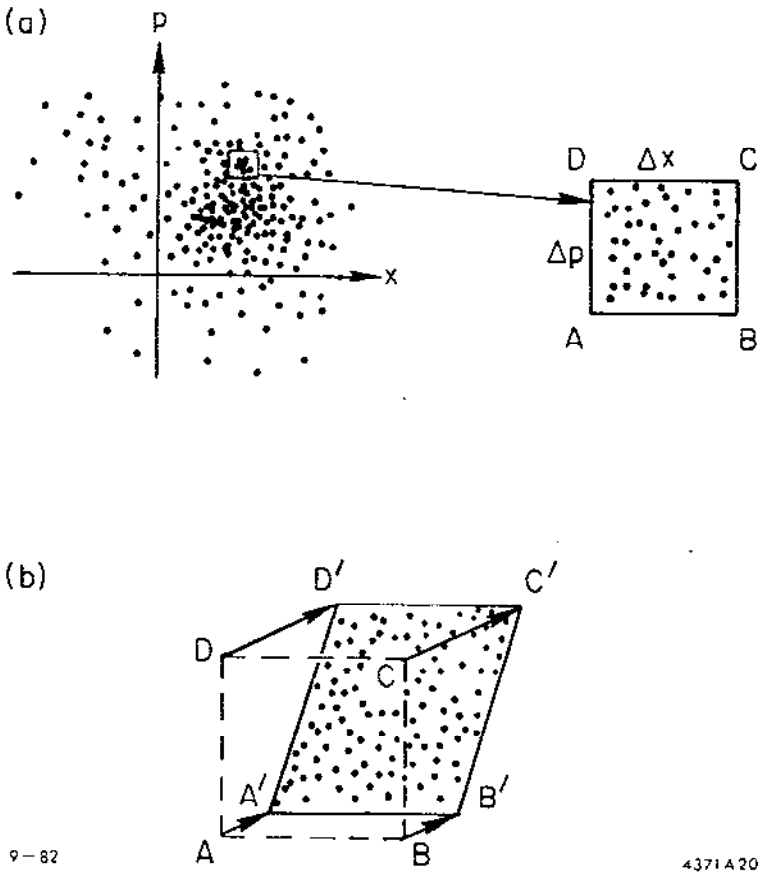

Fig. 20. (a) Phase space distribution of particles at time t. A $\Delta x \Delta p$ box is drawn and magnified. (b) At a later time t+dt, the box moves and deforms. All particles inside the box move with the box.

This is because we do not want the box size to be vanishingly small but dt should be considered truely infinitesimal.

In general, the rectangular box deforms into a parallelogram. The only case in which the box remains rigid in shape as time evolves is the simple harmonic motion discussed before. The vertices of the parallelogram are

$$A' \; [x + f(x,p,t)dt, \; p + g(x,p,t)dt]$$

$$B' \; [x + \Delta x + f(x+\Delta x,p,t)dt, \; p + g(x+\Delta x,p,t)dt]$$

$$C' \; [x + \Delta x + f(x+\Delta x,p+\Delta p,t)dt, \; p + \Delta p + g(x+\Delta x,p+\Delta p,t)dt]$$

$$D' \; [x + f(x,p+\Delta p,t)dt, \; p + \Delta p + g(x,p+\Delta p,t)dt] \quad .$$

The condition that no particles leak into or out of the box now takes the form

$$\psi(x,p,t)\, \text{area}(ABCD) = \psi(x + fdt, \; p + gdt, \; t + dt) \times \text{area}(A'B'C'D') \quad . \tag{3.4}$$

For a Hamiltonian system, we have the condition (3.2), which implies the area of the box is conserved:

$$\text{area}(A'B'C'D') = \left| \overrightarrow{A'B'} \times \overrightarrow{A'D'} \right|$$

$$= \Delta x \, \Delta p \left[1 + \left(\frac{\partial f}{\partial x} + \frac{\partial g}{\partial p} \right) dt \right]$$

$$= \Delta x \, \Delta p = \text{area}(ABCD) \quad . \tag{3.5}$$

Equation (3.4) then gives

$$\psi(x,p,t) = \psi(x+fdt,\ p+gdt,\ t+dt)$$

$$= \psi + \frac{\partial\psi}{\partial x} fdt + \frac{\partial\psi}{\partial p} gdt + \frac{\partial\psi}{\partial t} dt$$

or, after cancelling out ψ on both sides,

$$\frac{\partial\psi}{\partial t} + f \frac{\partial\psi}{\partial x} + g \frac{\partial\psi}{\partial p} = 0 \quad . \tag{3.6}$$

Equation (3.6) is the Vlasov equation -- especially when the forces involved are electromagnetic in origin. It can also be put in the form

$$\psi = \text{constant in time} \quad . \tag{3.7}$$

Equation (3.7), which we somewhat loosely refer to as the Liouville theorem,* states that the local particle density does not change if (an important if) the observer moves with the flow of boxes, but it does not tell how the boxes flow. The Vlasov form (3.6), on the other hand, does not have this problem since it contains explicitly the single particle information f and g.

---

* The Vlasov equation applies to a system of many particles. Strictly, the Liouville theorem applies to an "ensemble" of many systems, each containing many particles. Furthermore, we are ignoring the "collision terms" in Eq. (3.6). When included, we obtain the Boltzmann equation. For a discussion on the Boltzmann equation, as well as discussions on the Vlasov equation and the Liouville theorem, the reader should refer to textbooks on statistical mechanics.[7a]

Problem 9. Solve the Vlasov equation for a simple harmonic motion with $f = \omega p$ and $g = -\omega x$. Show that the general solution is

$$\psi(x,p,t) = \text{any function of } (r,\ \phi+\omega t) \quad ,$$

where r and ϕ are the polar coordinates defined by $x = r\cos\phi$ and $p = r\sin\phi$.

3.2. Potential Well Distortion of Bunch Shape

As a first application of the Vlasov technique, we will study the effect of longitudinal wake fields on a distortion of the equilibrium shape of a particle bunch.[13,56,57] The mechanism is a static one; no part of the beam bunch is executing collective motion. The dynamics of the bunch shape oscillations will be postponed until later sections.

Consider a bunched beam that travels along the axis of the accelerator pipe. We assume the beam does not have any transverse dimension, i.e., the beam is an infinitesimally thin thread. Such a beam does not generate transverse wake fields; only the m = 0 wake is excited by the beam.

As we mentioned before, the Vlasov equation is constructed by first writing down the single particle equations of motion. In the present case, the equations are

$$\begin{aligned} \frac{d}{ds}\tau &= -\frac{\alpha}{c}\delta \\ \frac{d}{ds}\delta &= g(\tau) \quad . \end{aligned} \tag{3.8}$$

The notations are the same as those used in Eq. (2.1) except that here we have used the longitudinal coordinate along the accelerator, s, as the independent variable. The same variable s was used in Section 2.6. We have left the $d\delta/ds$ equation open for the time being, except that we do know g is not a function of δ because the system is Hamiltonian. [See Eq. (3.2).]

The Vlasov equation corresponding to (3.8) is*

$$\frac{\partial\psi}{\partial s} - \frac{\alpha\delta}{c}\frac{\partial\psi}{\partial\tau} + g(\tau)\frac{\partial\psi}{\partial\delta} = 0 \qquad (3.9)$$

where we will set $\partial\psi/\partial s = 0$ since we are looking for a static distribution. The general solution, it turns out, can be written as

$$\psi(\tau,\delta) = \text{any function of } H \quad , \qquad (3.10)$$

where H is given by

$$H = \frac{\delta^2}{2} + \frac{c}{\alpha}\int_0^\tau g(\tau')\,d\tau' \quad . \qquad (3.11)$$

In what follows, we will take ψ to be an exponential function of H, i.e.**

---

* A subtlety arises if one (incorrectly) uses time t, instead of s, as the independent variable. The difference, however, is negligibly small. What happens is that the quantity $Z(\omega')/\omega'$ of Eq. (3.28) later will be replaced by $Z(\omega')/p\omega_0$. See Ref. 70.

** Out of the infinity of possible solutions (3.10), Eq. (3.12) is the only relevant solution for an electron beam. To show that, one needs to modify the Vlasov equation by taking into account the effects of external damping and diffusion to obtain another equation called the Fokker-Planck equation.[75,76] It then follows from the Fokker-Planck equation that (3.12) is indeed the unique solution of the stationary beam distribution. For a proton beam, the distribution does not have to be given by Eq. (3.12), but analysis very similar to this section still applies.

$$\psi = \frac{1}{\sqrt{2\pi}\,\sigma_\delta} e^{-\delta^2/2\sigma_\delta^2} \rho(\tau) \qquad (3.12)$$

with the longitudinal beam shape

$$\rho(\tau) = A_0 \exp\left[-\frac{c}{\alpha\sigma_\delta^2} \int_0^\tau g(\tau')\, d\tau' \right] . \qquad (3.13)$$

In these expressions, σ_δ is the rms relative energy spread, A_0 is a constant determined by the normalization condition $\int d\tau\ \rho = N$. Note that the energy distribution of the beam is always Gaussian, regardless of the form of $g(\tau)$.

Ideally, $g(\tau) = \omega_s^2\tau/\alpha c$ [see Eq. (2.2)]. The equilibrium distribution is then also Gaussian in τ. In the presence of longitudinal wake fields, however, the τ-distribution will be distorted out of a Gaussian shape.

Suppose the wake has dissipated before the beam completes one revolution. We have

$$\begin{aligned} g(\tau) &= \frac{\omega_s^2}{\alpha c}\tau - \frac{e}{T_0 E c} V(\tau) \\ V(\tau) &= eL \int_\tau^\infty d\tau'\ \rho(\tau')\, W(\tau'-\tau) \quad , \end{aligned} \qquad (3.14)$$

where V is the retarding voltage caused by the wake fields; it involves integrating the wake left by all charges in front of the particle under consideration; L is the total length of the pipe structure in which the wake is generated and T_0 is the revolution period.

The H in Eqs. (3.10) and (3.11) is just the Hamiltonian of the system. The second term on the right hand side of (3.11) can be regarded as a potential well term. In the absence of wake effects, the potential well is parabolic, as we expect for simple harmonic motions. The well distorts when wake fields are included.

Substituting (3.14) into (3.13) gives a transcendental integral equation for ρ:

$$\rho(\tau) = A_0 \exp\left[-\frac{\omega_s^2}{2\alpha^2 \sigma_\delta^2}\tau^2 + \frac{e^2 L}{\alpha \sigma_\delta^2 E T_0} \times \int_0^\tau d\tau' \int_{\tau'}^\infty d\tau'' \, \rho(\tau'') \, W(\tau''-\tau') \right] . \qquad (3.15)$$

Obviously this equation is not easy to handle and often needs to be solved numerically. Figure 21 shows one such attempt.[77] The bunch shape calculated according to (3.15) is plotted assuming a given wake function. (See the discussion towards the end of Section 3.5.) The bunch shape is Gaussian at low beam intensities, but clearly distorts as beam intensity is increased. Another feature of Fig. 21 is that the high intensity distributions lean toward the front so that the parasitic energy losses can be compensated by the rf voltage.

It is not clear whether a static solution for ρ satisfying Eq. (3.15) always exists for an arbitrary wake function W. Also being asked is the question of what are the implications when a solution does not exist (for example, does it mean the beam is unstable?) or even if it exists, the numerical convergence of Eq. (3.15) is poor.[78]

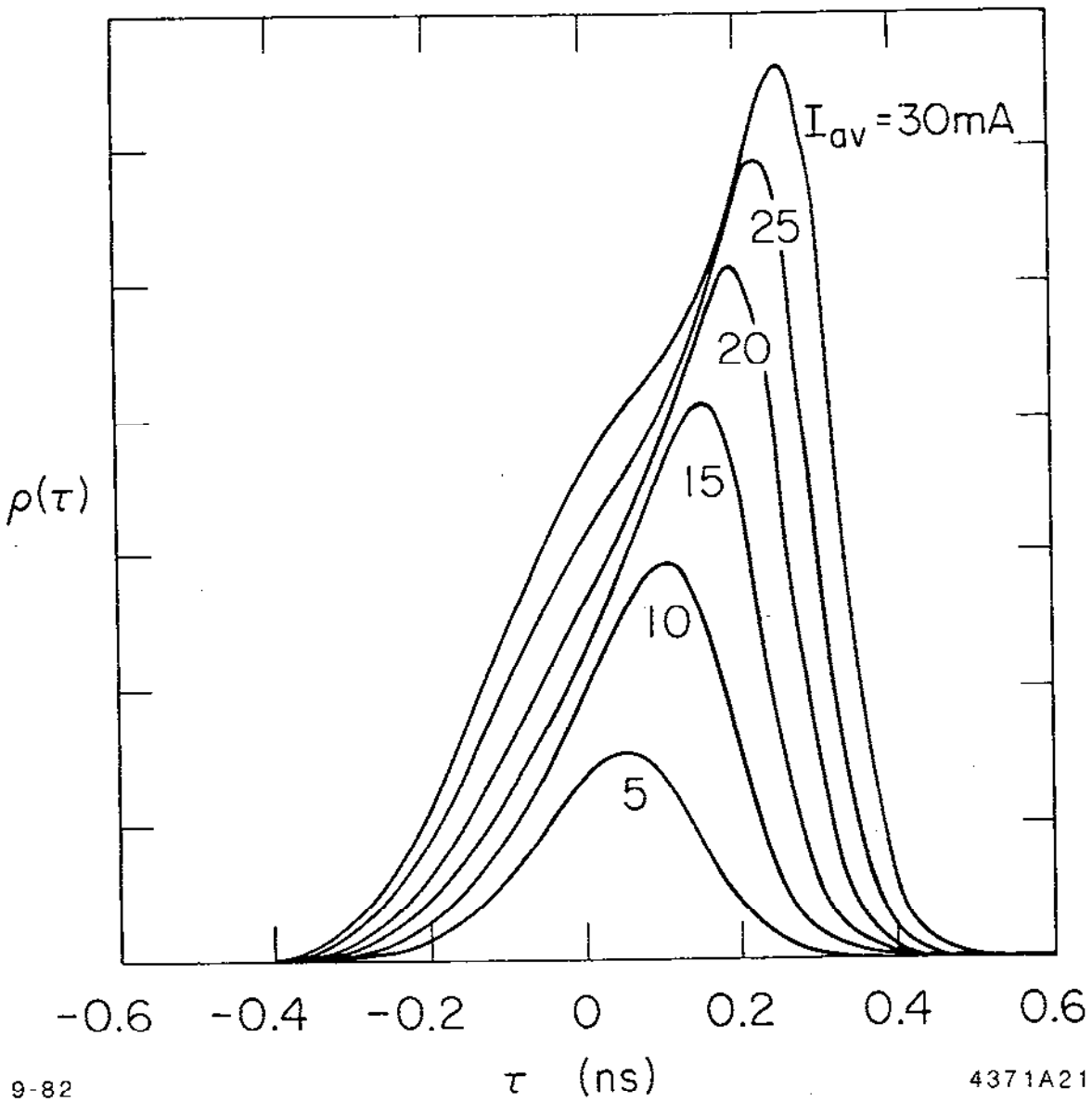

Fig. 21. Potential well distortion of bunch shape for various beam intensities calculated for the storage ring SPEAR. The unit for $\rho(\tau)$ is not specified and I_{av} is the average beam current in the ring.

3.3. Linearization of the Vlasov Equation

On top of the static distortion of the bunch shape, particles execute accidental collective motions. Although they may have only infinitesimal amplitudes originally, these motions grow exponentially under unfavorable conditions. When this happens, the beam is unstable. Some of these instabilities were studied before, using simplified beam models. In this and following sections, the Vlasov technique will be applied to treat this subject. The approach basically follows that of Sacherer's.[58,59] The result contains all the instabilities of Section II as special cases.

Consider again a thread beam. At first, let us switch off the wake field and let the beam have an initial phase-space distribution ψ_0. Being an equilibrium distribution, ψ_0 is only a function of r, i.e.

$$\psi_0 = \psi_0(r) \quad , \tag{3.16}$$

where we have introduced the polar coordinates

$$\begin{aligned} \tau &= r \cos\phi \\ \frac{\alpha}{\omega_s}\delta &= r \sin\phi \quad . \end{aligned} \tag{3.17}$$

Note that r is related to the unperturbed Hamiltonian by $H = \omega_s^2 r^2/2\alpha^2$ and (3.16) follows from (3.10).

Now we turn on the wake fields and suppose there is a disturbance on the distribution so that now we have*

---

* Strictly speaking, ψ_0 now should be given by the potential well distorted distribution. However, to first order in the disturbance, we shall ignore the potential well distortion on ψ_0. As we shall see later, the potential well distortion is just one of the modes -- the one with mode frequency $\Omega = 0$.

$$\psi(r,\phi,s) = \psi_0(r) + \psi_1(r,\phi)\, e^{-i\Omega s/c} \quad . \tag{3.18}$$

We have assumed the disturbance has a single frequency Ω, i.e., it contains contribution from only one single mode of oscillation. We will consider the disturbance to be small.

The mode frequency Ω and the mode distribution ψ_1 are not arbitrary. First, the disturbance ψ_1 generates a wake field. Then, being an oscillation mode, the additional disturbance on the beam distribution caused by this wake must have the same pattern as the original disturbance ψ_1. The beam-wake system therefore has to be solved self-consistently. As a result, only a discrete set of values are possible for Ω and, associated with each value of Ω, there is a well-defined distribution ψ_1. Below, we will show how to obtain these solutions for Ω and ψ_1 using the Vlasov technique.

If we project ψ_1 onto the τ-axis, we get the longitudinal distribution

$$\rho_1(\tau)\, e^{-i\Omega s/c} = \int_{-\infty}^{\infty} d\delta\ \psi_1(r,\phi)\, e^{-i\Omega s/c} \quad . \tag{3.19}$$

This $\rho_1(\tau)$ is the distribution observed at a fixed location (the location of the impedance, for instance) in the accelerator. One revolution before, the beam observed at the same location has a distribution $\rho_1(\tau)\exp[-i\Omega(s/c - T_0)]$ with T_0 the revolution period.

The wake field excited by ρ_1 produces a retarding voltage. The voltage at location s seen by a particle at $c\tau$ is [compare Eq. (3.14)

and see Fig. 22]

$$V(\tau,s) = eL \int_{-\infty}^{\infty} d\tau' \sum_{k=-\infty}^{\infty} \rho_1(\tau')\, e^{-i\Omega[(s/c)-kT_0]}\, W(kT_0+\tau'-\tau) \quad . \tag{3.20}$$

In writing down this expression, we have included the multi-turn wakes and have used the causality property that $W(\tau) = 0$ if $\tau < 0$.

Since we anticipate solving the problem in the frequency domain, we will now introduce the Fourier transform of ρ_1 according to Eq. (1.56) and the Fourier transform of W according to Eq. (1.48). Equation (3.20) then becomes

$$V(\tau,s) = e\omega_0\, e^{-i\Omega s/c} \sum_{p=-\infty}^{\infty} \tilde{\rho}_1(p\omega_0+\Omega)\, e^{i(p\omega_0+\Omega)\tau}\, Z(p\omega_0+\Omega) \tag{3.21}$$

where $Z(\omega)$ is the longitudinal impedance of the accelerator, $\omega_0 = 2\pi/T_0$ and we have made use of the identity (1.60).

Note that the beam distribution observed at a fixed time, i.e. a snapshot, is given by $\rho_1(\tau)\exp[-i\Omega(s/c+\tau)]$. The corresponding frequency spectrum is therefore related to $\tilde{\rho}_1(\omega)$ by

$$\tilde{\rho}_1(\omega)\Big|_{\text{snapshot}} = \tilde{\rho}_1(\omega + \Omega) \quad . \tag{3.22}$$

Had we used the snapshot spectrum in Eq. (3.21), the frequency off-set in the argument of $\tilde{\rho}_1$ drops out.

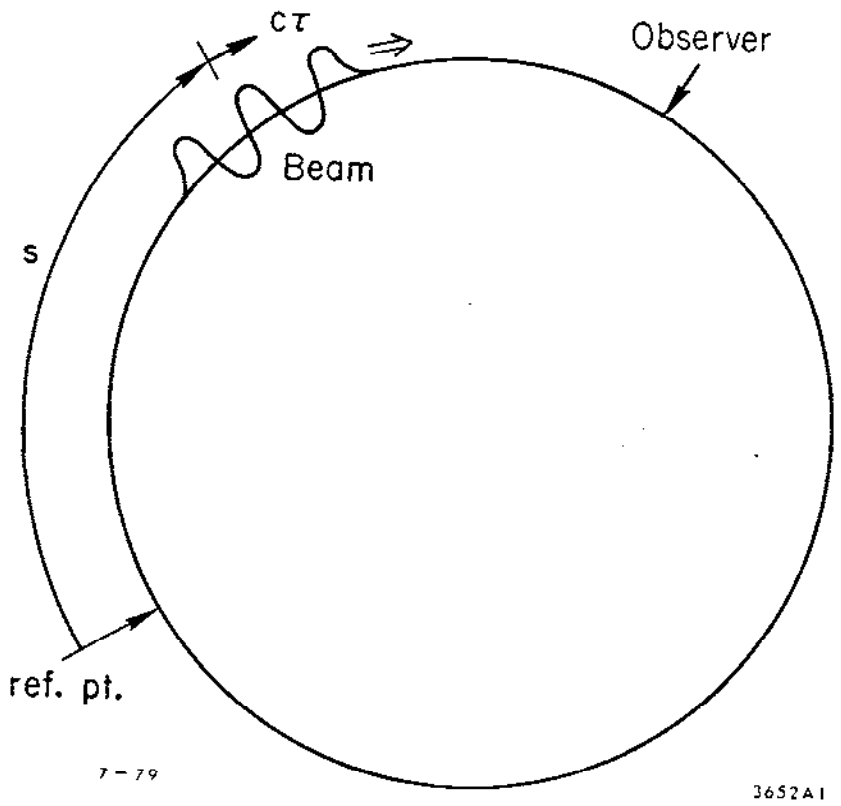

Fig. 22. Disturbance on the beam as observed at a fixed location in a circular accelerator.

Having obtained $V(\tau,s)$, the Vlasov equation (3.9) can be written as

$$\frac{\partial\psi}{\partial s} - \frac{\alpha\delta}{c}\frac{\partial\psi}{\partial\tau} + \frac{\omega_s^2}{\alpha c}\tau\frac{\partial\psi}{\partial\delta} - \frac{e}{T_0Ec}V(\tau,s)\frac{\partial\psi}{\partial\delta} = 0 \quad .$$

The two middle terms can be simplified if we use polar coordinates (3.17), yielding

$$\frac{\partial\psi}{\partial s} + \frac{\omega_s}{c}\frac{\partial\psi}{\partial\phi} - \frac{e}{T_0Ec}V(\tau,s)\frac{\partial\psi}{\partial\delta} = 0 \quad . \tag{3.23}$$

We now substitute (3.18) into the above equation, linearize it by keeping only the first order terms in ψ_1. Remembering that V is already first order* and that ψ_0 depends only on r, we obtain the linearized Vlasov equation

$$-i\Omega\psi_1 + \omega_s\frac{\partial\psi_1}{\partial\phi} - \frac{\alpha e^2\,\omega_0}{T_0E\,\omega_s}\sin\phi\;\psi'_0(r)$$

$$\times\sum_p \tilde{\rho}_1(p\omega_0+\Omega)\,e^{i(p\omega_0+\Omega)\tau}\,Z(p\omega_0+\Omega) = 0 \quad . \tag{3.24}$$

Note that we have linearized with respect to the perturbation ψ_1, not with respect to the impedance or the beam intensity. The impedance and the beam intensity do not have to be small in this linearization procedure.

---

* Actually, ψ_0 also produces a wake field, which means V contains a zeroth order term. Such a term is equivalent to imposing a potential well on the motion of ψ_1; it will be dropped since it is not essential if we only want to study the stability of the beam. However, the potential well does contribute to a frequency shift in ω_s. As a result, all ω_s's from here on should be added a shift $\Delta\omega_s$. See Problem 10 later.

3.4. Longitudinal Modes

Next, let us Fourier expand ψ_1 according to

$$\psi_1(r,\phi) = \sum_{\ell=-\infty}^{\infty} \alpha_\ell R_\ell(r) e^{i\ell\phi} \quad . \tag{3.25}$$

This is possible since ψ_1 must be periodic in ϕ with period 2π. We have used ℓ as the summation index in anticipation that it actually is the longitudinal mode index used in Fig. 19 in the limit of weak beam intensities.

Substituting (3.25) into (3.24), we get

$$-i \sum_{\ell'} \alpha_{\ell'} R_{\ell'}(r) e^{i\ell'\phi} (\Omega-\ell'\omega_s) - \frac{\alpha e^2 \omega_0}{T_0 E \omega_s} \sin\phi \psi'_0(r)$$

$$\times \sum_p \tilde{\rho}_1(\omega') Z(\omega') e^{i\omega' r\cos\phi} = 0$$

where ω' in the summation is an abbreviation for $p\omega_0+\Omega$. Multiply the equation by exp $(-i\ell\phi)$ and integrate over ϕ from 0 to 2π, and repeat it for all values of ℓ. We obtain an infinite set of equations:

$$-i(\Omega-\ell\omega_s) \alpha_\ell R_\ell(r) + \frac{\alpha e^2 \omega_0}{T_0 E \omega_s} \ell i^\ell \frac{\psi'_0(r)}{r} \sum_p \tilde{\rho}_1(\omega') \frac{Z(\omega')}{\omega'} J_\ell(\omega' r) = 0$$

$$\ell = 0, \pm 1, \pm 2, \ldots \quad . \tag{3.26}$$

In (3.26), $J_\ell(x)$ is the Bessel function.* Some properties of the Bessel functions are given in Table III.

We still need an expression for $\tilde{\rho}_1(\omega')$ in Eq. (3.26). This is done below:

$$\tilde{\rho}_1(\omega') = \frac{1}{2\pi}\int_{-\infty}^{\infty} d\tau\, e^{-i\omega'\tau}\, \rho_1(\tau)$$

$$= \frac{1}{2\pi}\int_{-\infty}^{\infty} d\tau \int_{-\infty}^{\infty} d\delta\, e^{-i\omega'\tau}\, \psi_1(r,\phi)$$

$$= \frac{\omega_s}{2\pi\alpha}\int_0^{2\pi} d\phi \int_0^{\infty} r dr\, \exp(-i\omega' r\cos\phi) \sum_{\ell'} \alpha_{\ell'}\, R_{\ell'}(r)\, e^{i\ell'\phi}$$

$$= \frac{\omega_s}{\alpha}\sum_{\ell'}\int_0^{\infty} r dr\, \alpha_{\ell'}\, R_{\ell'}(r)\, i^{-\ell'}\, J_{\ell'}(\omega' r) \qquad (3.27)$$

When (3.27) is substituted into (3.26), we find Sacherer's integral equation for the longitudinal (m = 0) instabilities:

$$(\Omega - \ell\omega_s)\,\alpha_\ell\, R_\ell(r) = -i\,\frac{e^2\omega_0}{T_0 E}\,\ell\,\frac{\psi'_0(r)}{r}\sum_{\ell'}\int_0^{\infty} r'dr'$$

$$\times\, \alpha_{\ell'}\, R_{\ell'}(r')\, i^{\ell-\ell'} \sum_p \frac{Z(\omega')}{\omega'}\, J_\ell(\omega' r)\, J_{\ell'}(\omega' r') \,. \qquad (3.28)$$

---

* One may regard the Bessel functions as nothing more than the sine and cosine functions expressed in polar coordinates.

TABLE III

Some properties of the Bessel functions

$$\frac{1}{2\pi}\int_0^{2\pi} d\phi\, e^{i\ell\phi - ix\cos\phi} = i^{-\ell} J_\ell(x)$$

$$J_\ell(-x) = (-1)^\ell J_\ell(x) = J_{-\ell}(x)$$

$$J_\ell(0) = \delta_{\ell 0}$$

$$\frac{1}{2\pi}\int_0^{2\pi} d\phi\, \sin\phi\, e^{-i\ell\phi + ix\cos\phi} = -i^\ell \frac{\ell}{x} J_\ell(x)$$

$$\int_0^\infty x^{-\alpha} dx\, J_\ell(x)\, J_{\ell'}(x) = \frac{\Gamma(\alpha)\,\Gamma\left(\frac{\ell+\ell'-\alpha+1}{2}\right)}{2^\alpha \Gamma\left(\frac{-\ell+\ell'+1+\alpha}{2}\right)\Gamma\left(\frac{\ell+\ell'+1+\alpha}{2}\right)\Gamma\left(\frac{\ell-\ell'+1+\alpha}{2}\right)}$$

Given the impedance Z and the initial distribution ψ_0, we have to find the $R_\ell(r)$'s and α_ℓ's to satisfy the Sacherer equation. This is not easy to do in general and is currently one important research area; but without losing any essentials, we will proceed by choosing a simplified model of ψ_0, namely

$$\psi_0(r) = \begin{cases} 0 & \text{if} \quad r > \hat{\tau} \\ \dfrac{N\alpha}{\pi\hat{\tau}^2\omega_s} & \text{if} \quad r < \hat{\tau} \end{cases} \quad . \tag{3.29}$$

The impedance, on the other hand, is left to be general.

The distribution (3.29) is called the water-bag model.[58,73] Its phase space distribution and projection onto the τ-axis are shown in Fig. 23. The distribution is normalized so that $\int d\delta \int d\tau\ \psi_0 = N$.

Any perturbation on a water-bag beam will have to occur around the edge of the bag, i.e., around $r = \hat{\tau}$. As a result, all R_ℓ's are δ-functions, i.e.

$$R_\ell(r) = \delta(r - \hat{\tau}) \quad . \tag{3.30}$$

This result also follows from Eq. (3.28) by inspection if we note that $\psi'_0 \propto \delta(r-\hat{\tau})$. Having obtained (3.30), the Sacherer equation (3.28) reduces to a set of equations for the coefficients α_ℓ:

$$(\Omega-\ell'\omega_s)\ \alpha_{\ell'} = i\,\frac{Ne^2\ \alpha\omega_0}{\pi\omega_s\ T_0E\ \hat{\tau}^2}\,\ell' \sum_{\ell''} \alpha_{\ell''}\, i^{\ell'-\ell''}$$

$$\times \sum_p \frac{Z(\omega')}{\omega'}\, J_{\ell'}(\omega'\hat{\tau})\ J_{\ell''}(\omega'\tau) \quad ; \quad \ell' = 0,\pm1,\pm2,\ldots \quad . \tag{3.31}$$

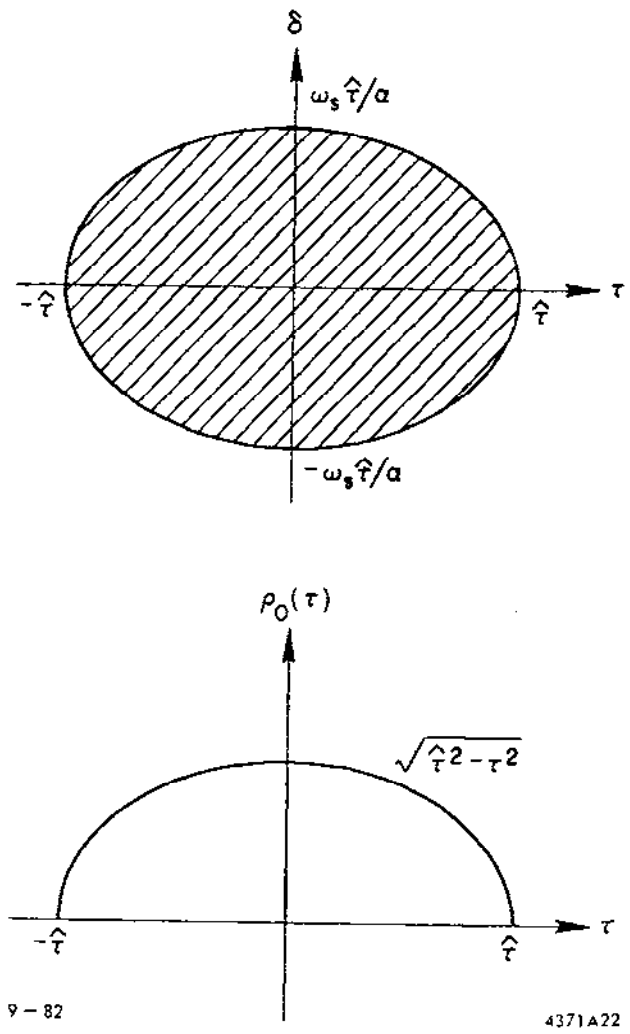

Fig. 23. Phase space distribution and longitudinal distribution of a water-bag beam. For this distribution, $\tau_{rms} = \hat{\tau}/2$.

We are now finally ready to discuss modes. First note that when $N = 0$, i.e., in the zero intensity limit, the solutions to (3.31) are

$$a_{\ell'(\ell)} = \begin{cases} 1 & \text{if} \quad \ell' = \ell \\ 0 & \text{if} \quad \ell' \neq \ell \end{cases}$$

$$\Omega^{(\ell)} = \ell\omega_s \quad , \tag{3.32}$$

where ℓ is an integer specifying the mode number. In other words, the ℓ-th mode is described by

$$\psi_1^{(\ell)} = \underbrace{\delta(r-\hat{\tau})\, e^{i\ell\phi}}_{\text{long. dist.}} \cdot \underbrace{e^{-i\ell\omega_s s/c}}_{\text{time dependence}} \quad . \tag{3.33}$$

These are the modes shown in Fig. 19(a). Projections of these modes onto the τ-axis, without the time dependences, are drawn in Fig. 24.

In case the beam intensity is nonzero but still weak, we can find the ℓ-th mode frequency by substituting the zero-th order solution (3.32) into the right-hand-side of (3.31), i.e.

$$\Omega^{(\ell)} - \ell\omega_s = i \frac{Ne^2 \alpha \omega_0}{\pi\omega_s T_0 E \hat{\tau}^2} \ell \sum_{p=-\infty}^{\infty} \frac{Z(\omega')}{\omega'} J_\ell^2(\omega'\hat{\tau}) \quad , \tag{3.34}$$

where ω' represents $p\omega_0 + \ell\omega_s$.

Some result on instabilities at last! Given the impedance, Eq. (3.34) gives the complex mode frequencies for a water-bag beam with relatively weak intensities. In particular, the real part of Eq. (3.34) gives the

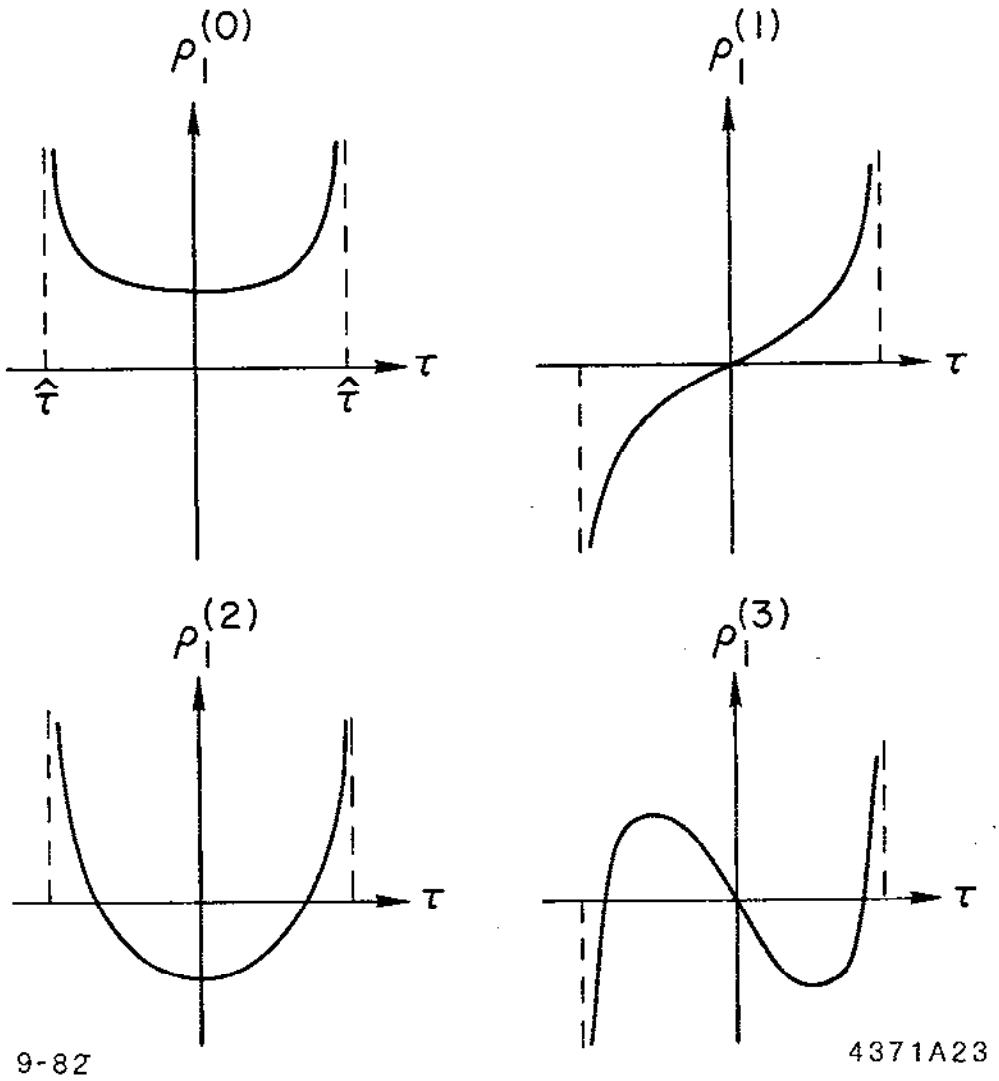

Fig. 24. The longitudinal distribution $\rho_1^{(\ell)}$ of the modes $\ell = 0,1,2,3$ in the zero intensity limit.

mode frequency shift, $\Delta\Omega^{(\ell)}$, while the imaginary part gives the instability growth rate $\tau^{-1(\ell)}$. This result is obviously more powerful than that obtained using one- or two-particle models which are restricted to $\ell \leq 1$ or 2.

One should be careful in obtaining the $\Delta\Omega^{(\ell)}$ from Eq. (3.34) because it does not contain all the contributions. A frequency shift term has been dropped when we linearized the Vlasov equation back in Eq. (3.24). See the footnote there and also Problem 10.

Take the $\ell = 1$ mode as an illustration. Let us assume the beam bunch is short enough so that $\omega'\hat{\tau} \ll 1$. Then $J_1(\omega'\hat{\tau}) \approx \omega'\hat{\tau}/2$ and we have rediscovered the Robinson growth rate,[27] Eq. (2.9). Equation (3.34), when applied to $\ell > 1$, gives the growth rates of the "higher order Robinson effect."

Problem 10. From Eq. (3.14), obtain the frequency shift for small oscillation particles in the potential well:

$$\Delta\omega_s = -\frac{e\alpha}{2T_0E\ \omega_s}\frac{\partial V(\tau)}{\partial\tau}\bigg|_{\tau=0}$$

$$= \frac{e^2\alpha\omega_0^2}{2T_0E\omega_s}\sum_p \tilde{\rho}_0(p\omega_0)p\ \mathrm{Im}\ Z(p\omega_0) \quad .$$

Show that the above $\Delta\omega_s$ gives the first term in the Robinson frequency shift (2.8) by letting $\rho_0(\tau) = N\delta(\tau)$. This potential well frequency shift $\Delta\omega_s$ has been dropped when we linearized the Vlasov equation and, as a result, Eq. (3.34) gives only the second term of (2.8).

The procedure followed in this section resembles closely the perturbation technique used in quantum mechanics. Indeed, since the Bessel function J_ℓ is actually the ℓ-th component of $\tilde{p}_1(\omega')$ [see (3.27)], the right hand side of Eq. (3.31) can be expressed in a quantum mechanical notation:

$$\sum_{\ell''} \langle \ell' \mid Z/\omega \mid \ell'' \rangle \quad . \tag{3.35}$$

It should be mentioned that the water-bag beam is particularly simple since one can readily solve $R_\ell(r)$ in Eq. (3.30). The price we pay here is that all radial structures are degenerate and some information is lost. For more realistic beams (such as a Gaussian beam), the problem becomes more complicated. These complications are not essential for our purposes which are mostly pedagogical. Readers interested in the more complete treatments should study at least Refs. 62 to 69.

In Ref. 69, the results obtained for a water-bag beam are compared with the Gaussian beam results and it is found that they agree rather well numerically, at least for the lowest few modes. This means to some extent the stability criterion does not depend critically on the unperturbed distribution ψ_0. On the other hand, this conclusion is not to be taken for granted. Shown in Figs. 25(a) and 25(b) are two possible unperturbed beam distributions. For an impedance that has a significant high-frequency tail, one can imagine a situation in which a beam with distribution 25(a) is stable while distribution 25(b) is unstable. The significance of the instability of distribution 25(b) is rather limited because after losing the particles in the spike, the beam becomes stable again.

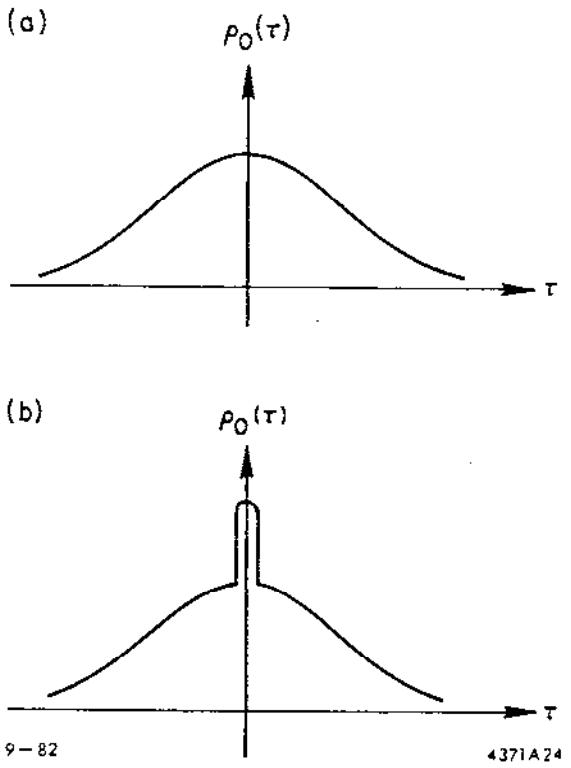

Fig. 25. Two possible unperturbed beam distributions. Distribution (b) has a δ-function spike at the origin. Depending on the impedance, they may have very different stability criteria; but the significance of the difference is rather limited.

3.5. Bunch Lengthening

The only instability that the weak beam result, Eq. (3.34), allows is of the Robinson type. That is, instability occurs only when the impedance consists of sharp peaks like that shown in Fig. 11(b) below cut-off, or equivalently, when the wake field lasts longer than a revolution period. In case the impedance is a smooth function in frequency, i.e., if the impedance is "broad-banded," one can approximate $Z(p\omega_0 + \ell\omega_s)$ by $Z(p\omega_0)$. The right hand side of Eq. (3.34) then becomes purely real. (Remember the real part of the impedance is an even function in frequency.) All modes are, therefore, necessarily stable.

If we further increase the beam intensity, however, Eq. (3.34) breaks down and instabilities will appear even for a broad-band impedance. What happens then is that the frequency shifts are comparable to ω_s so that a linear mixture of several unperturbed modes, Eq. (3.33), is needed to describe a single perturbed mode. Such a phenomenon, sometimes referred to as "mode mixing" or "turbulence",* can lead to instabilities other than the Robinson type.

For a broad-band impedance, we will drop the Ω from the argument of the impedance in Eq. (3.31), i.e., replace ω' by $p\omega_0$. The problem reduces to that of solving for the eigenvalues of a linear system. The eigenvalue Ω is determined by the condition

---

* The term "turbulence" has a well-defined meaning in fluid dynamics. It is not clear how this term gets to be used here, but somehow it has managed.

$$\det\left[M - \frac{\Omega}{\omega_s} I \right] = 0 \tag{3.36}$$

where I is a unit matrix and M is a matrix with elements

$$M_{\ell\ell'} = \ell\delta_{\ell\ell'} + i \frac{Ne^2\alpha}{\pi\omega_s^2 T_0 E \hat{\tau}^2} \ell i^{\ell-\ell'} \int_{-\infty}^{\infty} d\omega \frac{Z(\omega)}{\omega} J_\ell(\omega\hat{\tau}) J_{\ell'}(\omega\hat{\tau}) \,. \tag{3.37}$$

We have replaced the summation over p by an integration. By doing so, we have in effect ignored the multi-turn wakes. Written out explicitly, M has the form

$$M = \begin{bmatrix} \cdots & & & & & & \\ \cdots & & & & & & \\ & 2+I & R & I & R & I & \\ & R & 1+I & R & I & R & \\ & 0 & 0 & 0 & 0 & 0 & \\ & R & I & R & -1+I & R & \\ & I & R & I & R & -2+I & \\ & & & & & & \cdots \\ & & & & & & \cdots \end{bmatrix} \tag{3.38}$$

where the $\ell = 0$ elements all vanish; I's and R's are some real quantities, all different from one another, with I coming from only Im Z and R coming only from Re Z. Note that if we drop all the off-diagonal mode-coupling terms, we will obtain (3.34). Note also that $\Omega = 0$ is always a solution; this is the mode that describes the static potential-well distortion.

Let us proceed again with an example. Let the impedance be given by

$$Z(\omega) = R_0 \left|\omega_0/\omega\right|^{1/2} [1 + i \, \mathrm{sgn}\,(\omega)] \quad , \tag{3.39}$$

where R_0 is a real positive constant. This impedance corresponds to a wake function $W(z) \propto z^{-1/2}$. Then the matrix elements of M are

$$M_{\ell\ell'} = \ell\delta_{\ell\ell'} - \eta \frac{\ell}{2} C_{\ell\ell'} \tag{3.40}$$

with

$$C_{\ell\ell'} = \frac{\Gamma\left(\dfrac{\ell+\ell'-1/2}{2}\right)}{\Gamma\left(\dfrac{\ell'-\ell+5/2}{2}\right)\Gamma\left(\dfrac{\ell+\ell'+5/2}{2}\right)\Gamma\left(\dfrac{\ell-\ell'+5/2}{2}\right)} \begin{cases} (-1)^{[\ell-\ell']/2} & \text{if } \ell-\ell' = \text{even} \\ (-1)^{[\ell-\ell'-1]/2} & \text{if } \ell-\ell' = \text{odd} \end{cases}$$

where we have defined a dimensionless parameter

$$\eta = \frac{Ne^2 \alpha R_0}{\omega_s^2 \, T_0^{3/2} E \, \hat{T}^{3/2}} \quad , \tag{3.41}$$

and $\Gamma(x)$ is the gamma function.* Use has been made of Table III.

We have evaluated numerically the eigenvalues Ω/ω_s using (3.36) with the matrix (3.40). The results for the lowest few modes are shown in Fig. 26.** The mode frequencies Ω/ω_s are plotted against the parameter

---

* Gamma functions are generalized factorials. One is certainly familiar with the factorial of an integer; the gamma function defines how to take factorials of fractional numbers as well.

** Remember these results ignore the shift in ω_s due to potential well distortion.

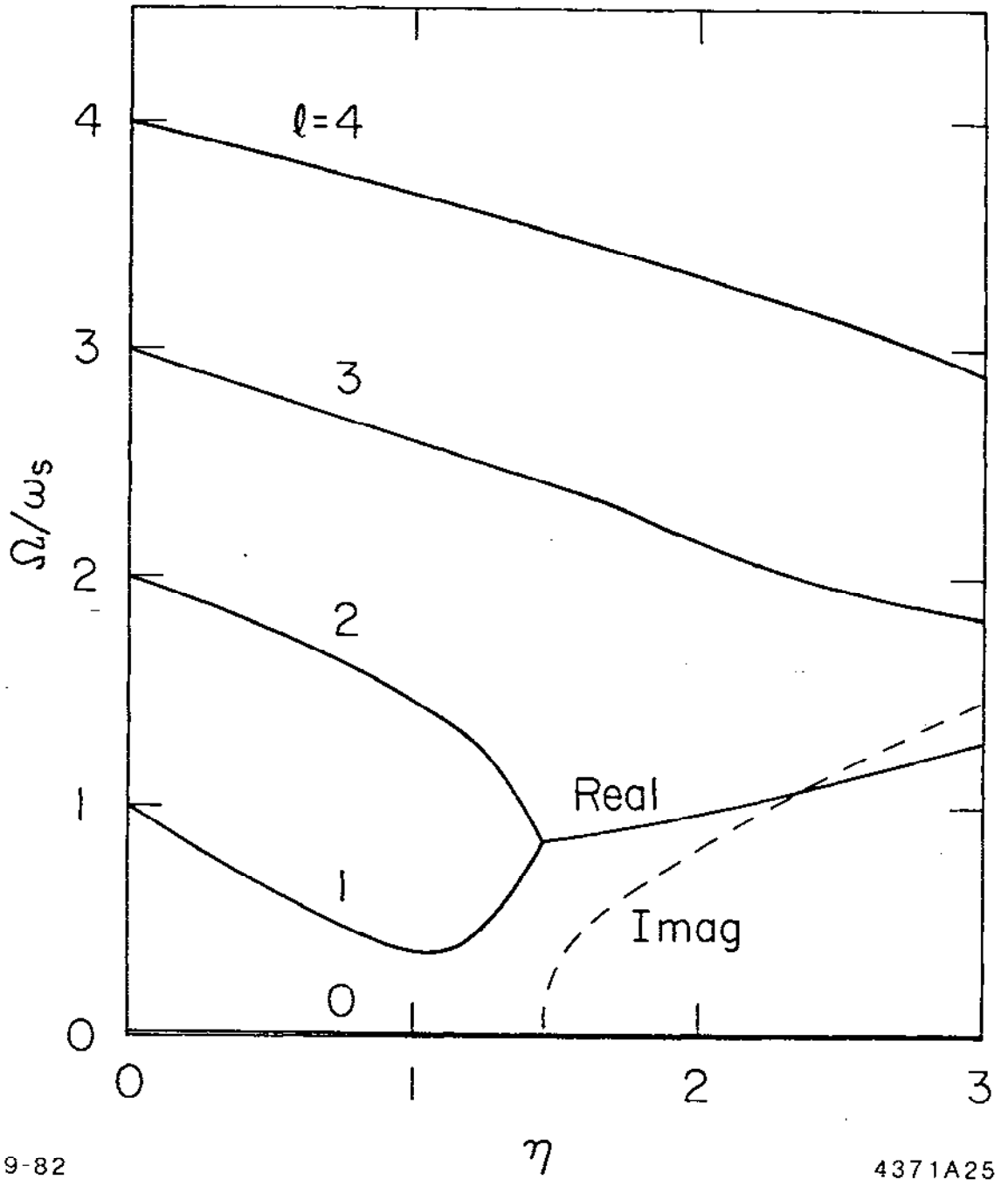

Fig. 26. Longitudinal mode frequencies Ω/ω_s vs the parameter η for a water-bag beam with the impedance (3.39). Instability occurs when $\eta > \eta_{th} \approx 1.45$ and the $\ell = 1$ and $\ell = 2$ mode frequency lines merge and become imaginary. The solid curves give the real part of the mode frequencies while the dashed curve is the imaginary part of the the $\ell = 1$ and $\ell = 2$ mode frequencies above threshold. There is always a static mode with $\Omega/\omega_s = 0$. The spectra for $\ell < 0$ are mirror images with respect to the $\Omega = 0$ line.

η. At $\eta = 0$, the mode frequencies are simply multiples of ω_s. As η increases, the mode frequencies shift. As η reaches the critical value $\eta_{th} \approx 1.45$, two of the mode frequencies become equal; then above η_{th}, they become imaginary and the beam is unstable. The parameter η_{th} thus defines the stability threshold of the beam. Note that the instability growth rate increases sharply as soon as η exceeds η_{th}. This is a general property of the mode mixing instabilities and is sometimes referred to as "phase transition" for the case of a long bunch in which many modes participate.[66,67] See also the discussion at the end of Section 2.4.

The matrix (3.38) has infinite dimensions. The eigenvalues are evaluated with the matrix truncated. For the truncation procedure to converge, the beam spectrum, as well as the impedance, must not have long tails at high frequencies. For a water-bag model, the impedance at high frequencies must decrease with frequency at least as fast as a power law. This impedance (3.39) and also (3.70) and (3.75) later are chosen with these considerations in mind. In case the truncation procedure does not converge, the formalism that follows from the expansion (3.25) breaks down. A better convergence may be achieved by expanding ψ_1 in terms of the "coasting beam" modes that are expressed in the Cartesian coordinates τ and δ,[64-67] instead of the present polar coordinates r and ϕ.

Let us suppose a beam of "natural" bunch length $\hat{\tau}_0$ and intensity N is stored in the accelerator. If the intensity is such that $\eta < \eta_{th}$, the beam is going to keep its length $\hat{\tau}_0$ and not much will happen. But if $\eta > \eta_{th}$, the instability takes over and $\hat{\tau}$ starts to lengthen. An

inspection of (3.41) shows that as the beam lengthens, η drops and when η drops below η_{th}, the beam becomes stable again. In equilibrium, the beam will be lengthened just enough so that η stays at the stability threshold. When this happens, we have

$$\hat{\tau} = \left[\frac{Ne^2 \alpha R_0}{\omega_s^2 T_0^{3/2} E \eta_{th}} \right]^{2/3} . \qquad (3.42)$$

The behavior of bunch length as a function of beam intensity therefore looks like Fig. 27(a). For the impedance (3.39), the curve above the bunch lengthening threshold has $\hat{\tau} \propto N^{2/3}$. Below threshold, we have shown a slight potential-well distortion effect on $\hat{\tau}$.

The change of bunch distribution due to potential-well distortion and that due to instability are distinctly different. In the former case, the energy distribution of the beam is unaffected [see Eq. (3.12)], while in the latter case, the synchrotron oscillation brings the changes in $\hat{\tau}$ rapidly into changes in energy spread $\hat{\delta}$. As a result, the energy spread of the beam behaves like that shown in Fig. 27(b). Below the bunch lengthening threshold, $\hat{\delta}$ is constant; above threshold, $\hat{\delta} \propto N^{2/3}$.

We have been using the impedance (3.39) as an illustration. It turns out that, in general, for a given accelerator with an arbitrary impedance, $\hat{\tau}$ above threshold depends only on the single parameter

$$\xi = \frac{\alpha I_{av}}{\nu_s^2 E} . \qquad (3.43)$$

In other words, the accelerator may be operated with various possible values of the average beam current $I_{av} = Ne/T_0$, momentum compaction

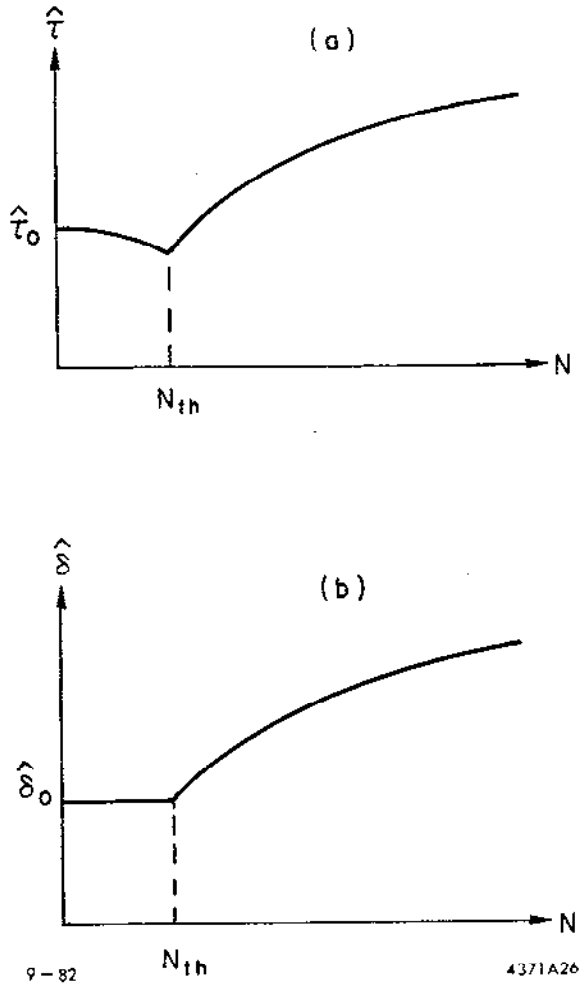

Fig. 27. Bunch length $\hat{\tau}$ and energy spread $\hat{\delta}$ as functions of beam intensity N. Below a certain bunch lengthening threshold N_{th}, $\hat{\tau}$ changes (shortens in the case shown) due to potential-well distortion while $\hat{\delta}$ stays constant. Above N_{th}, both $\hat{\tau}$ and $\hat{\delta}$ increases with N. If impedance is given by Eq. (3.39), then $\hat{\tau}$ and $\hat{\delta}$ are proportional to $N^{2/3}$ in the region $N > N_{th}$.

factor α, synchrotron tune $\nu_s = \omega_s/\omega_0$ and beam energy E, but the bunch length above the lengthening threshold depends only on these factors combined together as given by (3.43). This behavior is called the scaling law and ξ is the scaling parameter.[73,79] Equation (3.42) of course obeys the scaling. Figure 28 shows some experimental data for the storage ring SPEAR.[80] The scaling property of these data is quite obvious.

There is more. It is not difficult to show that if the impedance behaves like

$$Z(\omega) \propto \omega^a \quad , \tag{3.44}$$

then the bunch length above the lengthening threshold will behave with

$$\hat{\tau} \propto \xi^{1/(2+a)} \quad . \tag{3.45}$$

For example, the impedance (3.39) has a = -1/2 and thus $\hat{\tau} \propto \xi^{2/3}$. Figure 28 shows that for SPEAR, $\sigma_z \propto \xi^{0.76}$, from which we deduce that a = -0.68.

The behavior $Z(\omega) \propto \omega^{-0.68}$ for SPEAR of course is valid only in the frequency range of interest, which covers roughly from c/σ_z to a few times c/σ_z. These bunch length data, combined with measurements on the parasitic losses,[80] indicate that the SPEAR impedance looks more or less like that shown in Fig. 29. This impedance is in fact the one used to obtain the potential well distortion shown in Fig. 21.

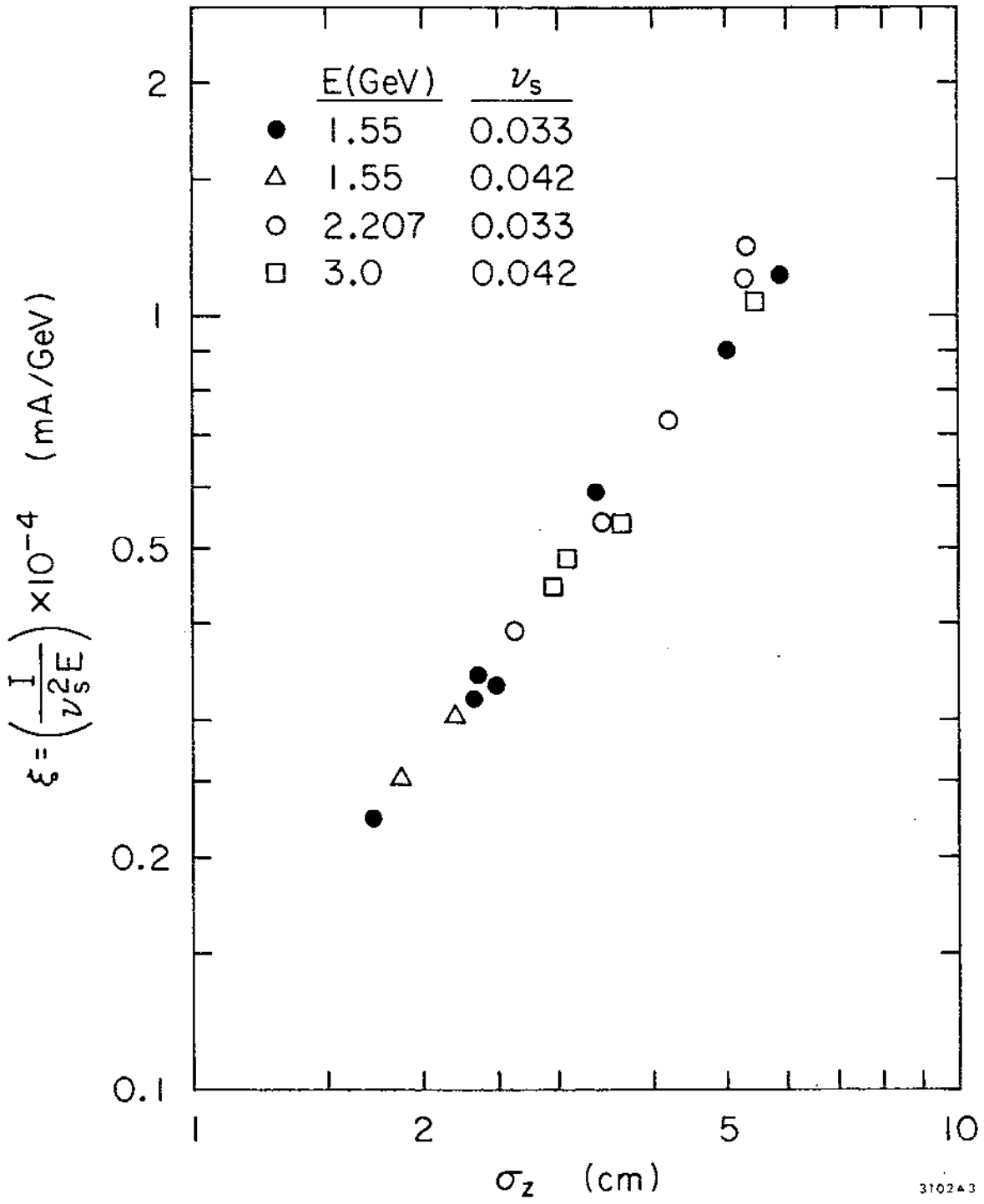

Fig. 28. Bunch length vs the scaling parameter for the storage ring SPEAR. Data are taken above the lengthening threshold. The momentum compaction factor α was kept constant in these experiments and σ_z is the rms bunch length.

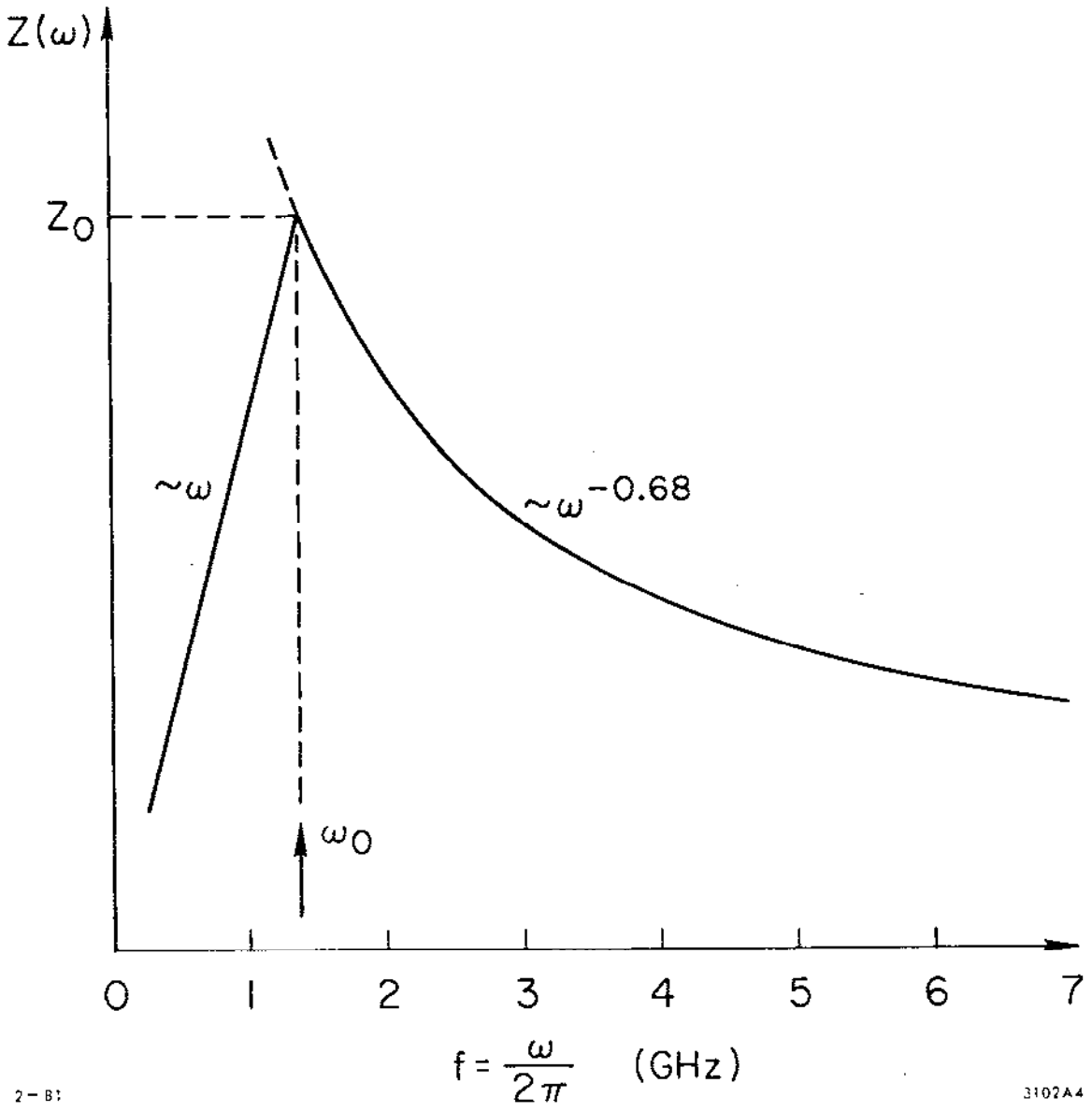

Fig. 29. A sketch of the real part of the SPEAR longitudinal impedance.

3.6. Transverse Modes

By the transverse modes here, we mean those modes with m = 1, i.e., the beam has a dipole moment (pointing, say, in the vertical y-direction) in the transverse plane. The dipole moment is not necessarily constant longitudinally from the bunch head to the bunch tail. Instead, it may go positive and negative and, depending on the longitudinal mode number ℓ, its longitudinal structure may be simple or complicated as sketched in Fig. 19(b).

What we will do in this section is to study these transverse modes. Note that, although called the transverse modes, the transverse structure of these modes is simple (How complicated can a dipole be?) and our main task is in fact to find their longitudinal structures.

It may seem that the problem is going to be much more complicated than the longitudinal case treated in the previous few sections. The Vlasov equation, for example, now needs to take into account both the transverse and the longitudinal phase spaces. Fortunately however, the transverse structure of the beam is simple and can be solved with ease, and the strategy is that, after removing the transverse dimensions from the Vlasov equation, we are left with an equation very similar to Eq. (3.24). The analysis developed for the longitudinal case can then be followed straightforwardly for the transverse case as well.

The phase space distribution $\Psi(y,P_y,\tau,\delta,s)$ satisfies the Vlasov equation

$$\frac{\partial\Psi}{\partial s} + y'\frac{\partial\Psi}{\partial y} + P_y'\frac{\partial\Psi}{\partial P_y} + \tau'\frac{\partial\Psi}{\partial\tau} + \delta'\frac{\partial\Psi}{\partial\delta} = 0 \quad , \tag{3.46}$$

where a prime means taking the derivative with respect to s. The dynamics of the beam is contained in the single particle equations of motion

$$\begin{aligned} y' &= P_y \\ P_y' &= -\left[\frac{\omega_\beta}{c}\right]^2 y + \frac{1}{E}F_y(\tau,s) \\ \tau' &= -\frac{\alpha}{c}\delta \\ \delta' &= \frac{\omega_s^2}{\alpha c}\tau + \frac{y}{cE}\frac{\partial F_y(\tau,s)}{\partial\tau} \end{aligned} \tag{3.47}$$

The quantity F_y is the transverse wake force generated by the dipole moment of the beam, E is the particle energy, ω_β and ω_s are the unperturbed betatron and synchrotron frequencies.

In Eq. (3.47), we have included a wake field term in the δ' equation. It comes from the fact that a dipole moment generates not only a transverse deflection force but also a longitudinal retarding force. (See Table II.) In what follows, however, this term will be dropped. (The system is therefore non-Hamiltonian.) Thus the betatron motion is affected by the wake while the synchrotron motion is treated as unperturbed. This is a good approximation provided the synchro-betatron resonance conditions $\omega_\beta \pm \ell\omega_s = n\omega_0$ are avoided and the transverse beam

size has not grown to become too large. See the discussion following Eq. (2.1) and also Problem 11 later.

We now transform the longitudinal and the transverse coordinates into their polar forms defined by Eq. (3.17) and

$$\begin{aligned} y &= q\cos\theta \\ P_y &= -\frac{\omega_\beta}{c} q\sin\theta \quad . \end{aligned} \tag{3.48}$$

The phase space coordinates are shown in Fig. 30. Equation (3.46) then becomes

$$\frac{\partial\psi}{\partial s} + \frac{\omega_\beta}{c}\frac{\partial\psi}{\partial\theta} + \frac{1}{E} F_y(\tau,s) \frac{\partial\psi}{\partial P_y} + \frac{\omega_s}{c}\frac{\partial\psi}{\partial\phi} = 0 \quad . \tag{3.49}$$

The unperturbed stationary distribution of the beam is a function only of r and q. On top of the unperturbed distribution, we will consider a small perturbation that describes a transverse dipole oscillation mode. The distribution is therefore written as

$$\psi = f_0(q)\, g_0(r) + f_1(q,\theta)\, g_1(r,\phi)\, e^{-i\Omega s/c} \quad , \tag{3.50}$$

where Ω is the mode frequency, f_1 and g_1 describe the transverse and longitudinal beam structures of the mode. As we did for the longitudinal instabilities, our job now is to look for self-consistent solutions for Ω, f_1 and g_1.

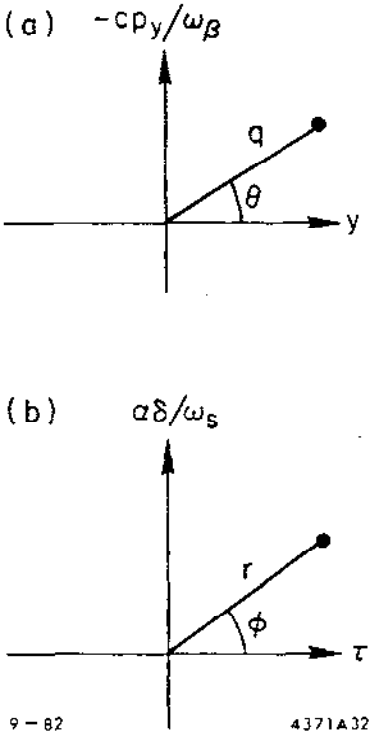

Fig. 30. Phase space coordinates (a) in the betatron plane and (b) in the synchrotron plane. Particles stream in the counter-clockwise direction in both cases.

In writing down (3.50), we have implicitly assumed that the center of the unperturbed beam coincides with the accelerator pipe axis. Effects associated with a distorted beam trajectory (i.e., a distorted closed-orbit) are therefore excluded from our study. We will discuss this again towards the end of Section 3.7. We will also discuss in Section 3.7 the fact that the perturbation distribution factorizes into f_1 and g_1 as given by (3.50).

We next introduce a complication that comes from the head-tail effect discussed in Section 2.6. What happens is that the betatron frequency is not a constant; it actually depends on δ through the chromaticity ξ. The quantity ω_β in (3.49) is therefore replaced by $\omega_\beta + \xi\omega_0\delta$, using Eq. (2.51), where ω_0 is the revolution frequency. Substituting (3.50) into (3.49) and linearize with respect to the perturbation, keeping in mind that F_y is already first order, we find

$$\left\{-i\frac{\Omega}{c} f_1 g_1 + \frac{\omega_\beta+\xi\omega_0\delta}{c}\frac{\partial f_1}{\partial\theta} g_1 + \frac{\omega_s}{c} f_1 \frac{\partial g_1}{\partial\phi}\right\} e^{-i\Omega s/c} - \frac{c}{E\omega_\beta}\sin\theta\, F_y f_0' g_0 = 0 \quad . \tag{3.51}$$

As we mentioned before, the transverse structure f_1 is easy to solve. Indeed, since it describes a dipole motion, we anticipate a solution

$$f_1(q,\theta) = -D\, f_0'(q)\exp(i\theta) \quad , \tag{3.52}$$

where D is the dipole moment of this distribution:

$$\frac{\int y\, f_1 q\, dq\, d\theta}{\int f_0 q\, dq\, d\theta} = D \quad . \tag{3.53}$$

This dipole motion is sketched in Fig. 31.

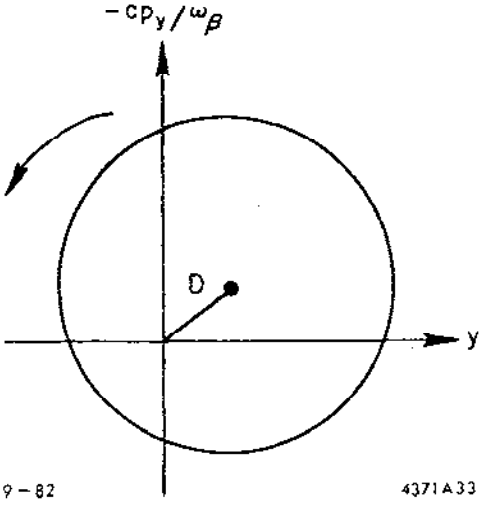

Fig. 31. Dipole motion in the transverse phase space. The unperturbed distribution $f_0(q)$ is displaced by a distance D. The displaced distribution then rotates.

Substitute (3.52) into (3.51) to obtain a reduced Vlasov equation that involves only longitudinal coordinates

$$\left[i(\Omega - \omega_\beta - \xi\omega_0\delta)g_1 - \omega_s \frac{\partial g_1}{\partial \phi} \right] De^{-i\Omega s/c} - \frac{c^2}{2iE\omega_\beta} F_y g_0 = 0 \ . \tag{3.54}$$

In obtaining (3.54), the factor sin θ in Eq. (3.51) has been replaced by exp(iθ)/2i. Rigorously one needs both exp(iθ) and exp(-iθ) components in (3.52), but the exp(-iθ) component can be ignored if the frequency shifts due to the wake field is small compared with the betatron frequency ω_β.

The solution for g_1 can be written as

$$g_1(r,\phi) = \sum_{\ell=-\infty}^{\infty} a_\ell R_\ell(r) e^{i\ell\phi} e^{i\xi\omega_0\tau/\alpha} \ . \tag{3.55}$$

This Fourier expansion is in analogy to Eq. (3.25) except that, due to the chromaticity, we now have an additional head-tail phase factor. The same factor appeared in our two-particle treatment in Section 2.6. From here on, the treatment is very similar to what we did for the longitudinal case.

Substituting (3.55) into (3.54), we find the chromaticity term is cancelled except the phase factor, and we have

$$i \sum_{\ell'} (\Omega-\omega_\beta-\ell'\omega_s)\, a_{\ell'} R_{\ell'}(r) e^{i\ell'\phi} De^{-i\Omega s/c}$$

$$- \frac{c^2}{2iE\omega_\beta} F_y(\tau,s)\, g_0(r)\, e^{-i\xi\omega_0\tau/\alpha} = 0 \ . \tag{3.56}$$

We need to find F_y. The dipole moment of the beam, observed at location s as a function of τ, is

$$De^{-i\Omega s/c}\int_{-\infty}^{\infty} d\delta\; g_1(r,\phi) \;=\; De^{-i\Omega s/c}\,\rho_1(\tau) \quad . \qquad (3.57)$$

The deflecting force is then obtained by summing the wake in all previous revolutions:

$$F_y(\tau,s) \;=\; De^2\int_{-\infty}^{\infty} d\tau' \sum_{k=-\infty}^{\infty} \rho_1(\tau')\, e^{-i\Omega[(s/c)-kT_0]}\, W(kT_0+\tau'-\tau) \quad . \qquad (3.58)$$

The longitudinal counterpart of this expression is Eq. (3.20). The wake function here is of course the transverse one.

Going to the frequency domain, Eq. (3.58) reads

$$F_y(\tau,s) \;=\; i\,\frac{De^2\omega_0}{cT_0}\, e^{-i\Omega s/c} \sum_p \tilde{\rho}_1(\omega')\, e^{i\omega'\tau}\, Z(\omega') \qquad (3.59)$$

where ω' represents $p\omega_0+\Omega$ and $Z(\omega)$ is the total transverse impedance in the accelerator. Substitute (3.59) into (3.56), multiply the result by $\exp(-i\ell\phi)$ and integrate over ϕ from 0 to 2π, we get an infinite set of equations:

$$i(\Omega - \omega_\beta - \ell\omega_s)\,\alpha_\ell\, R_\ell(r) = \frac{ce^2\omega_0}{2E\omega_\beta T_0}\, i^\ell\, g_0(r)$$

$$\times \sum_p \tilde{\rho}_1(\omega')\, Z(\omega')\, J_\ell\left(\omega' r - \frac{\xi}{\alpha}\,\omega_0 r\right) \quad , \ \ell = \text{all integers} \quad . \qquad (3.60)$$

Furthermore, similar to Eq. (3.27), we have

$$\tilde{p}_1(\omega') = \frac{\omega_s}{\alpha} \sum_{\ell} \int_0^{\infty} r dr\, \alpha_\ell\, R_\ell(r)\, i^{-\ell}\, J_\ell\left(\omega' r - \frac{\xi}{\alpha} \omega_0 r \right) \quad . \tag{3.61}$$

Note that the chromaticity has caused a shift in the spectrum $\tilde{p}_1$ and in Eqs. (3.60) and (3.61). Equations (3.60) and (3.61) form Sacherer's integral equations for m = 1.

To proceed further, we will assume a simple model of the longitudinal distribution, namely[46,58]

$$g_0 = \frac{N_\alpha}{2\pi\omega_s \hat{\tau}} \delta(r-\hat{\tau}) \quad . \tag{3.62}$$

In this distribution, shown in Fig. 32, particles populate an elliptical ring in the phase space. This is called a hollow-beam model, or an "air-bag" model.

The advantage of using the air-bag model is obvious; all R_ℓ's degenerate into $\delta(r-\hat{\tau})$, i.e., we have Eq. (3.30) and consequently Eq. (3.60) reduces to

$$(\Omega - \omega_\beta - \ell'\omega_s)\alpha_{\ell'} = -i \frac{Ne^2 c}{2ET_0{}^2\omega_\beta} \sum_{\ell''} \alpha_{\ell''}\, i^{\ell'-\ell''}$$

$$\times \sum_p Z(\omega')\, J_{\ell'}\left[\omega'\hat{\tau} - \frac{\xi}{\alpha}\omega_0\hat{\tau}\right] J_{\ell''}\left[\omega'\hat{\tau} - \frac{\xi}{\alpha}\omega_0\hat{\tau}\right] , \ \ell' = 0, \pm 1, \pm 2, \ldots \quad . \tag{3.63}$$

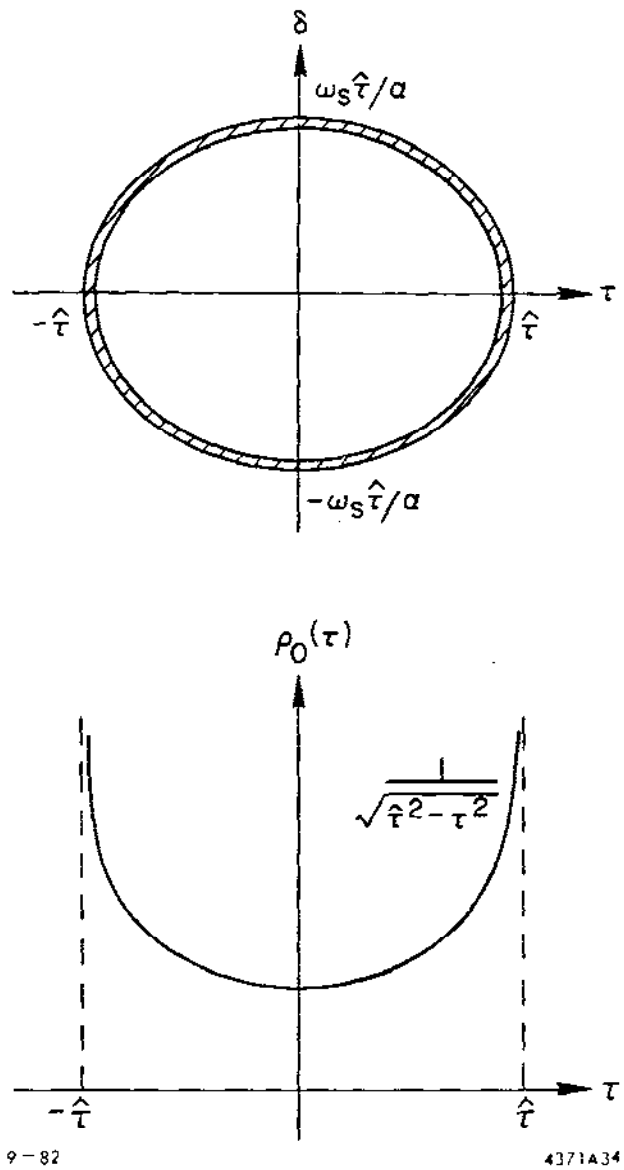

Fig. 32. Phase space distribution and the longitudinal distribution of a hollow beam, or an "air-bag" beam. For this distribution, $\sigma_{rms} = \hat{\tau}/\sqrt{2}$.

A mode is now specified by the mode frequency $\Omega^{(\ell)}$ and the set of coefficients $a_{\ell',(\ell)}$, where ℓ is the mode index. In the absence of the wake field, the right hand side of (3.63) vanishes; the ℓ-th mode is described by

$$a_{\ell',(\ell)} = \begin{cases} 1 & \text{if} \quad \ell' = \ell \\ 0 & \text{if} \quad \ell' \neq \ell \end{cases} \tag{3.64}$$

$$\Omega^{(\ell)} = \omega_\beta + \ell\omega_s \quad .$$

The distribution of this mode is given by

$$\underbrace{f'_0(q)e^{i\theta}}_{\text{trans. dist.}} \cdot \underbrace{\delta(r-\hat{\tau})e^{i\ell\phi}}_{\text{long. dist.}} \cdot \underbrace{e^{i\xi\omega_0\tau/\alpha}}_{\text{head-tail phase factor}} \cdot \underbrace{e^{-i(\omega_\beta+\ell\omega_s)s/c}}_{\text{time dependence}} \quad . \tag{3.65}$$

These modes, without the head-tail phase factor, are those sketched in Fig. 19(b). The longitudinal projection onto the τ-axis of these modes are the same as those shown in Fig. 24 if $\xi = 0$.

In case of a weak beam intensity and frequency shifts small compared with ω_s, one can obtain the first order perturbation by substituting (3.64) into the right hand side of (3.63) to obtain

$$\Omega^{(\ell)} - \omega_\beta - \ell\omega_s = -i \frac{Ne^2c}{2ET_0{}^2\omega_\beta} \sum_{p=-\infty}^{\infty} Z(\omega') \, J_\ell{}^2\left(\omega'\hat{\tau} - \frac{\xi}{\alpha}\omega_0\hat{\tau} \right) , \tag{3.66}$$

where $\omega' = p\omega_0 + \omega_\beta + \ell\omega_s$. Again, the real part of this expression gives the mode frequency shifts and the imaginary part gives the instability growth rate.

Problem 11. The wake term in the δ' equation of Eq. (3.47) was dropped. To see the significance of this term, let us keep it but drop the wake term in the P_y' equation. Follow closely this section, assume f_0 = Gaussian and g_0 = water-bag. Show that

$$f_1 = D \frac{qf_0}{\sigma_y^2} e^{i\theta}$$

and that

$$(\Omega-\omega_\beta-\ell'\omega_s)\alpha_{\ell'} = i \frac{Ne^2c\omega_0}{2\pi E T_0 \omega_s} \alpha \left(\frac{\sigma_y}{c\hat{\tau}} \right)^2 \ell' \times \sum_{\ell''} \alpha_{\ell''} i^{\ell'-\ell''} \sum_p \frac{\omega' Z(\omega')}{\omega' - \xi\omega_0/\alpha} J_{\ell'} J_{\ell''} .$$

Compare with (3.63). Show that this wake effect can be ignored if σ_y is small compared with $\sqrt{\omega_s/\alpha\omega_\beta}$ times the bunch length $c\hat{\tau}$.

If there is a longitudinal impedance Z'' present, one can also compare the above result with Eq. (3.31). Show that this effect can be ignored if $Z(\omega)$ is much less than $cZ''(\omega)/\omega\sigma_y^2$. If $Z''(\omega)$ is related to $Z(\omega)$ through Eq. (1.58), then the criterion becomes $\sigma_y \ll b$. Both the conditions $\sigma_y \ll c\hat{\tau}\sqrt{\omega_s/\alpha\omega_\beta}$ and $\sigma_y \ll b$ are fulfilled in most accelerators.

Problem 12. Consider an air-bag beam executing mode (3.65). Show that the center-of-mass of the beam as a whole has an oscillation amplitude proportional to $J_\ell(\xi\omega_0\hat{\tau}/\alpha)$. Therefore, if $\xi = 0$, a pickup electrode will see only the $\ell = 0$ mode, but all modes show up if the head-tail phase $\xi\omega_0\hat{\tau}/\alpha$ becomes substantial.

3.7. Transverse Instabilities

Let us first consider the weak beam result (3.66). The $\ell = 0$ mode describes a rigid-beam mode in which the dipole moment of the beam does not have an oscillating longitudinal structure. In the limit of a short bunch length, we have for the $\ell = 0$ mode

$$\Omega^{(0)} - \omega_\beta = -i \frac{Ne^2c}{2ET_0{}^2\omega_\beta} \sum_p Z(p\omega_0 + \omega_\beta) \quad . \tag{3.67}$$

This result has been obtained before in Eq. (2.12) using a one-particle model. As pointed out in Section 2.2, Eq. (3.67) leads to the transverse Robinson instability if the impedance has sharp peaks with widths $\Delta\omega \lesssim [\omega_\beta]$, where $[\omega_\beta]$ is the betatron frequency modulus the revolution frequency ω_0, and it also leads to the resistive wall instability studied by Courant and Sessler in Ref. 32.

Equation (3.66) is more general than Eq. (2.12) in two ways. First, it can be applied to the $\ell \neq 0$ modes as well, and secondly, it contains the chromaticity information that leads to the head-tail instability. Obviously a sharply peaked impedance would introduce transverse Robinson

instabilities in the $\ell \neq 0$ modes. What is interesting nevertheless, is the head-tail instability. To study that, let us consider a broad band impedance (single turn wake field) so that the summation in (3.66) can be approximated by an integral. The growth rate then reads

$$\tau^{-1}(\ell) = -\frac{Ne^2c}{4\pi ET_0\omega_\beta}\int_{-\infty}^{\infty} d\omega' \ \mathrm{Re}\ Z(\omega')\ J_\ell{}^2\left[\omega'\hat{\tau} - \frac{\xi}{\alpha}\omega_0\hat{\tau}\right] . \qquad (3.68)$$

The real part of the transverse impedance, Re Z, is odd in ω. If $\xi = 0$, the integral vanishes and there will be no instability. For finite but small ξ, Eq. (3.68) becomes, keeping only a first order term in the head-tail phase $\xi\omega_0\hat{\tau}/\alpha$,

$$\tau^{-1}(\ell) = \frac{Ne^2c}{\pi ET_0\omega_\beta}\cdot\frac{\xi}{\alpha}\omega_0\hat{\tau}\int_0^\infty d\omega\ \mathrm{Re}\ Z(\omega)\ J_\ell(\omega\hat{\tau})\ J'_\ell(\omega\hat{\tau}) . \qquad (3.69)$$

As an illustration, let us consider an impedance that gives rise to a constant wake (2.28), namely

$$Z(\omega) = cT_0W_0\left[\frac{1}{\omega} - i\pi\delta(\omega)\right] . \qquad (3.70)$$

The integration in (3.69) can be performed using Table III, yielding the head-tail instability growth rate

$$\tau^{-1}(\ell) = \frac{Ne^2c^2W_0}{\pi E\ \omega_\beta}\cdot\frac{\xi}{\alpha}\omega_0\hat{\tau}\cdot\frac{2}{\pi(4\ell^2-1)} . \qquad (3.71)$$

The same result was obtained in Ref. 48. One can compare (3.71) with the result (2.62) obtained using the two-particle model. The present expression is clearly superior in that it gives the growth rate for all modes. Note that the two-particle model predicts $\tau^{-1}(1) = -\tau^{-1}(0)$, while

in the present model $\tau^{-1(1)}$ is suppressed by the form factor $1/(4\ell^2-1) = 1/3$.

According to (3.71), the $\ell = 0$ mode is unstable if $\xi < 0$ and the higher order modes are unstable if $\xi > 0$. This behavior is model dependent. If the impedance is different from (3.70) or if the head-tail phase is not small compared with unity, this conclusion may change. Figure 33 shows the growth rates $\tau^{-1(\ell)}$ versus $\xi\omega_0\hat{\tau}/\alpha$ for $\ell = 0, \pm 1$ and ± 2 assuming the impedance is given by (3.70). Equation (3.71) gives only the linear portion of these curves for small $\xi\omega_0\hat{\tau}/\alpha$.

Problem 13. From Eq. (3.68), show that

$$\sum_{\ell=-\infty}^{\infty} \tau^{-1(\ell)} = 0 \quad .$$

That is, the sum of the growth rates and damping rates of all modes is zero. In other words, the existence of damped modes implies the existence of at least one antidamped mode, and vice versa. This result is valid for arbitrary impedance and head-tail phase.

Problem 14. The imaginary part of the impedance (3.70) gives rise to a mode frequency shift. Show that

$$\Delta\Omega^{(\ell)} = -\frac{Ne^2c^2W_0}{4E\ \omega_\beta} J\ell^2 \left[\frac{\xi}{\alpha} - \omega_0\hat{\tau} \right] \quad .$$

For small ξ, the only mode that suffers a frequency shift is $\ell = 0$; the shift is negative and is almost independent of ξ.

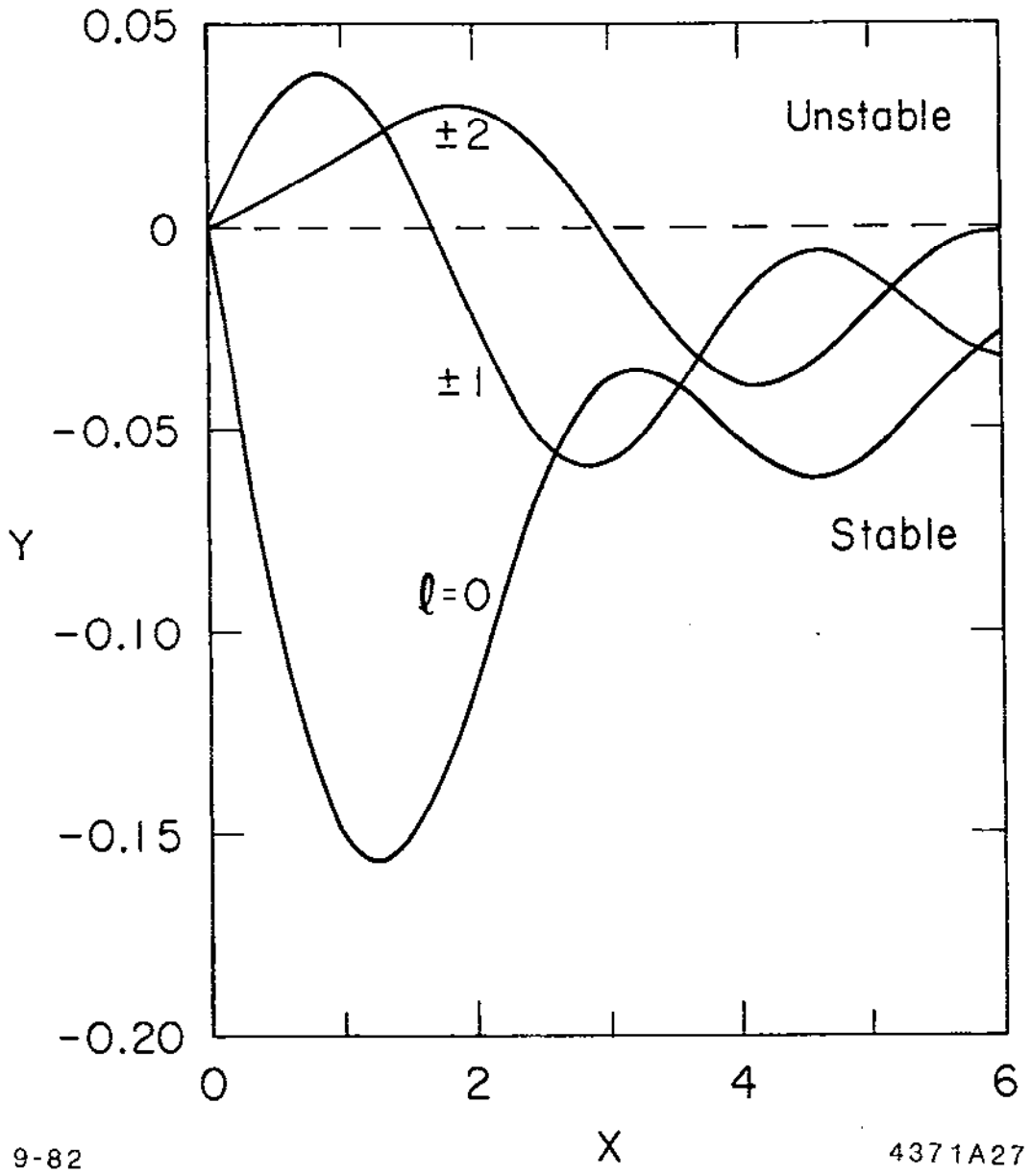

Fig. 33. The growth rate $\tau^{-1}(\mathcal{R})$ versus the head-tail phase $x = \xi\omega_0\hat{\tau}/\alpha$ for the impedance (3.70). The vertical axis y is $\tau^{-1}(\mathcal{R})$ normalized by $Ne^2c^2W_0/E\omega_\beta$. For $x < 0$, τ^{-1} can be obtained using the fact that τ^{-1} is an odd function of x.

As the beam intensity increases, expression (3.66) breaks down. One has to consider the general case described by Eq. (3.63). A mode therefore is no longer approximately given by Eq. (3.64). Instead, it has to be described as a linear mixture of all the unperturbed modes. This phenomenon has been referred to as "mode mixing,"[62,63,68-70] "transverse turbulence"[71] and "strong head-tail",[46] depending on the authors. The associated instability mechanism has been illustrated by a two-particle model in Section 2.4.

Consider a broad-band impedance and $\xi = 0$. Equation (3.63) can be written as an eigenvalue problem, i.e.,

$$\det\left\{ M - \frac{\Omega-\omega_\beta}{\omega_s} I \right\} = 0 \quad , \tag{3.72}$$

which is the same as Eq. (3.36) except for a shift in Ω by ω_β. The matrix elements of M are

$$M_{\ell\ell'} = \ell\delta_{\ell\ell'} - i \frac{Ne^2c}{4\pi E T_0 \omega_\beta \omega_s} i^{\ell-\ell'} \int_{-\infty}^{\infty} d\omega\, Z(\omega)\, J_\ell(\omega\hat{\tau})\, J_{\ell'}(\omega\hat{\tau}). \tag{3.73}$$

The form of the matrix M looks like

$$M = \begin{bmatrix} \cdots & & & & & & \\ \cdots & & & & & & \\ & 2+I & R & I & R & I & \\ & R & 1+I & R & I & R & \\ & I & R & I & R & I & \\ & R & I & R & -1+I & R & \\ & I & R & I & R & -2+I & \\ & & & & & & \cdots \\ & & & & & & \cdots \end{bmatrix} \qquad (3.74)$$

The symbols are the same as those used in Eq. (3.38). Note that, unlike Eq. (3.38), the $\ell = 0$ row does not vanish. The elements of M are all real.

We will illustrate by an example. Take the impedance

$$Z(\omega) = \frac{2c}{b^2\omega_0} R_0 \left| \frac{\omega_0}{\omega} \right|^{3/2} [\mathrm{sgn}(\omega) + i] \quad . \qquad (3.75)$$

This impedance is related to the longitudinal impedance (3.39) through the relationship (1.58). The transverse wake function associated with (3.75) is $W(z) \propto z^{1/2}$. Substituting (3.75) into (3.73), we find

$$M_{\ell\ell'} = \ell\delta_{\ell\ell'} + \frac{n'}{4} C_{\ell\ell'} \quad , \qquad (3.76)$$

where $C_{\ell\ell'}$ are the coefficients given by Eq. (3.40) and η' is a dimensionless parameter related to the longitudinal scaling parameter η, Eq. (3.41), by

$$\eta' = \eta \left[\frac{c\hat{\tau}}{b} \right]^2 \frac{\omega_s}{\alpha\omega_\beta} \quad . \tag{3.77}$$

As a rough estimate of whether the longitudinal or the transverse instabilities dominate the beam behavior, we can compare η and η'. If $\eta' > \eta$, the beam stability threshold is probably determined by the transverse instability, while if $\eta' < \eta$, the longitudinal instability has a lower threshold.*

Figure 34 shows the results of a numerical calculation using Eq. (3.72) and the matrix (3.76). The eigenvalues $(\Omega-\omega_\beta)/\omega_s$ are plotted versus the transverse scaling parameter η' for several ℓ's. At $\eta' = 0$, the mode frequencies are located at ω_β, $\omega_\beta \pm \omega_s$, $\omega_\beta \pm 2\omega_s$, etc. As η' increases, the mode frequencies shift and at $\eta' \approx 0.28$, the two modes $\ell = 0$ and $\ell = -1$ become degenerate. At this value of η', the other modes have shifted only slightly. Further increase of η' makes the beam unstable. The threshold $\eta'_{th} = 0.28$ is substantially lower than the longitudinal threshold $\eta = 1.45$ found in Section 3.5.

---

* As an alternative to (3.77), one can write $\eta'/\eta = 4\sigma_z\sigma_\delta\beta_z/b^2$, where σ_z is the rms bunch length, σ_δ is the rms relative energy spread, β_z is the beta-function at the location of the transverse impedance. The replacement of ω_β by $1/\beta_z$ occurs because we have assumed a smooth focusing while in a real accelerator, the focusing contains a weight function β.

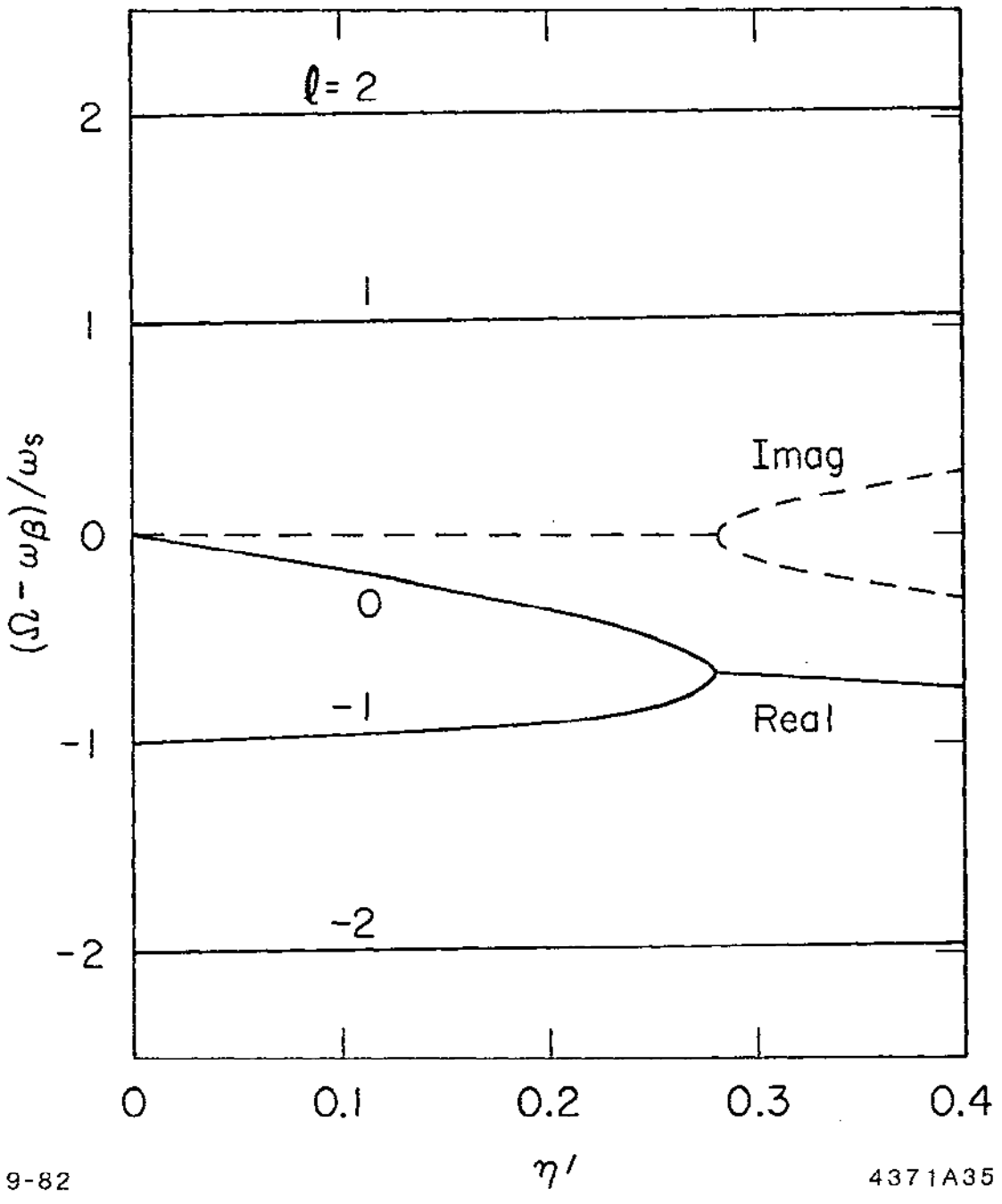

Fig. 34. Transverse mode frequencies $(\Omega-\omega_\beta)/\omega_s$ versus the parameter η' for an air-bag beam with the impedance (3.75). Instability threshold is located at $\eta' \approx 0.28$ where the modes $\ell = 0$ and -1 become degenerate. The dashed curves give the imaginary part of mode frequencies for $\ell = 0$ and -1.

It may seem that the beam is more stable for shorter bunch lengths since $\eta' \propto \hat{\tau}^{1/2}$, but this is very model dependent. For a different impedance, the reverse may turn out to be true. The scaling with respect to the other parameters, on the other hand, is not model dependent. For example, for a given accelerator and given bunch length $\hat{\tau}$, the threshold beam intensity obeys*

$$N_{th} \propto \omega_s \omega_\beta E \quad . \tag{3.78}$$

The same scaling is obeyed by the two-particle analysis, Eqs. (2.34) and (2.37), as it should.

Problem 15. Show that for the impedance (3.70), the matrix M has the elements

$$M_{\ell\ell'} = \ell\delta_{\ell\ell'} + \frac{\eta_1}{\pi^2}\begin{cases} \dfrac{4}{\pi(\ell^2-\ell'^2)} & \text{if } \ell-\ell' = \text{odd} \\ -\pi\delta_{\ell 0}\delta_{\ell' 0} & \text{if } \ell-\ell' = \text{even} \end{cases} ,$$

where η_1 is the parameter defined by (2.34) when we studied the two-particle model using the same impedance. Using the two-particle model, we obtained Fig. 16. Using the matrix M above, we obtain Fig. 35. Compare the two figures.

---

* An alternative to Eq. (3.78) is $I_{th} \propto \nu_s E/\beta_Z$ for a given bunch length, where I_{th} is the threshold beam current, $\nu_s = \omega_s/\omega_0$ is the synchrotron tune.

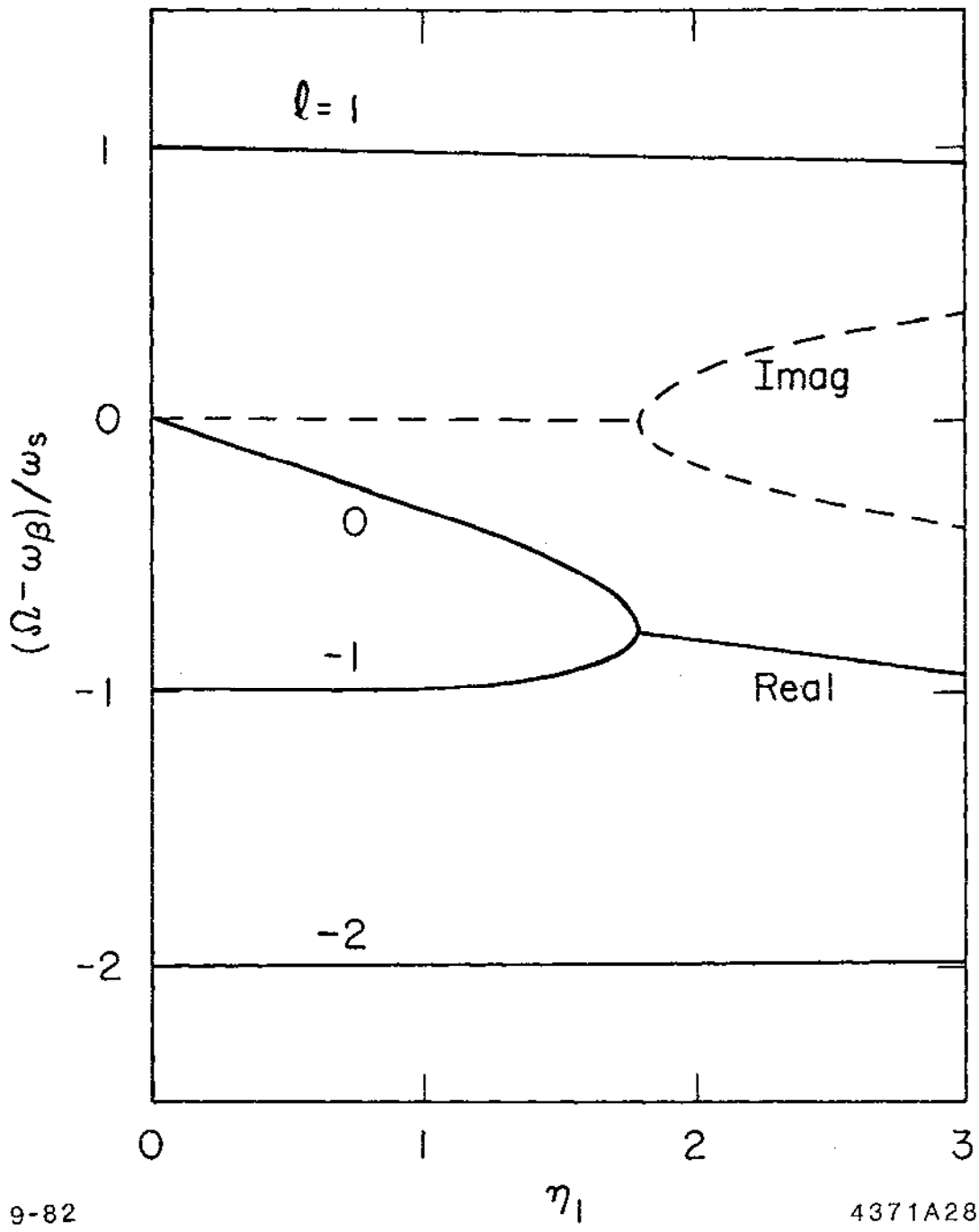

Fig. 35. Transverse mode frequencies $(\Omega-\omega_\beta)/\omega_s$ versus the parameter η_1 for an air-bag beam with impedance (3.70). The instability threshold is located at $\eta_1 \approx 1.8$. At the threshold, the $\ell = 0$ mode frequency has shifted down from ω_β by $\sim 0.8\ \omega_s$. The dashed curves are the imaginary part of the mode frequencies for $\ell = 0$ and $\ell = -1$.

In both Figs. 34 and 35, the $\ell = 0$ mode frequency shifts downward as η' increases from 0. This in fact is a general behavior for short bunches regardless of the details of the impedance. What happens is that the transverse wake force produced by an off-axis beam has the polarity that the beam is deflected further away from the pipe axis. (See discussions following Table II.) This force therefore acts as a defocusing force and as a result the rigid beam mode (the $\ell = 0$ mode) frequency shifts downward. (See also Problem 14.) For experimental observation of this effect, see Refs. 81 and 82 for instance. For long bunches, this property is not necessarily true because the transverse wake function $W(z)$ may change its polarity at some finite z.

Recall that in the longitudinal case, as the beam becomes unstable, the bunch lengthens without losing beam particles. The same thing does not happen in the transverse case. As soon as the threshold is crossed, beam particles will be lost, at least according to the linear theory.

Aside from this apparent difference, however, the transverse and longitudinal instabilities are almost exactly parallel. For each longitudinal effect, there is a transverse analogue, and vice versa. For example, we have mentioned that the Robinson instability has its transverse counterpart and that at high beam intensities, both the longitudinal and the transverse cases have the mode coupling instabilities.

One may ask then if there is a head-tail instability in the longitudinal case and if there is a transverse counterpart of the potential well distortion. The answer to both questions is yes. The

longitudinal head-tail instability[83] results from the fact that the momentum compaction factor α is not strictly a constant; it depends on the instantaneous energy error δ just as the betatron frequency ω_β does. The longitudinal beam distribution then acquires a head-tail phase and instability may arise as a result.

The transverse analogue of the potential well distortion comes from having the unperturbed beam off-centered from the accelerator pipe axis.[84] Such a displacement of the unperturbed beam may come from a closed-orbit error caused by imperfections of the accelerator magnets. The transverse wake field associated with the closed-orbit error deflects the bunch tail by a fixed amount every time the beam passes by the impedance. The result is that the beam is distorted into a banana shape and this distortion is static in time.

In the most general description, Sacherer's equation (3.28) for $m = 0$ and (3.60) for $m = 1$ are part of a grand scheme in which modes with different m's and ℓ's are all coupled together. To study the beam stability, one then has to solve the eigenvalue problem of a doubly infinite matrix, of which we have separately studied only the $m = 0$ and the $m = 1$ components. In reality, as long as the mode frequency shifts are small compared with ω_β, the matrix degenerates into blocks, each with a distinct value of m. If the mode frequency shifts are small even compared with ω_s, further degeneracy occurs and indeed we obtain results like Eqs. (3.34) and (3.66). The factorization of the perturbation distribution into f_1 and g_1 in Eq. (3.50) is the result of assuming the mode frequency shifts are small compared with ω_β.

3.8. Multi-Bunch Instabilities

In the previous sections, we have assumed that there is only one bunch of particles in the accelerator. We will now show that with a slight modification, the analysis can be applied to a beam of M bunches, provided the bunches are equally spaced and equally populated.

Consider first the longitudinal instabilities. A mode of the multi-bunch beam is described by

$$\psi_n(r,\phi,s) = \psi_0(r) + \psi_1(r,\phi)\exp\left[-i\Omega\left(\frac{s}{c} + \frac{nT_0}{M}\right)\right]\exp\left[-2\pi i\,\frac{n\mu}{M}\right]$$

$$n = 0, 1, \ldots, M-1 \quad , \tag{3.79}$$

where ψ_n is the distribution function of the n-th bunch observed at a fixed location s, ψ_0 is the unperturbed distribution normalized by $\int d\tau \int d\delta\ \psi_0 = N$ = number of particles per bunch, ψ_1 is the perturbation distribution (same for all n's), μ is the multi-bunch mode index that assumes the values $0,1,\ldots,M-1$. Successive bunches oscillate with a phase difference of $2\pi\mu/M$ if the phases are compared at a given time so that bunches are separated by distances cT_0/M. When $M = 1$, Eq. (3.79) reduces to (3.18). The mode number μ and the phase factor $\exp(-2\pi i n\mu/M)$ have been discussed in Section 2.7.

We will concentrate on the reference bunch for which $n = 0$. The wake voltage seen by particles in this bunch is

$$V(\tau,s) = eL \int_{-\infty}^{\infty} d\tau' \sum_{k=-\infty}^{\infty} \rho_1(\tau')$$

$$\times \sum_{n=0}^{M-1} \exp\left[-i\Omega\left(\frac{s}{c} + \frac{nT_0}{M} - kT_0\right) - 2\pi i \frac{n\mu}{M}\right] W\left[kT_0 - \frac{nT_0}{M} + \tau' - \tau\right] . \quad (3.80)$$

Compared with Eq. (3.20), this expression contains an additional summation over the M bunches. The quantity ρ_1 is the projection of Ψ_1 onto the τ-axis; it has been defined in Eq. (3.19). In the frequency domain, Eq. (3.80) reads

$$V(\tau,s) = Me\omega_0 \, e^{-i\Omega s/c} \sum_{p=-\infty}^{\infty} \tilde{\rho}_1(\omega') \, e^{i\omega'\tau} \, Z(\omega') \quad (3.81)$$

where

$$\omega' = Mp\omega_0 + \mu\omega_0 + \Omega \quad . \quad (3.82)$$

Compared with Eq. (3.21), Eq. (3.81) has an additional factor of M in front but the summation over p is M times more sparse.

We then follow the procedures of Sections 3.3 and 3.4 to set up and linearize the Vlasov equation for the 0-th bunch. For a waterbag distribution (3.29), we obtain again Eq. (3.31) with the modifications that the right hand side is multiplied by M and that ω' is replaced by (3.81). A similar result was obtained in Eq. (2.69).

The Robinson instability occurs if the impedance has a sharp peak (i.e., long wake field) at $\omega_R \approx (Mp+\mu)\omega_0$. For the accelerating cavities, the fundamental mode peaks at $\omega_R \approx h\omega_0$, where h is the harmonic number

and is necessarily an integral multiple of M. This means the most important Robinson instability (or Robinson damping) occurs for the $\mu = 0$ mode in which all bunches oscillate in phase. Under these conditions, the growth rate is proportional to M, i.e., it is determined essentially by the total beam current, not the single bunch current.

For a broad-band impedance (i.e., short wake field), the summation over p is replaced by an integral. The replacement removes the factor of M in front and one obtains results identical to the single bunch results Eqs. (3.36) and (3.37). This is not surprising since broad-band impedance means the wake force is short-ranged and instability is a result of a local interaction among particles in a single bunch.

Treatment of the transverse motion of a multi-bunch beam is again very similar. For an air-bag beam, for example, one obtains Eq. (3.63) with the same modifications as for the longitudinal case. Similar discussions on instability also apply.

ACKNOWLEDGEMENTS

In the preparation of the manuscript, I have enjoyed and benefited from numerous discussions with Matthew Allen, Karl Bane, Richard Cooper, Andrew Hutton, Norman Kroll, Phillip Morton, Helmut Wiedemann, and Perry Wilson. Phillip Morton has also contributed in clarifying the manuscript on several occasions. Karl Bane also provided Figs. 8 and 10, and Tom Knight provided Fig. 33. The analysis of the quadrupole instability of Section 2.5 was done in cooperation with Semyon Kheifets. Richard Cooper carefully proofread the manuscript. I am very grateful for their generous help.

REFERENCES

1. J. D. Jackson, "Classical Electrodynamics," 2nd edition, Wiley, New york, 1975.

2. L. Landau and E. Lifshitz, "The Classical Theory of Fields," Pergamon, New York, 1975.

3. P. L. Morton, V. K. Neil and A. M. Sessler, J. Appl. Phys. 37, 3875 (1966).

4. M. J. Lee, F. E. Mills and P. L. Morton, SLAC Report 76 (1967).

5. A. Piwinski, DESY Report 72/72 (1972).

6. M. J. Lighthill, "Introduction to Fourier Analysis and Generalized Functions," Cambridge University Press, Cambridge, 1958.

7. P. B. Wilson, 1981 Summer School on High Energy Particle Accelerators, AIP Proc. 87, p. 450.

8. K. W. Robinson, Storage Ring Summer Study, SLAC Report 49 (1965), p. 32.

9. W. K. H. Panofsky and W. A. Wenzel, Rev. Sci. Instrum. 27, 967 (1956).

10. G.A. Voss and T. Weiland, DESY Report M-82-10 (1982), unpublished.

11. R. J. Briggs, T. J. Fessenden and V. K. Neil, IX International Conference on High Energy Accelerators, SLAC, 1974, p. 278.

12. T. Lockner and M. Friedman, IEEE Trans. Nucl. Sci. NS-26, 4237 (1979).

13. A. Papiernik, M. Chatard-Moulin and B. Jecko, Proceedings of the IX International Conference on High Energy Accelerators, SLAC, 1974, p. 375.

14. A. W. Chao and P. L. Morton, SLAC Report PEP-105 (1975), unpublished.

15. B. Zotter, SLAC Report PEP-310 (1979), unpublished.

16. M. Chatard-Moulin and A. Papiernik, IEEE Trans. Nucl. Sci. 26, 3523 (1979).

17. R. K. Cooper, S. Krinsky and P. L. Morton, Part. Accel. 12, 1 (1982).

18. S. Kheifets, Proceedings of the XI International Conference on High Energy Accelerators, Geneva, 1980, p. 586.

19. H. G. Hereward, CERN/ISR-DI/75-47 (1975), unpublished.

20. E. Keil, Nucl. Instrum. Methods 100, 419 (1972).

21. K. Halbach and R. Holsinger, Part. Accel. 7, 213 (1976).

22. K. Bane and B. Zotter, Proceedings of the XI International Conference on High Energy Accelerators, Geneva, 1980, p. 581.

23. T. Weiland, Proceedings of the XI International Conference on High Energy Accelerators, Geneva, 1980, p. 570.

24. T. Weiland, DESY Report 82-015 (1982).

25. J. Mathews and R. L. Walker, "Mathematical Methods of Physics," 2nd Edition, W. A. Benjamin, New York, 1970, p. 131.

26. B. Zotter and F. Sacherer, Proceedings of the International School of Particle Accelerators, Erice, 1976, CERN 77-13, p. 175.

27. K. Robinson, CEAL Report TM-183 (1969), unpublished.

28. M. Lee and R. McConnell, SLAC Report SR-30 (1973), unpublished.

29. A. Hofmann, Proceedings of the International School of Particle Accelerators, Erice, 1976, CERN 77-13, p. 139.

30. M. Sands, Orsay Report 3-76 (1976), unpublished.

31. M. Sands, SLAC Report 121 (1970).

32. E. D. Courant and A. M. Sessler, Rev. Sci. Instrum. 37, 1579 (1966).

33. C. Pellegrini, 1981 Summer School on High Energy Particle Accelerators, API Proc. 87, p. 77.

34. C. Pellegrini, "Physics with Intersecting Storage Rings," International School of Physics, Enrico Fermi, Academic Press, New York, 1971, p. 221.

35. G. Loew, 1982 Summer School on High Energy Particle Accelerators, SLAC, 1982.

36. L. D. Landau and E. M. Lifshitz, "Mechanics," Pergamon, 1960, p. 82.

37. R. F. Koontz, G. A. Loew, R. H. Miller and P. B. Wilson, IEEE Trans. Nucl. Sci. 24, 1493 (1977).

38. R. Helm and G. Loew, "Linear Accelerators," North Holland, Amsterdam, 1970, Chapter B.1.4.

39. W. K. H. Panofsky and M. Bander, Rev. Sci. Instrum. 39, 206 (1968).

40. V. K. Neil, L. S. Hall and R. K. Cooper, Part. Accel. 9, 213 (1979).

41. A. W. Chao, B. Richter and C. Y. Yao, Nucl. Instrum. Methods 178, 1 (1980).

42. A. W. Chao and R. K. Cooper, SLAC Collider Note CN-142 (1982), submitted for publication.

43. R. D. Kohaupt, DESY Report M-80/19 (1980), unpublished.

44. R. Talman, CERN/ISR-TH/81-17 (1981), unpublished.

45. R. Talman, Nucl. Instrum. Methods 193, 423 (1982).

46. A. W. Chao, P. Morton, J. Rees, M. Sands, and P. Wilson, to appear as a SLAC-PEP-Note (1982).

47. C. Pellegrini, Nuovo Cimento 64, 447 (1969).

48. M. Sands, SLAC-TN-69-8 (1969).

49. Y. Miyahara and K. Takata, Part. Accel. 10, 125 (1980).

50. The SPEAR Group, IX International Conference on High Energy Accelerators, SLAC, 1974, p. 338.

51. J. Gareyte and F. Sacherer, IX International Conference on High Energy Accelerators, SLAC, 1974, p. 341.

52. F. Sacherer, Proceedings of the Spring Study on Accelerator Theory, Geneva, 1972, p. 175.

53. Littauer, 1982 Summer School on High Energy Particle Accelerators, SLAC, 1982.

54. F. F. Chen, "Introduction to Plasma Physics," Plenum, New York, 1977.

55. S. Chandrasekhar, "Plasma Physics," University of Chicago, 1960, Chapter VI.

56. C. Pellegrini and A. M. Sessler, Nuovo Cimento 3A, 116 (1971).

57. J. Haissinski, Nuovo Cimento 18B, 72 (1973).

58. F. Sacherer, CERN/SI-BR/72-5 (1972), unpublished.

59. F. Sacherer, IEEE Trans. Nucl. Sci. 24, 1393 (1977).

60. J. L. Laclare, Proceedings of the XI International Conference on High Energy Accelerators, Geneva, 1980, p. 526.

61. G. Besnier, Nucl. Instrum. Methods 164, 235 (1979).

62. B. Zotter, CERN SPS/81-18, CERN SPS/81-19 and CERN SPS/81-20 (1981), unpublished.

63. K. Satoh, SLAC Reports PEP-357 and PEP-361 (1981), unpublished.

64. J. M. Wang and C. Pellegrini, Proceedings of the XI International High Energy Accelerators, Geneva, 1980, p. 554.

65. C. Pellegrini, IEEE Trans. Nucl. Sci. NS-28, 2413 (1981).

66. R. D. Ruth and J. M. Wang, IEEE Trans. Nucl. Sci. NS-28, 2405 (1981).

67. R. D. Ruth, Ph.D. thesis, BNL 51425 (1981).

68. K. Satoh and Y. Chin, KEK Preprint 82-2, submitted to Nucl. Instrum. Methods (1982).

69. T. Suzuki and K. Yokoya, submitted to Nucl. Instrum. Methods (1982).

70. T. Suzuki, KEK Preprint 82-10, submitted to Part. Accel. (1982).

71. R. D. Kohaupt, DESY Report 80/22 (1980).

72. R. D. Kohaupt, Proceedings of the XI International Conference on High Energy Accelerators, Geneva, 1980, p. 562.

73. A. W. Chao and J. Gareyte, SLAC Report SPEAR-197/PEP-224 (1976), unpublished.

74. K. Huang, "Statistical Mechanics," John Wiley, New York (1963).

75. S. Chandrasekhar, Rev. Mod. Phys. 15, 1 (1943).

76. J. LeDuff, SLAC Report PEP-64 (1973), unpublished.

77. K. Bane, A. W. Chao and M. J. Lee, SLAC Report SPEAR-213 (1978), unpublished.

78. P. Wilson, SLAC Report PEP-232 (1977), unpublished.

79. M. Month and E. Messerschmid, IEEE Trans. Nucl. Sci. NS-24, 1208 (1977).

80. P. B. Wilson et al., IEEE Trans. Nucl. Sci. NS-24, 1211 (1977).

81. J. C. Denard et al., IEEE Trans. Nucl. Sci. NS-28, 2474 (1981).

82. D. Rice et al., IEEE Trans. Nucl. Sci. NS-28, 2446 (1981).

83. H. G. Hereward, Rutherford Laboratory Report RL-75-021 and EPIC/MC/70 (1975), unpublished.

84. A. W. Chao and S. Kheifets, SLAC Report PEP-365 (1981), unpublished.